

Implementation and Validation of Experimental Test Bench for Laboratory-Scale Microgrid

by

Huan LIU

THESIS PRESENTED TO ÉCOLE DE TECHNOLOGIE SUPÉRIEURE
IN PARTIAL FULFILLMENT FOR A MASTER'S DEGREE
WITH THESIS IN ELECTRICAL ENGINEERING
M.A.Sc.

MONTREAL, MAY 1ST, 2023

ÉCOLE DE TECHNOLOGIE SUPÉRIEURE
UNIVERSITÉ DU QUÉBEC



Huan Liu, 2023



This Creative Commons licence allows readers to download this work and share it with others as long as the author is credited. The content of this work can't be modified in any way or used commercially.

BOARD OF EXAMINERS
THIS THESIS HAS BEEN EVALUATED
BY THE FOLLOWING BOARD OF EXAMINERS

Mr. Louis A. Dessaint, Thesis Supervisor
Department of Electrical Engineering, École de technologie supérieure

Mr. Kamal AI Haddad, President of the Board of Examiners
Department of Electrical Engineering, at École de technologie supérieure

Mr. Pierre Jean Lagacé, Member of the jury
Department of Electrical Engineering, at École de technologie supérieure

THIS THESIS WAS PRESENTED AND DEFENDED
IN THE PRESENCE OF A BOARD OF EXAMINERS AND PUBLIC
ON APRIL 18, 2023
AT ÉCOLE DE TECHNOLOGIE SUPÉRIEURE

FOREWORD

This thesis provides 30 credits out of 45 credits for my master's degree in Electrical Engineering with a concentration in Microgrid at École de technologie supérieure under the guidance of Professor Louis-A. Dessaint. The research aims to construct a campus microgrid based on ÉTS and validate the economic optimization algorithm with a Battery Energy Storage System.

ACKNOWLEDGMENT

This long journey of studying while working is about to come to an end. I have mixed emotions, and it seems that there is much to be said for not saying much. So many people have helped me along the path that I wish to genuinely thank. At the top of this list is my advisor, Professor Louis-A. Dessaint. He has consistently provided me with support, confidence, and accessibility. He knows how to maintain my motivation through insightful guidance and outstanding dedication.

My appreciation also extends to the jury members who took the necessary time to evaluate and appraise my work.

My gratitude also goes to Nicolas Mary for his cooperation and enlightened advice. He is more like my mentor, whenever he can answer my questions and clear my doubts. Especially during the testing period, he faced difficulties alongside me and assisted me in overcoming the obstacles. I would like to thank Yohann Geli as well, when I took over this project from him, he supported me get started with LabVIEW.

This thesis not only highlights my efforts at the keyboard but also a milestone that represents the culmination of accomplishments of successive groups of master's and doctor's students at ÉTS and specifically in GREPCI. The effective establishment of the test bench is attributable to Youssef Bekbouti, Éric Pilot, and Jorge Rojas-Rodriguez, the technical support team of the Electrical Engineering Department.

I really like to express my appreciation to my colleagues at Service des Enseignements Généraux, such as Nathalie Jalbert, Rachid Bouacha, Hugo Bélise, Youri Juteau, Paul-Ernest Grenier, Yannick Cloutier, and Céline Beaudry. No matter in the mind or the work, they are my unwavering support, continually encouraging me to advance.

VIII

I am obliged to my dear friends Xiaofan Fu, Long Kong, Zijian Zhao, Anna Li, Nathalie Dabin, and Nathalie Jalbert for their real friendship, their counsel, and all the assistance they could provide during my thesis completion.

Finally, I would like to thank my family for their support. I am indebted to my parents Xianfa Liu and Huali Han for their unconditional love and continuous encouragement. Special thanks to my love Patrice Gauthier, whose inspiration, understanding, and daily assistance. I would also like to thank my four years old daughter Léana Gauthier for her sacrifice of mother-daughter time to enable me to accomplish this thesis.

Réalisation et validation d'un banc d'essai expérimental pour un micro-réseau à l'échelle laboratoire

Huan LIU

RÉSUMÉ

En raison de l'épuisement des énergies non renouvelables, de l'importance de la pollution de l'environnement et de son impact sur le climat mondial, les communautés locales recherchent des solutions énergétiques fiables et efficaces. Tout ceci s'intègre dans une notion plus générale du micro-réseau. Avec l'évolution de la société et le développement rapide de la science et de la technologie, les systèmes reliés en micro-réseaux constituent une partie intégrante du secteur de l'électricité, car ils peuvent combiner efficacement plusieurs systèmes de production d'électricité distribués et ont un taux de pénétration significativement élevé des énergies renouvelables. Actuellement, tous les pays du monde construisent des bancs d'essais expérimentaux de micro-réseaux et des projets de démonstration recherchant et appliquant vigoureusement ces derniers.

L'objectif principal de ce mémoire est de mettre au banc d'essai le contrôle de la coordination de la puissance de micro-réseaux, le paramétrage en temps réel, la prédiction de la charge à court terme et les stratégies de programmation d'optimisation énergétique. Tout cela s'inscrit dans l'atteinte d'un écrêtage des pics de charge et l'amélioration des avantages économiques du stockage de l'énergie produite.

En premier lieu, ce mémoire fournit le contexte de la recherche sur les micro-réseaux, passe en revue les projets expérimentaux les plus importants et les pilotes de ces micro-réseaux, étudie la conception du système les gérant et développe une plate-forme complète de test physique, appliquée à ces derniers.

En second lieu, l'architecture globale de ce banc d'essai pour un micro-réseau type est développée par le biais d'un concept de contrôle hiérarchique conformément à la structure traditionnelle du système de micro-réseau connecté au grand réseau électrique, y compris un ensemble de passerelle de micro-réseau, un compteur de puissance, un pack de charge et un système de stockage d'énergie. LabVIEW et SQLite fonctionnent simultanément comme outils de développement pour créer un système de contrôle centralisé du micro-réseau intégrant la surveillance des données en temps réel, le contrôle intelligent, l'analyse de la qualité de l'alimentation et la gestion de la base de données. De plus, la communication entre le contrôleur, les dispositifs de stockage énergétique et le compteur emprunte le protocole Modbus.

En définitive, ce mémoire apporte un raisonnement clair sur les tests de performance qui confirment la fiabilité et la précision de ce banc d'essai. En évaluant les changements dans les

demandes de charge et en combinant la prévision de charge théorique à court terme. En prenant comme référence initiale l'idée d'un réseau neuronal, les essais viennent valider les algorithmes du fonctionnement économique ainsi que les techniques de gestion de l'énergie. Le test de performance s'est tenu un jour de fin de semaine en 2019, alors que la consommation de la puissance était relativement inférieure à celle d'une journée de semaine et le fonctionnement du système est peu affecté par l'algorithme. Toutefois, les tests de validation sont programmés sur deux jours ouvrables considérés comme étant plus représentatifs en consommation énergétique, lors des essais de 2019, et plus précisément en saison d'hiver et d'été. Ces deux jours d'analyses possèdent la consommation de la puissance la plus élevée. Ils permettent donc de mieux optimiser l'opération d'écrêtage de la puissance de charge.

Les résultats expérimentaux indiquent que ce système possède une forte évolutivité et une fiabilité plus représentative servant à l'évaluation complète, le diagnostic de problèmes et les analyses de faisabilité et de rentabilité économiques.

Mots-clés : Micro-réseau; LabVIEW ; banc d'essai expérimental ; Modbus ; interface de contrôle central

Implementation and validation of experimental test bench for laboratory-scale microgrid

Huan LIU

ABSTRACT

Due to the depletion of non-renewable energy sources, the severity of environmental pollution, and their impact on the global climate, local communities were looking for a reliable and efficient electricity solution. As a result, the notion of microgrid has emerged as the times dictate. With the advancement of society and the rapid development of science and technology, microgrid systems have become an integral part of the power sector, since it can efficiently combine several distributed power generation systems and has a high renewable energy penetration rate. Currently, every country in the world is constructing microgrid experimental platforms and demonstration projects, and vigorously researching and applying microgrids.

The primary objective of this thesis is to establish a microgrid experimental platform and conduct experiments and verifications on this test bench, including microgrid power coordination control, real-time calculation, short-term load forecasting, and energy optimization scheduling strategies, to achieve peak load shaving and improve the economic benefits of distributed storage.

First of all, this paper provides a background on microgrid research and reviews important experimental and pilot projects related to microgrids. It then studies the microgrid system design and develops a complete physical test platform for microgrids, which includes a battery bank, a load pack, an inverter, and a power meter.

Secondly, the overall design of this microgrid test bench is developed utilizing a hierarchical control concept in accordance with the traditional grid-connected microgrid system structure. This includes a microgrid gateway cabinet, power meter, load, and energy storage system. To incorporate optimization algorithms, LabVIEW and SQLite were used concurrently as development tools to create a centralized microgrid control system with features such as real-time data monitoring, intelligent control, power quality analysis, and database management. Additionally, the communication among the controller, energy storage devices, and the power meters is facilitated using the Modbus protocol.

Ultimately, this thesis concludes with performance tests of this grid-connected microgrid test bench, which confirm its reliability and accuracy. By assessing changes in load demands and combining the theoretical short-term load forecasting based on neural network algorithms, the economic operation algorithms and energy management techniques have been validated. The performance test was conducted on a weekend day in 2019, whose power consumption was relatively lower than that on a weekday and the system operation is minimally affected by the algorithm. However, the validation tests are mainly scheduled on two days that are considered

more representative in 2019, specifically winter and summer. Those two days have the highest power usage and are also the most crucial for load power shaving operation.

The experimental results indicate that this system has strong scalability and a user-friendly interface, providing reliable support for comprehensive evaluations, problem diagnostics, and economic analysis.

Keywords: Microgrid; LabVIEW; experimental test bench; Modbus; central control interface

TABLE OF CONTENTS

	Page
INTRODUCTION	1
CHAPTER 1 CONTEXT	5
1.1 Background	5
1.1.1 Microgrid Concept	5
1.1.2 Microgrid Control System	9
1.2 Outline and Contributions	10
1.3 Literature Review	11
1.4 Motivation & Research Objectives	24
1.5 Concluding Remarks	25
CHAPTER 2 OVERALL STRUCTURE AND HARDWARE ARCHITECTURE OF THE MICROGRID TEST BENCH.....	27
2.1 Introduction.....	27
2.2 Overall Structure of the Test Bench.....	27
2.3 Hardware Implementation	31
2.3.1 MG Gateway Cabinet	31
2.3.2 Power Meter Selection and Setting.....	33
2.3.3 Load Selection and Setting	34
2.3.4 Energy storage unit selection and setting.....	36
2.4 Communication Method and Communication Protocol Selection	38
2.4.1 Communication Method	38
2.4.2 Communication Protocol	39
2.5 Chapter Summary	39
CHAPTER 3 TEST BENCH SOFTWARE SYSTEM IMPROVEMENT	41
3.1 Real-Time System Implementation	41
3.1.1 Inverter Control Module Development.....	43
3.1.1.1 Communication.....	43
3.1.1.2 Inverter Monitoring System.....	44
3.1.1.3 Inverter Control System.....	47
3.1.1.4 Inverter protection setup	53
3.1.2 Electrical Load Control Module Improvement.....	55
3.1.2.1 Communication.....	56
3.1.2.2 Data Extraction	57
3.1.3 Power Meter Monitoring Module Design.....	58
3.1.3.1 Communication.....	58
3.1.3.2 Measurement.....	59
3.2 Test Bench Device Software Modules Integration	60
3.2.1 Terminals Assignment and Icons definition	60
3.2.2 Integration	61

	3.2.2.1	XW Pro Inverter integration	61
	3.2.2.2	Chroma Load integration	62
	3.2.2.3	PM5340 Power Meter integration.....	62
3.3		Test Bench Virtual Interface Improvement	63
	3.3.1	MGCCP Main Interface	64
	3.3.2	BMS Interface	66
	3.3.3	Test Parameters Configuration Interface	66
	3.3.4	Load Control Panel	68
	3.3.5	Optimal Power Control Panel	69
3.4		Chapter Summary	69
CHAPTER 4 TEST BENCH PERFORMANCE TEST			71
4.1		Communication Function Test.....	71
	4.1.1	PM5430 Power meter Communication Test.....	71
	4.1.2	Chroma 63480 AC/DC Load Communication Test.....	72
	4.1.3	XW Pro 6848 NA Inverter Communication Test	75
4.2		Data Transceiver Test	76
	4.2.1	PM5340 Power meter Test.....	76
	4.2.2	Chroma 63804 AC/DC Load Test with Constant Power Mode	79
	4.2.3	XW Pro Inverter Test and Validation with Conext Gateway interface	81
4.3		System Operation Test.....	86
	4.3.1	Test Condition and Set Up.....	86
		4.3.1.1 Test mode selection.....	86
		4.3.1.2 Test Date selection.....	87
		4.3.1.3 Power ratio determination.....	87
		4.3.1.4 Time ratio determination.....	88
		4.3.1.5 SOC associated parameter identification.....	89
	4.3.2	Test result.....	92
		4.3.2.1 Load Power and Grid Power Consumption	93
		4.3.2.2 Battery Bank Charging and Discharging Oscillation.....	93
4.4		Chapter Summary	97
CHAPTER 5 VALIDATION AND VERIFICATION OF CONTROL STRATEGIES TEST RESULTS.....			99
5.1		Energy Management Control Architecture	99
	5.1.1	Neural network input data.....	100
	5.1.2	MG Load Power Forecasting.....	101
	5.1.3	Power Optimization Dispatch Strategy.....	103
		5.1.3.1 Objective Function.....	103
		5.1.3.2 Constraints	105
		5.1.3.3 Charge and Discharge Scheduling	106
5.2		Simulation and Validation Tests on test bench with 3 rd January, 2019	107
	5.2.1	Past Time Simulation and Test with Perfect Load Prediction Algorithm.....	108
	5.2.2	Past Time Simulation and Test with ANN Prediction Algorithm	111

5.3	Simulation and Validation Tests on test bench with 2 nd July, 2019	115
5.3.1	Past Time Simulation and Test with Perfect Load Prediction Algorithm.....	115
5.3.2	Past Time Simulation and Test with ANN Prediction Algorithm	118
5.4	Chapter Summary	122
	CONCLUSION.....	123
	RECOMMENDATIONS.....	125
APPENDIX I	POWER METER PM5340 DATASHEET.....	127
APPENDIX II	XW PRO 6848 HYBRID INVERTER DATASHEET	130
APPENDIX III	SIMPLIPHI PHI 3.8 BATTERY DATASHEET.....	133
APPENDIX IV	CONEXT GATEWAY DATASHEET.....	135
APPENDIX V	LABVIEW INVERTER READ AND WRITE PROGRAM	139
APPENDIX VI	LABVIEW INVERTER INITIALIZATION PROGRAM.....	143
APPENDIX VII	LABVIEW CHROMA LOAD PROGRAM.....	145
APPENDIX VIII	LABVIEW POWER METER PROGRAM	147
APPENDIX IX	XW PRO INVERTER READ PROGRAM INTEGRATION.....	149
APPENDIX X	CONEXT BATTERY MONITOR DATASHEET.....	151
	LIST OF BIBLIOGRAPHICAL REFERENCES.....	153

LIST OF TABLES

		Page
Table 1.1	Comparison of hierarchical control and distributed control for microgrid.....	9
Table 1.2	A Summary of the CANREL components.....	13
Table 1.3	MICROGRID Testbed Specifications	16
Table 1.4	Components of Energy Conversion Systems.....	19
Table 1.5	Experimental AC/DC-MG, General Parameters.....	21
Table 2.1	Chroma 63804 Specification.....	35
Table 3.1	Modbus Map in Gateway for XW Pro Inverter Grid Side Measurement.....	50
Table 3.2	Modbus Map in Gateway for XW Pro Inverter Battery Side Measurement.....	50
Table 3.3	Modbus Map in Gateway for XW Pro Inverter Mode and Status Surveillance.....	51
Table 3.4	Modbus Map in Gateway for XW Pro Inverter Sending Instruction Registers.....	51
Table 3.5	Device, Charger, Inverter Status Details.....	52
Table 3.6	Settings for SimpliPhi PHI 3.8 kWh 48V Battery with Schneider Conext XW Pro & XW+ Inverters	54
Table 3.7	Modbus Map for Inverter Protection	54
Table 4.1	Observation results of grid voltage at HMI and LabVIEW	77
Table 4.2	Grid Frequency Reading from HMI and LabVIEW	78
Table 4.3	Chroma Load Pack reading from HMI and LabVIEW	81
Table 4.4	Comparison of battery pack voltage and discharge power in both LabVIEW and Gateway interface.....	85
Table 5.1	Parameter Value Configuration	107

LIST OF FIGURES

		Page
Figure 1.1	Price Pressure Energy Inflation is Soaring across G-7 Economies	5
Figure 1.2	Major Power Supply Challenges from Mid-2020 Through 2021	6
Figure 1.3	Conceptual Modern Architecture of a Microgrid Operating System.....	7
Figure 1.4	The Infrastructure of an ACMG System.....	8
Figure 1.5	The Infrastructure of a DCMG System.....	8
Figure 1.6	Modern Architecture Design of AC/DC Hybrid MG (HMG) Systems.....	9
Figure 1.7	The CANREL Containerized Testbed	12
Figure 1.8	The CANREL One-line Diagram. SIM: Simulator; CAP: Capacitor; EV: Electric Vehicle	12
Figure 1.9	The CANREL system components: the (a) containerized design solution,.....	13
Figure 1.10	Microgrid Testbed QEERI (Hardware)	15
Figure 1.11	Hybrid AC/DC Microgrid Testbed Components.....	16
Figure 1.12	Experimental Set Up of Laboratory Scale of MG System.....	18
Figure 1.13	Description of Proposed Education Laboratory-Scale Microgrid	19
Figure 1.14	Example of a 3-phase AC MG Implemented.....	22
Figure 1.15	General Topology of Implemented Hybrid MG	23
Figure 2.1	Overall Structure Diagram of MG in Laboratory of ÉTS.....	28
Figure 2.2	Communication Topology Diagram	29
Figure 2.3	Functional Architecture Diagram	30
Figure 2.4	MG Gateway Cabinet	32
Figure 2.5	Schneider PM5340 Power and Energy Meter.....	33
Figure 2.6	Chroma Programmable AC/DC Electronic Load	34

Figure 2.7	XW Mini Distribution Panel.....	36
Figure 2.8	Schneider XW Pro 6848 hybrid Inverter	37
Figure 2.9	Simpliphi PHI 3.8 Battery.....	37
Figure 3.1	MGCCP Host Computer.....	42
Figure 3.2	Modbus Master by Plasmionique Inc.	42
Figure 3.3	Open TCP Session	44
Figure 3.4	Read Holding Registers	45
Figure 3.5	Source Block Diagram Code of Reading Grid Frequency.....	45
Figure 3.6	Source Block Diagram Code of Reading Grid Voltage.....	46
Figure 3.7	Source Block Diagram Code of Reading Grid Current	46
Figure 3.8	Conversion program of Hexadecimal to Decimal	46
Figure 3.9	Data Precision Selection	48
Figure 3.10	Write Single/ Multiple Registers	49
Figure 3.11	Source block diagram code of writing operation.....	49
Figure 3.12	Source Block Diagram Code of Converting Code to String.....	53
Figure 3.13	Inverter Initialization Program Segment.....	53
Figure 3.14	Open Selected Load by VISA Write Function	56
Figure 3.15	Block Diagram of VISA Write Function.....	57
Figure 3.16	Data extraction program	57
Figure 3.17	Data extraction Block Diagram	58
Figure 3.18	Source Block Diagram of PM5340 Communication	59
Figure 3.19	Measurement system of PM5340.....	59
Figure 3.20	Measurement of Energy Delivered to Load.....	60
Figure 3.21	XW Pro Inverter Write Program Integration Block Diagram.....	61

Figure 3.22	Chroma Load Integration Program	62
Figure 3.23	PM5340 Power Meter Integration Program.....	63
Figure 3.24	Microgrid Central Control Platform	64
Figure 3.25	MGCCP Main Interface	64
Figure 3.26	Logging Interface.....	65
Figure 3.27	BMS Interface	66
Figure 3.28	Tab 1 of Parameter Setting Interface	67
Figure 3.29	Tab2 of Parameters Setting Interface.....	67
Figure 3.30	Load Control Panel	68
Figure 3.31	Optimal Power Control Panel	69
Figure 4.1	Communication Time between Host Computer and PM5340.....	71
Figure 4.2	Communication Test of PM5340 Power Meter	72
Figure 4.3	GPIB-ENET/1000 Configuration Web Page	73
Figure 4.4	Master Chroma Load information from NI MAX	74
Figure 4.5	Reading load information from LabVIEW	74
Figure 4.6	Communication Time between Host Computer and XW Pro Inverter.....	75
Figure 4.7	Communication Test of XW PRO 6848	76
Figure 4.8	Grid Voltage Read from PM5340 in LabVIEW	77
Figure 4.9	Grid Voltage Read from HMI.....	77
Figure 4.10	Grid Frequency Read from LabVIEW	78
Figure 4.11	Grid Frequency Read from HMI.....	78
Figure 4.12	Chroma load configuration in LabVIEW	79
Figure 4.13	Chroma Load Pack Measurement via LabVIEW	80
Figure 4.14	Chroma Load Pack Measurement via Control Panel	80

Figure 4.15	XW Pro Inverter Initial Configuration in LabVIEW	82
Figure 4.16	XW Pro Inverter Initial configuration displayed in Gateway Interface.....	83
Figure 4.17	XW Pro Inverter Sell-to-Grid with 6.4kW showing in Gateway.....	84
Figure 4.18	XW Pro Inverter Sell-to-Grid with 6.4kW showing in LabVIEW	84
Figure 4.19	XW Pro Inverter Sell-to-Grid with more information showing in Gateway	85
Figure 4.20	LiFePO4 Charge Voltage vs. SOC	90
Figure 4.21	SimpliPhi Battery Discharge Voltage vs SOC.....	90
Figure 4.22	System Functional Test Result Segment.....	Erreur ! Signet non défini.
Figure 4.23	Charging when DC voltage is out of required range	95
Figure 4.24	Discharge with DC voltage less than 53V	95
Figure 4.25	Sunday, September 8, 2019 the operating curve of the MG test bench.....	96
Figure 5.1	Energy Management System, Taken from (Mary, 2022)	99
Figure 5.2	2019-01-03 Simulation Power Curve with Perfect Load Prediction	108
Figure 5.3	2019-01-03 on Test Bench with Perfect Load Prediction.....	109
Figure 5.4	Battery SOC change during the test for 2019-01-03	110
Figure 5.5	2019-01-03 Simulation Power Curve with ANN Load Forecasting.....	112
Figure 5.6	2019-01-03 On Test Bench with ANN Load Forecasting	113
Figure 5.7	Battery SOC with ANN on 2019-01-03.....	114
Figure 5.8	2019-07-02 Simulation Power Curve with Perfect Load Prediction	115
Figure 5.9	Battery SOC change during the test for 2019-07-02	116
Figure 5.10	2019-07-02 on Test Bench with Perfect Load Prediction.....	117
Figure 5.11	2019-07-02 Simulation Power Curve with ANN Load Forecasting.....	119
Figure 5.12	2019-07-02 On Test Bench with ANN Load Forecasting	120
Figure 5.13	Battery SOC with ANN on 2019-07-02.....	121

LIST OF ABBREVIATIONS

HVDC	High-Voltage Direct Current
MG	Microgrid
DERs	Distributed Energy Resources
EMS	Energy Management System
MGCCP	Microgrid Central Control Platform
RT	Real-Time
PCS	Power Conversion System
CERTS	Consortium for Electric Reliability Technology Solutions
DSM	Demand-Side Management
BESS	Battery Energy Storage System
ACMG	AC Microgrid
DCMG	DC Microgrid
HMG	Hybrid Microgrid
CANREL	Canadian Renewable Energy Laboratory
RES	Renewable energy sources
DAQ	Data Acquisition
IGBT	Insulated Gate Bipolar Transistor
PWM	Pulse-width Modulation
MPPT	Maximum Power Point Tracking
FPGA	Field Programmable Gate Arrays
MCS	Microgrid Control System

XXIV

HMI	Human-machine interface
HIL	Hardware-in-the-loop
CR	Constant Resistance
DoD	Depth of Discharge
SOC	State of Charge
CP	Constant Power
RTT	Real-time Target
LAN	Local area network
GRÉPCI	The Power Electronics and Industrial Control Research Group
NEMA	National Electrical Manufactures Association
CSA	Canadian Securities Administrators
VI	Virtual Instrument
API	Application Programming Interface
NI MAX	NI Measurement & Automation Explorer
LTLF	Long Term Load Forecasting
MTLF	Medium Term Load Forecasting
STLF	Short Term Load Forecasting
VSTLF	Very Short-Term Load Forecasting
ANN	Artificial Neural Network
MPC	Model Predictive Control
FNN	A Feedforward Neural Network

LIST OF SYMBOLS AND UNITS OF MEASUREMENT

$P_{bat_set_point}$	Power Send to Battery Bank
C_{bat}	Battery Bank Capacity
$P_{inverter_command}$	Inverter Command Power
R_{power}	Power Ratio
R_t	Time Ratio
C_{bat_rep}	Represented Battery Bank Capacity
$P_{ÉTS}$	Real System Power (ÉTS Power)
P_{Chroma}	Test Bench Power (Load Power)
T_{real}	Real Time
T_{test}	Test Time
T_{acc}	Accelerated Test Time
P_{inv_max}	Maximum Inverter Power
P_{inv_rep}	Represented Inverter Power
SOC_{min}	Minimum SOC
SOC_{bat}	Battery SOC
P_{dis_inv}	Inverter Discharge Power
P_{cha_inv}	Inverter Charge Power
SOC_{max}	Maximum SOC
$SOC_{virtual}$	Virtual SOC
$SOC_{available}$	Available SOC
P_{load}	Load Power

XXVI

$P_{\text{grid-power}}$	Grid Power
e_{ME}	Mean Error
$L_{\text{real}}(t)$	Actual Load Power
$L_{\text{predict}}(t)$	Predicted Load Power
$L_{\text{corrected}}(t)$	Iterative Load Power
$\text{Cost}_{\text{ÉTS}}$	Electricity cost of ÉTS
$\text{Cost}_{\text{Degradation}}$	Maintenance Cost of Battery
λ_{grid}	Electricity Price
$\lambda_{\text{degradation}}$	Maintenance Price of Battery
$C_{\text{degradation}}$	Battery Capacity Lost
ME	Mean Error
Ah	Ampere hour
W	Watt
kW	kilo Watt
kWh	kilo Watt Hour
\$	Express the Amount in Canadian Dollars Currency
\$/kWh	Price per kilo Watt hour of Electricity

INTRODUCTION

With the accelerated progress of the power and utility industry and the rapid expansion of the electric power market, large-scale centralized power generation and High-Voltage Direct Current (Jabbar et al.) electric power transmission networks have become the primary methods of power production, transmission, and distribution due to their high energy utilization and significant economic benefits. However, in the last decades, the traditional power grid has faced unprecedented challenges such as the depletion of non-renewable energy sources, serious environmental pollution problems, global climate change, and a further increase in electricity demand. Among them, the damage to the power grid caused by extreme weather is the most difficult to predict, and it often results in large-scale power outages. For instance, the February 2021 Texas Power Crisis was caused by multiple severe winter storms and had a duration of 2 weeks and 3 days, which led to 4.5 million homes and businesses without power, and about 702 people lost their lives (2021 Texas power crisis, 2021).

Therefore, countries all over the world are looking for reliable and resilient power supply, particularly in remote or isolated areas. The concept of microgrid (MG) has been proposed to coordinate these contradictions.

A microgrid is a controlled structure connected to the main grid, consisting of distributed energy resources (DERs), various coordinated loads, and generation units, as well as it can be isolated from the grid (M. H. Saeed, 2021). The distributed power is connected from the consumer side in the MG; thus, it has the characteristics of low cost and less pollution emission. Microgrids can also provide localized power generation, distribution and storage, and it has the potential for low investment-high profit, and cost savings and efficiency improvements, which can provide new opportunities for energy entrepreneurship, job creation, and community development.

MG can be regarded as a dispatchable load to participate in grid energy management, and can also be considered as a customized power supply that can meet the specific needs of users.

Furthermore, it can effectively supplement the shortcomings of the main power grid, avoid large-scale power outage accidents caused by a single power supply mode, give the benefits of complete consideration of DG, and enhance the security, reliability, and flexibility of the power system.

With the increased maturity of MG theoretical research, it is necessary to develop a MG experimental testbed, which could help to provide systematic experimental data and a basis for a series of future studies on the selection of the control strategies and the improvement of the energy management system (EMS).

There are currently two main MG experimental platforms. One is based on power system software combined with corresponding control strategies, where researchers add and remove functions at the software level, and set observation points for monitoring the internal working process and data transmission of MG. This type of system has a clear structure, accurate data collection, easy expansion of functionalities, a friendly human-computer interface, and a short development cycle. However, due to the lack of actual equipment support, it may be difficult to validate the real-time control strategies.

The other type is based on actual physical devices combined with a simulated MG. Researchers use various sampling tools, add a host computer to display and store data and construct a complete MG operation experimental testbed. This type of system has an explicit architecture, is more perceptive, and can provide better learning opportunities while demonstrating the scientificity of the control strategy.

As mentioned above, it is important for further development of MG to implement the MG central control platform (MGCCP), which can monitor the status and internal operation data of the MG system and can achieve real-time (RT) control to fulfill peak load shaving requirements, and other features such as demand response and pricing optimization, among others. It also facilitates the transition from traditional grids to smart grids.

This thesis aims to improve the MGCCP in LabVIEW, a graphical programming environment, by combining it with neural network algorithms to establish an AC microgrid economic operation test bench. This AC microgrid consists of a battery pack, AC programmable loads, and a power conversion system (PCS). It is noteworthy that the experimentation apparatus has the potential to encompass renewable energy sources in its configuration. Furthermore, it is pertinent to state that subsequent to this research, a second student incorporated the photovoltaic panels including Conext MPPT 60/150 into the test bench.

CHAPTER 1

CONTEXT

1.1 Background

1.1.1 Microgrid Concept

The progress and development of science, technology, and social economy have greatly increased the consumption of electricity, and the traditional power grid is facing unparalleled pressure and challenges. According to Bloomberg New Energy Finance, global power demand is expected to rise by 60% by 2050 as the world transitions away from fossil fuels and towards electric automobiles, stoves, and heating systems (David R Baker, 2021). Due to the impact of the Covid-19 pandemic and the global economic recovery, worldwide electricity demand is outpacing the penetration of renewables, which is resulting in a significant increase in energy inflation (IEA, 2021). Figure 1.1 shows that energy inflation has tremendous growth in the last year, which has reached a 24-year high.

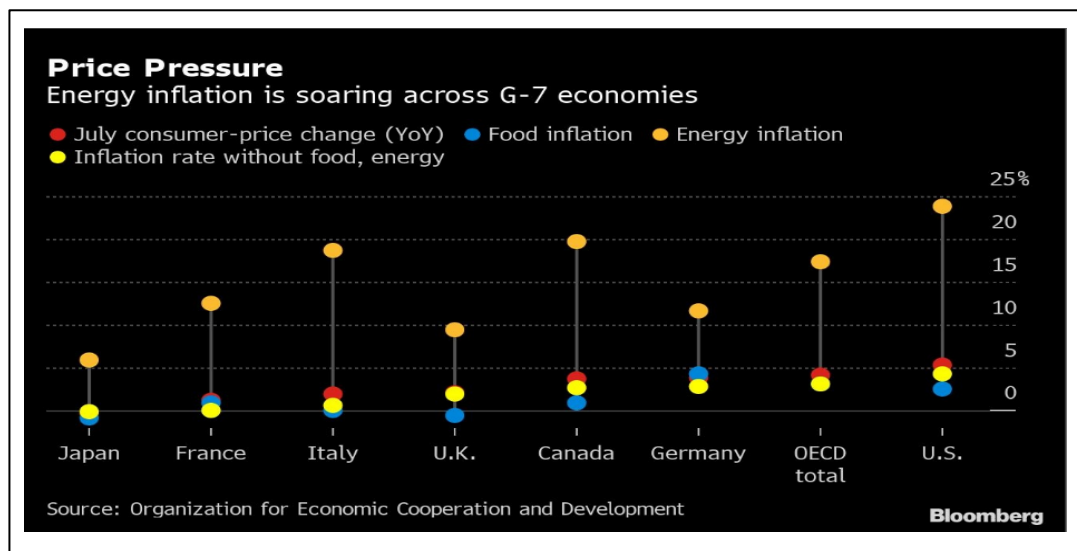


Figure 1.1 Price Pressure Energy Inflation is Soaring across G-7 Economies

Taken from David R Baker (2021)

Furthermore, as a result of climate change, extreme abnormal weather events are occurring more frequently, causing damage to power facilities and poses a serious threat to the stability and reliability of the power grid. As reported by Zakaria, 2022, over the last year, catastrophic power outages harmed at least 350 million people or more than 4% of the global population, Among them, the United States has experienced three major power outages events affecting 10.2 million citizens: winter storms in Texas, hurricane Ida in Louisiana, and heat wave in California (Zakaria, 2022).

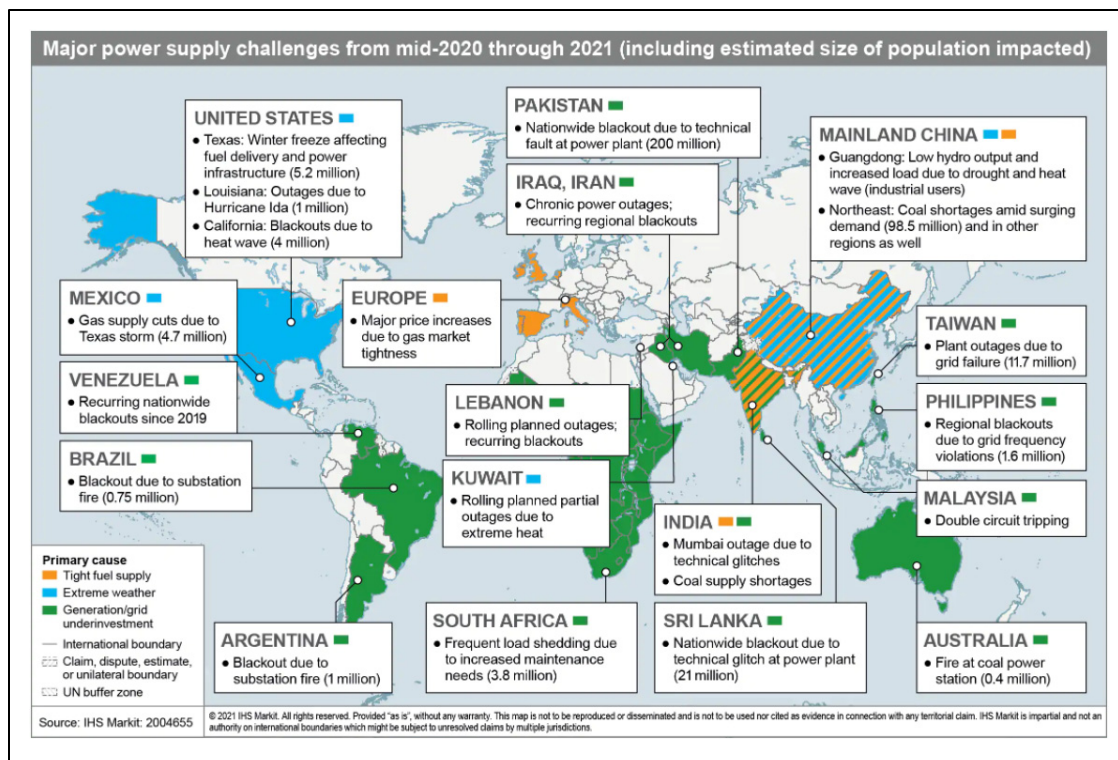


Figure 1.2 Major Power Supply Challenges from Mid-2020 Through 2021

Taken from Zakaria (2022)

Microgrids offer a feasible solution for communities and organizations such as hospitals and universities to keep their critical services running during power outages by generating their electricity. The Consortium for Electric Reliability Technology Solutions (CERTS) MG concept was created to increase power system reliability and efficiency by utilizing DER technology, such as Battery Energy Storage System (BESS), Photovoltaic (PV), and Hydraulic Engine, as shown in Figure 1.3 (Singh, 2021).

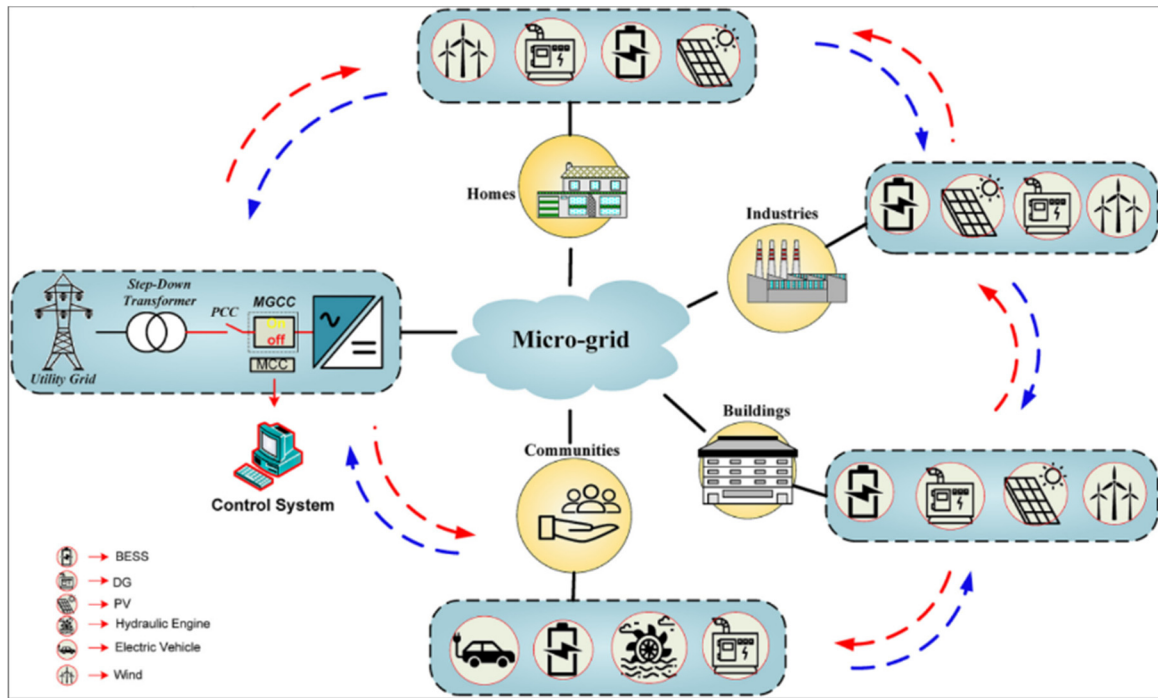


Figure 1.3 Conceptual Modern Architecture of a Microgrid Operating System
Interfaced with The Main Grid
Taken from Singh (2021)

In general, MGs can be powered by conventional grid, and also can be operated in islanded mode. During regular operation, the MG functions in parallel with the major grid. In this process, there is a variety of ways to lower the peak demand for electricity to reduce electricity bills, such as Demand-Side Management (DSM), which can be achieved through load-shifting, peak shaving, energy conservation, or valley filling (T. Mindra, 2022). Once the main grid fails, the MG must immediately switch to an independent operation mode to continue supplying power to the loads connecting to the grids.

Typically, according to the power supply type for the distribution networks, MGs are classified into AC microgrids (ACMG), DC microgrids (DCMG), and AC/DC or hybrid microgrids (HMG). ACMG system has better compatibility with AC-based loads, thus saving the investment cost. Since there is no reactive current, the DCMG system has higher transmission efficiency, and their control system is also relatively less complex due to no issues with

synchronization, harmonics, reactive power, and frequency control. The choice of microgrid type should depend on the application and the infrastructure. The basic structure diagrams of those three microgrids are presented in Figures 1.4, Figure 1.5, and Figure 1.6, respectively (Singh, 2021).

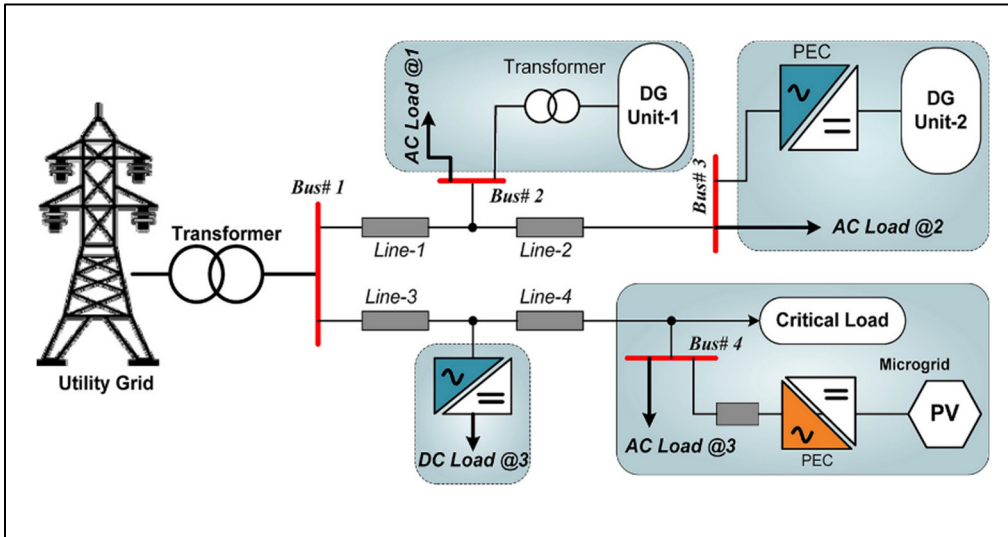


Figure 1.4 The Infrastructure of an ACMG System
Taken from Singh (2021)

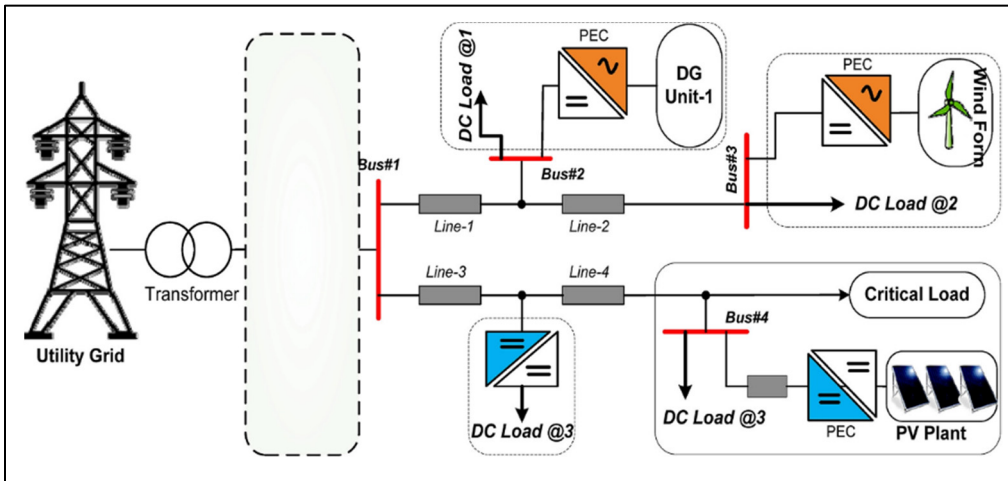


Figure 1.5 The Infrastructure of a DCMG System
Taken from Singh (2021)

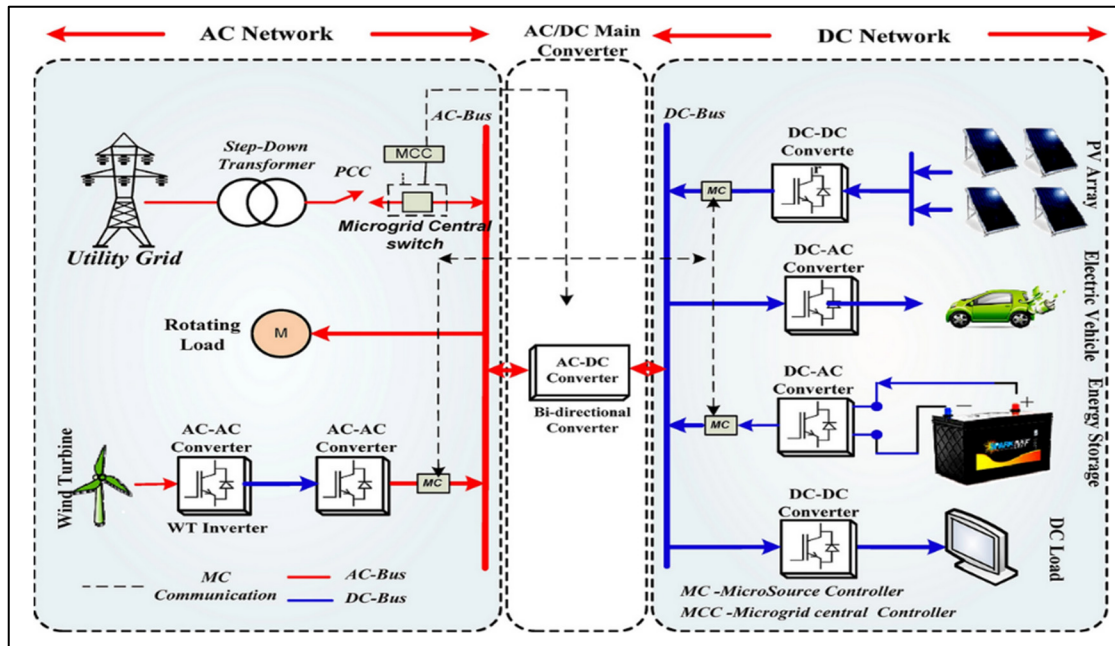


Figure 1.6 Modern Architecture Design of AC/DC Hybrid MG (HMG) Systems
 Taken from Singh (2021)

1.1.2 Microgrid Control System

Due to the particular control functions, the architecture and the software used for control systems are very different. It experienced a development process from centralized to distributed control. The comparison is shown in Table 1.1 (Xianyong Feng, 2017).

Table 1.1 Comparison of hierarchical control and distributed control for microgrid
 Taken from Xianyong Feng (2017)

Features	Economics	Reliability	Complexity	Scalability	Bandwidth
Hierarchical Or Centralized Control	Optimal	Control failure results losing coordination and optimal operation	Complex	Add DERs based on comprehensive communication architecture	Low
Distributed Control	Suboptimal	Reliable	Simple	Add more types of DERs with high quality algorithms	High

The centralized control system only uses a global database to process the system information, and each device is independently connected to the central controller unit. Therefore, as the microgrid becomes complex and more and more information needs to be processed, the response speed of the system could become slower, and the reliability could deteriorate.

The hierarchical control system adopts the master-slave layered control method, and its database structure is also hierarchical type, which greatly reduces the amount of data. The command response and communication between each unit are very flexible. However, if the upper layer fails, it will inevitably lead to the paralysis of the entire lower layer.

The distributed control system is composed of multiple entities that are both independent and interrelated. Each entity is in an equal position and has the right to make self-determination, thus reducing the complexity of the system and improving its scalability and reliability. However, because of the limitation of computational capabilities, it rarely deals with predictive control locally, consequently, its forecasting capacity may limit the overall system performance (Xianyong Feng, 2017).

More complex systems generate enormous amounts of data every second. Information and communication play a crucial role in the collection, transmission and procession of data. There is a consensus that centralized cloud computing is the most practical option. In cloud computing, globally dispersed hardware and software are networked to remote data centers that perform computation storage, monitoring, and management. However, there are several drawbacks, including diverse surroundings, and cyber security concern. Edge computing moves the computing frontier beyond the reach of centralized nodes and toward the edges of the communication network. Data analytics could be performed using computational resources that are physically located nearer to users. It is efficient to relieve the stress on cloud data centers.

1.2 Outline and Contributions

The main research contents of each chapter of this paper are as follows:

Chapter 1: This chapter mainly introduces the research background and the development of MG technology in countries around the world today.

Chapter 2: This chapter demonstrated the MG architecture and explains the hardware and communication unit selection.

Chapter 3: This chapter primarily improves the programming of the host computer LabVIEW to write the HMI, the design of the data optimization processing program of each device, and the communication program between software and hardware.

Chapter 4: This chapter describes the functionality tests that have been performed.

Chapter 5: This chapter is to compare and analyze the simulation results and on test bench test results.

1.3 Literature Review

A microgrid test bench is a physical simulation tool for designing, developing, and testing MG projects for both islanded operation and grid-connected operation (E. Nasr-Azadani, 2020). Unlike other small-scaled microgrid testbeds constructed in the last decade for research and development purposes, the Canadian Renewable Energy Laboratory (CANREL) built a MG test bench with containers (Figure 1.7) to offer performance demonstration and design validation services for industry customers, government utilities, and academia research.

This 600V low-voltage test bench is connected to the Guelph Hydro grid by a 13.8kV-600/347V transformer (Figure 1.8). As shown in Figure 1.9, this MG consists of two small MGs, which as associated with a 270kVA grid simulator, 90kW PV simulator, 100kW wind simulator, diesel generators, 10kW PV roof-top panels, 3kW wind turbine, 200kW programmable load banks, 200kWh BESS, 30kVar capacitor bank, and 7.2 kW EV chargers, table 1.2, (E. Nasr-Azadani, 2020).

CANREL provides the flexibility to meet a variety of different test characteristics such as supply, demand, and DERs. It is also equipped with full data acquisition, protection relays, and power meters for having detailed voltages, currents, and power in all experimental scenarios.



Taken from E. Nasr-Azadani (2020)

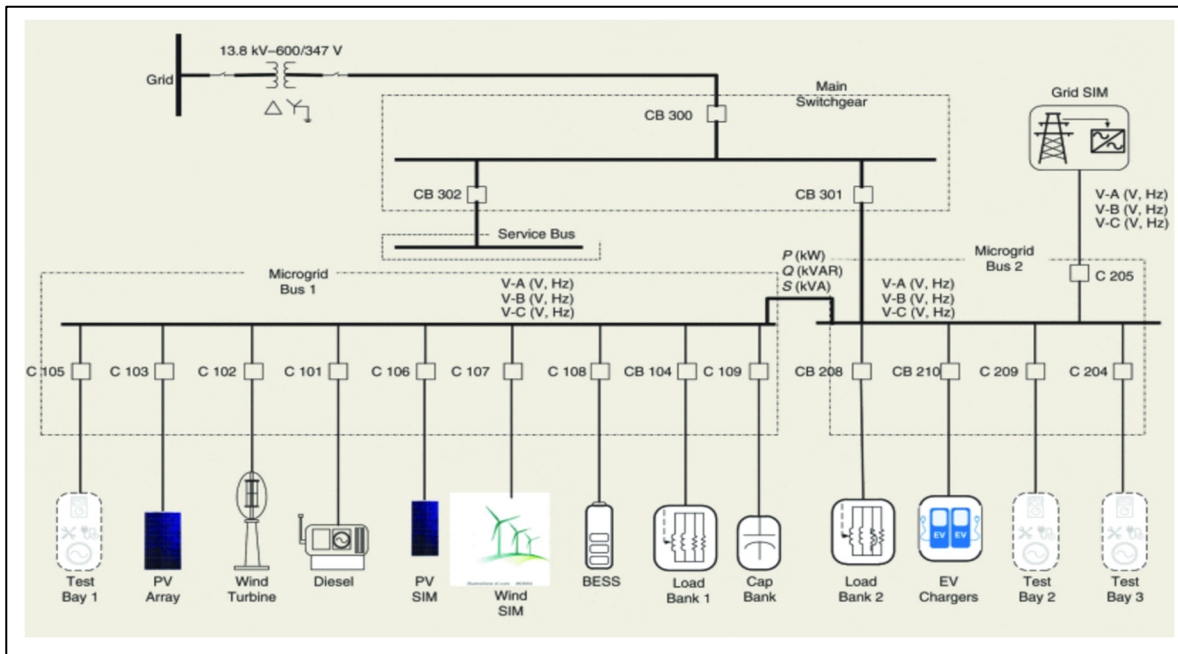


Figure 1.8 The CANREL One-line Diagram. SIM: Simulator; CAP: Capacitor; EV: Electric Vehicle

Taken from E. Nasr-Azadani (2020)

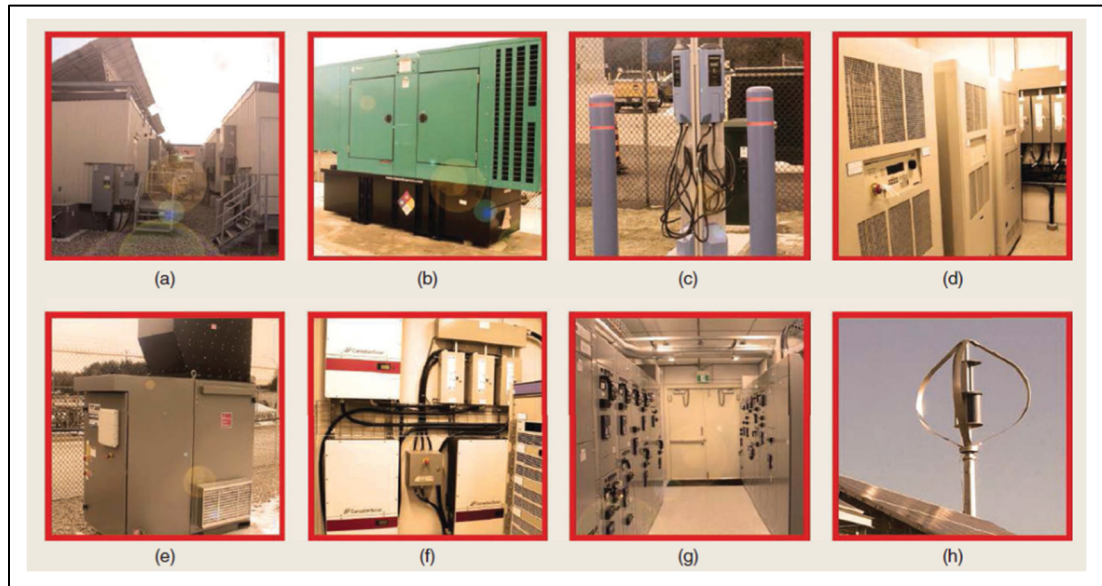


Figure 1.9 The CANREL system components: the (a) containerized design solution, (b) diesel generator, (c) EV chargers, (d) grid SIM, (e) programmable load banks,

(f) PV SIM, (g) two microgrid bus

Taken from E. Nasr-Azadani (2020)

Table 1.2 A summary of the CANREL components

Taken from E. Nasr-Azadani (2020)

Components	Description	Power Rating
Grid SIM	Bidirectional inverter-based grid SIM to simulate grid frequency and voltage abnormalities	270 kVA
Wind SIM	Bidirectional inverter-based wind SIM that dynamically simulates the active and reactive power output of a wind turbine	100 kW
Actual wind turbine	Vertical-axis wind-turbine generator to generate real wind-generation data	3 kW
PV array system SIM	A software-controlled dc source that simulates I-V and P-V curves of a PV array system	90 kW
PV inverter	String PV inverters with a maximum power point tracking control and external PQ curtailment control used for PV SIM	100 kW
Actual rooftop PV system	40 Canadian Solar PV panels CS6P-260P that cover the roof of two front rooms; equipped with a PV inverter	10 kW
ESS	Lithium-ion battery pack (equipped with a battery management system) and a bidirectional inverter	200 kW/200 kWh
Diesel generator	Diesel generator that can be operated in isochronous mode, droop mode, and PQ mode with a remote control	90 kW
Programmable load banks	Two programmable load banks with resistive and inductive load elements, which can be controlled remotely	200 kW
Capacitor bank	Three-phase capacitor bank to simulate capacitive inrush current scenarios and provide reactive power	30 kVar
EV charger	EV chargers serving as a test load to assess microgrid resources' response to electric-vehicle loads	7.2 kW
MCS	Hierarchical MCS to control and optimize microgrid operations	—

A hierarchical-based control approach is suggested and presented by CANREL for balancing the stable power and goal-oriented EMSs in both islanded and grid-tied modes (E. Nasr-Azadani, 2020). Multiple commercial communication protocols have been used in this microgrid control system (MCS), such as Modbus TCP/IP, Modbus RS485, analog input-output, and the human-machine interface (HMI) serves as a gateway to associate each controllable unit, where the primary control acts on. Therefore, the voltage and frequency control of the diesel generator, maximum power point tracking (MPPT) control of the PV inverters, and the voltage-frequency droop control of the BESS are all controlled at this level. The microgrid test bench also has a secondary control called a microgrid forming control system. It performs the monitoring of all parameters required and regulates their set points to maintain the voltage and frequency within the acceptable range. The tertiary control is reserved for setting up system limitations and constraints, which is independent of other level controls. When the MCS is not activated, the operator can manually operate each device in the corresponding mode and ensure the stability of the entire system.

CANREL has conducted several tests based on the percentage of renewable penetration and the operation modes. In low renewable penetration with no significant step changes in the load and PV, the diesel generator can regulate the frequency and voltage within the permitted range. However, a major step-change in the load might cause system instability. In high renewable penetration including PV simulator, wind simulation, and BESS, the frequency is successfully kept within the acceptable range of IEEE Standard 1547.4. In one-hundred percent renewable penetration, the BESS and the secondary controller regulate the system voltage and frequency inside the suitable range. Based on the experimental results, it can be concluded that the more renewable energy resources (RESs) are involved, the more unstable the system will be, which is reflected in the excessive fluctuation of the system frequency and the increase in the complexity of the voltage regulation. Overall, from the perspective of the composition and structure of the MG test bench, CANREL provides a strong experimental basis and guidance for designing and implementing other experimental platforms of the same types, such as equipment selection and installation structure.

Compared to the aforementioned CANREL testbed, the laboratory-level experimental platform is much smaller in scale, and the focus of validation is also different. As mentioned in Jabbar, 2019, considering the special requirements in building a MG testbed in Middle Eastern countries such as Qatar, which has limited access to certain technology and less flexibility in changing existing grid topologies, a 50kW MG testbed was built with multiple programmable sources and loads, grid emulator, and LCL grid filters, as shown in Figure 1.10.

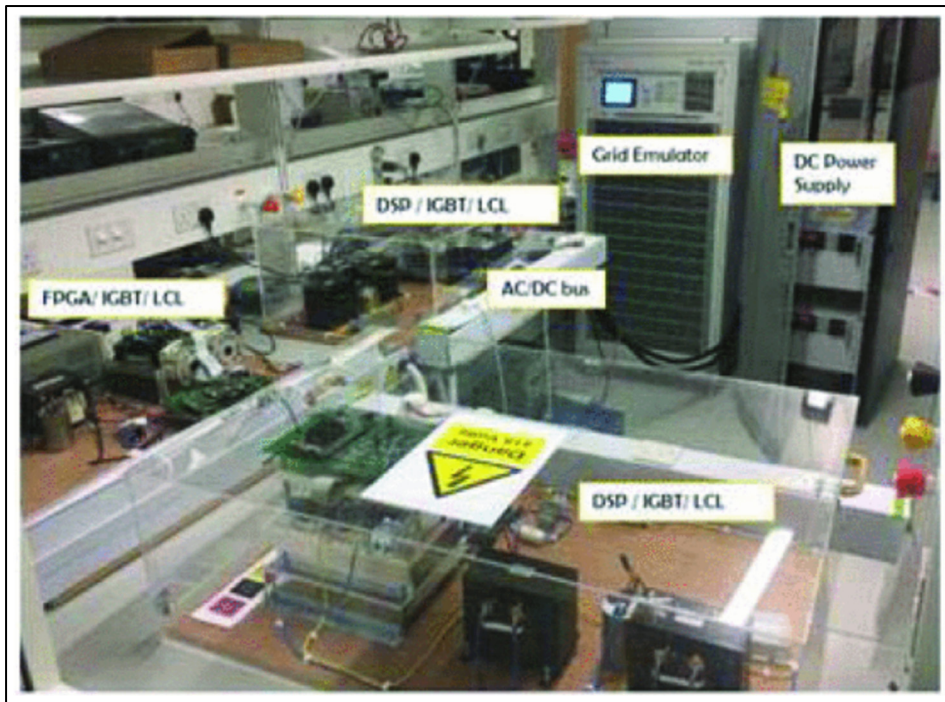


Figure 1.10 Microgrid Testbed QEERI (Hardware)

Taken from A. A. Jabbar (2019)

As presented in Figures 1.11, and Table 1.3, two 25kW/800V Magna Power programmable DC sources emulate non-linear PV energy feeding to a 50kW Chroma DC load, and the grid emulator powers up a 4.5kW Chroma AC load. The LCL grid filters, used for synchronizing the PV emulator to the AC grid, have ratings of 0.5mH, 45uF, and 0.5mH, respectively, and the cutting frequency is set to 1.5kHz by using the equation in (1) (A. A. Jabbar, 2019).

$$f = \frac{1}{2\pi} \sqrt{\frac{L_1 + L_2}{cL_2L_1}} \quad (1.1)$$

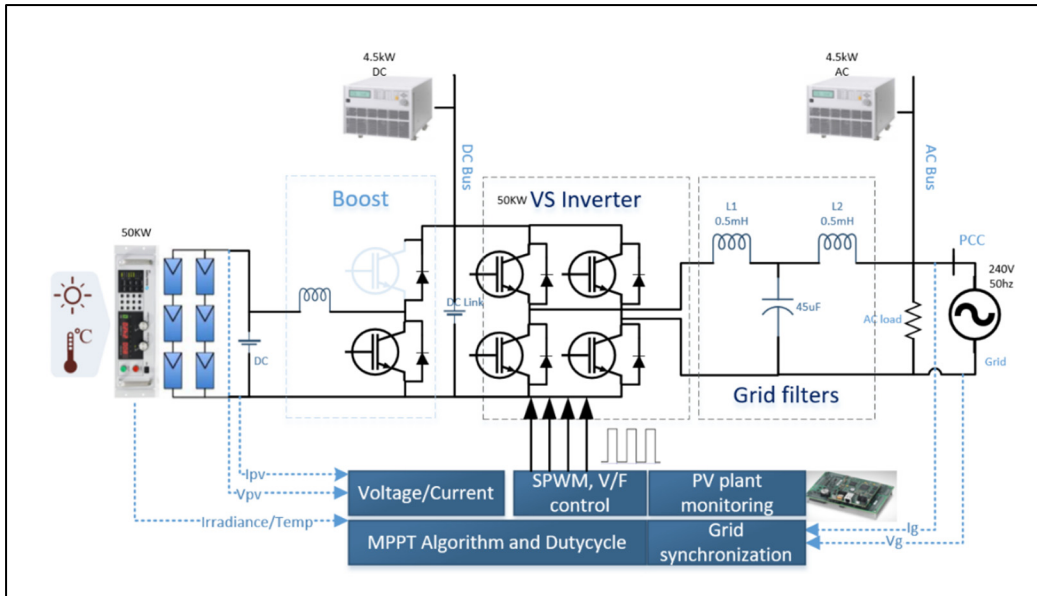


Figure 1.11 Hybrid AC/DC Microgrid Testbed Components

Taken from A. A. Jabbar (2019)

Table 1.3 MICROGRID Testbed Specifications

Taken from A. A. Jabbar (2019)

Component	Parameter
DC Programmable Power Supply 1	25kW 800V dc, 20A
DC Programmable Power Supply 2	25kW 800V dc, 20A
Grid Simulator	4.5kW
Programmable Load 1	4.5kW
Programmable Load 2	4.5kW
Programmable Load 3	50kW
IGBT Stack	FPGA Xilinx
Embedded Controllers	LCL (0.5mH, 45uF, 0.5mH)
Grid Filters	Switching Frequency 15kHz

The hierarchical control system and observation system are both realized in a graphical development environment – LabVIEW. The system is integrated with the real-time data acquisition (DAQ), Virtual Instrument Software Architecture (NI-VISA) platform, and Standard Commands for Programmable Instruments (SCPI). Similar to the CANREL testbed, GPIB, RS232, LAN, TCP/IP, and other communication protocols are utilized to remotely manage MG components.

Three control levels have been considered: the central level, local level, and low level. The central level control is not only able to collect accurate device information from the other two levels but also able to send system-level instructions such as voltage and current set points to secure the stability of MG. Different from the testbed introduced earlier, the secondary level control provides access to the PV emulator and load emulator with hardware-in-the-loop (HIL) configuration, as well as a 50-point IV profile. These emulators are modeled in LabVIEW as well, which is enable users to reach the required voltage and current by manipulating the connection methods of the PV cells targeted to purchase. Real-time measurements were performed by operating the programmable load under Constant Resistance (CR) mode from 400 ohms to 60 ohms with a constant voltage of 168V (A. A. Jabbar, 2019). The insulated Gate Bipolar Transistor (IGBT) is selected to build the grid filter, and the field-programmable gate arrays (FPGA) are used in the low-level control to construct the pulse-width modulation (PWM) and the maximum power point tracking (MPPT). Due to the fluctuation of temperature and solar radiation intensity caused by weather conditions, the Perturb and Observe (P&O) algorithm is described to examine the nonlinearity of the PV system. From simulation results with certain scenarios, the voltage setpoint change related to MPPT, which is controlled by the modulation index, has been regulated in an interval of 50ms with a step size of 40ms. Therefore, the P&O algorithm is effective.

This testbed mainly applies the HIL topology to simplify the requirements and reduce the investment in hardware devices. Despite the fact that this approach has not yet been adapted on the test bench to be introduced in this thesis at this time, the implementation of the control system by LabVIEW is instructive and valuable. The installation of the photovoltaic system

and MPPT is well underway, and generators will be deployed soon. Therefore, HIL will be helpful for further development.

Unlike the MG testbed in Qatar, A. N. Akpolat, 2021 presents a small-scale test system focusing on the study of BESS and EMS. As shown in Fig 1.12, Fig 1.13, and table 1.4, this testbed is structured by RESs (battery bank), power electronic converters, a PV array, a wind turbine, a fuel cell unit, and loads. This article lists a mathematical model for each subsystem. For instant, the inputs of solar irradiance and temperature have an impact on PV generation in the solar energy conversion system, which has a rating power of 1kW composed of four PV panels of 250W. The current of the PV cell is calculated with Kirchhoff's laws (1.2), and the five unknown parameters can be estimated from the values indicated in the data sheet and design requirements.

$$I_{CELL} = I_{PH} - I_0 \left(e^{\frac{V_{CELL} + I_{CELL} R_S}{nV_t}} - 1 \right) - \frac{V_{CELL} + I_{CELL} R_S}{R_{SH}} \quad (1.2)$$



Figure 1.12 Experimental Set Up of Laboratory Scale of MG System

Taken from A. N. Akpolat (2021)

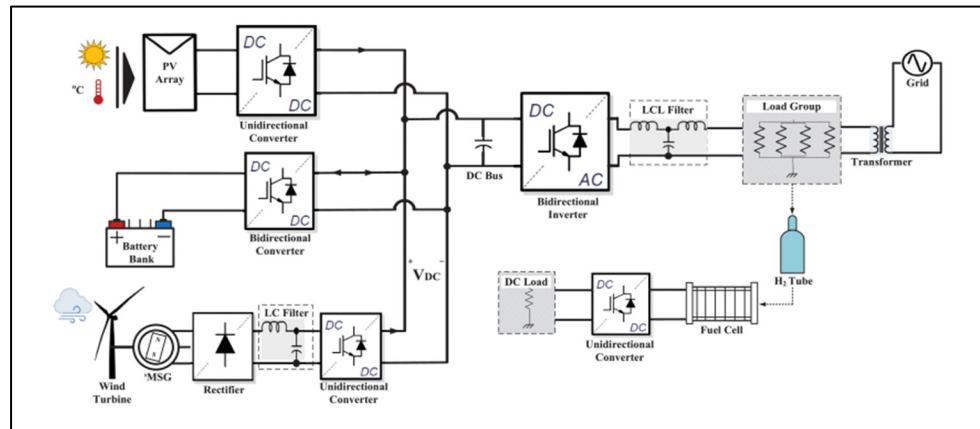


Figure 1.13 Description of Proposed Education Laboratory-Scale Microgrid
 Taken from A. N. Akpolat (2021)

Table 1.4 Components of Energy Conversion Systems
 Taken from A. N. Akpolat (2021)

PV Array	
Rated Maximum Power- P_m (kW)	1
Maximum Power Current- I_{mp} (A)	32.68
Maximum Power Voltage- V_{mp} (V)	30.6
Short Circuit Current- I_{sc} (A)	34.83
Open Circuit Voltage- V_{oc} (V)	36.3
Module Efficiency- η (%)	15.40
Wind Turbine	
Turbine Type	Horizontal Axis
Rotor Diameter (m)	1.17
Blades	(3) Injection moulded comp.
Generator Type	Permanent magnet sync.
Start-up Wind Speed (m/s)	3.58
Survival Wind Speed (m/s)	49.2
Output Voltage (V)	24
Rated Power (W)	400
Battery Bank	
Battery Type	Lead-Acid
Nominal Voltage (V)	12
Nominal Capacity (Ah)	200
Internal Resistance ($m\Omega$)	3.4
Cut-off Voltage (V)	9
Fully Charge Voltage (V)	13.9
Fuel Cell	
Nominal Power (kW)	1.2
Rated Current (A)	65
Operating Voltage (V_{DC})	20-35
Number of Cells	36
Efficiency	46
Max H_2 consumption (sl/min)	15

To accomplish a self-governing MG, a Lead Acid battery bank is chosen as the energy storage unit. Taking into account the recommended depth of discharge (DoD), the state of charge (SoC) is defined by equation (1.3):

$$\text{SoC} = 1 - \text{DoD} \quad (1.3)$$

Since the DoD of Lead Acid type battery is 50% (A. N. Akpolat, 2021), the SoC is operated in the range of 50% to 100%, which means that the battery bank needs to be charged when the SoC has dropped by half. The capacity of the battery bank is 14.4 kWh when it is fully charged. The formula for calculating battery power is as follows

$$\text{SoC} = \text{SoC}_i - \frac{1}{Q} \int_{t_2}^{t_1} i_{\text{Batt}} dt \quad (1.4)$$

Its control system also adopts the P&O MPPT algorithm with a switching frequency of 10 kHz in the PV inverter. Nonetheless, an IP controller is used to accommodate the voltage set point. According to the different operation modes, the power in the system can be studied as in (1.5):

$$P_{\text{NET}} = \begin{cases} P_{\text{BAT}}, & \text{if } \text{SoC}_{\text{min}} \leq \text{SoC} \leq \text{SoC}_{\text{max}} \text{ (Battery Mode ON)} \\ P_{\text{LOAD}}, & \text{if } \text{SoC} \leq \text{SoC}_{\text{min}} \text{ (Grid Mode ON)} \end{cases} \quad (1.4)$$

To validate the EMS algorithm and control strategies, a case study is analyzed by both simulation and RT experiments. As specified in Table 1-4, the PV power is 1kW and the wind power is 400W, where the total power is corresponding to the capacity of the battery bank. The test is performed for 30 minutes and the measurements are extracted every 30 seconds. Comparing the simulation and experimental results, it can be seen that the RT test results strongly support the simulation findings, despite the presence of disturbing harmonics. During the test run, the SoC of the battery bank didn't fall below the minimum requirement, and the frequency of AC load remained in the acceptable range. The interest of EMS analysis is to protect the battery bank as much as possible and extend its lifetime.

Espina (2020) presents a 24kW AC/DC hybrid MG test bench that is located at the MG Control Laboratory of the University of Chile. The test bench is comprised of three AC generation emulators and six DC distributed generation emulators. A series of operability tests are carried out to validate the control strategies and observe the behaviors and identify issues with this experimental AC/DC-MG. The specification of the test bench is listed in Table 1.5.

Table 1.5 Experimental AC/DC-MG, General Parameters
Taken from Espina (2020)

Description	DC	AC	IC
# of <i>DGs</i>	6	3	1
Nom. Voltage (V)	50 – 200	50 – 220*	-
MG's freq. (Hz)	-	50 – 60	-
Nom. Power ($\frac{\text{kW}}{\text{DG}}$)	2.5	3.0	3.0
Switch. freq. (kHz)	16		
Comm. rate (Hz)	10 – 16000		
* <i>Phase-to-neutral RMS voltage</i>			

Triphase controlled power inverter units, fabricated by National Instruments, are introduced as the DGs' emulators, which have a back-to-back structure and connect to the utility grid by an isolated transformer. The control of Triphase units is accomplished by real-time targets (RTT) with a Unix-based operating system, which is used in the environment of MATLAB Simulink. The communication between the control center and equipment is done using a local area network (LAN) (Espina, 2020). This test bench is also implemented HIL topology, which simulates the RERs and loads profiles to detect any disruption in the communication of controllers and any losses in the connection of DGs.

On the AC side, the Triphase PM15F120C with a rated power of 11.5kW contains two inverters to emulate two independent generation units (inverters 1 and 2 indicated in Figure 1.14), and the PM5F60R with a rated power of 5.5kW represents a three phases generation unit (inverter 3 shown in Figure 1.14). According to the selected operation mode, all units can be configured

as an LC, LCC, LCL, or LCLC filter (Espina, 2020). A functional experimental test has been performed to validate the economic dispatch and congestion management.

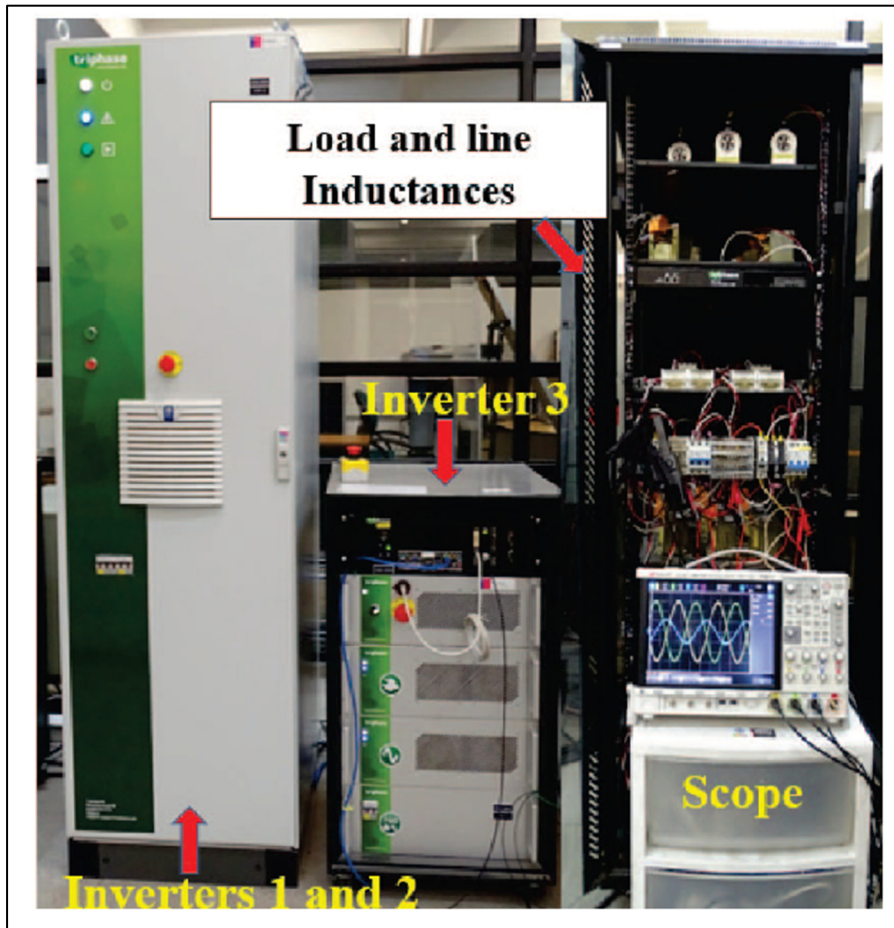


Figure 1.14 Example of a 3-phase AC MG Implemented
In the Laboratory for Research Purpose
Taken from Espina (2020)

On the DC-MG side, Triphase PM15160F06 presents six independent DC generators with a rating power of 30kW. It has the same back-to-back structure as the previously mentioned AC-MG inverters. As shown in Figure 1.15, PM5F42R with a rating power of 5.5kW is introduced as the interlink converter between the AC-MG and the DC-MG.

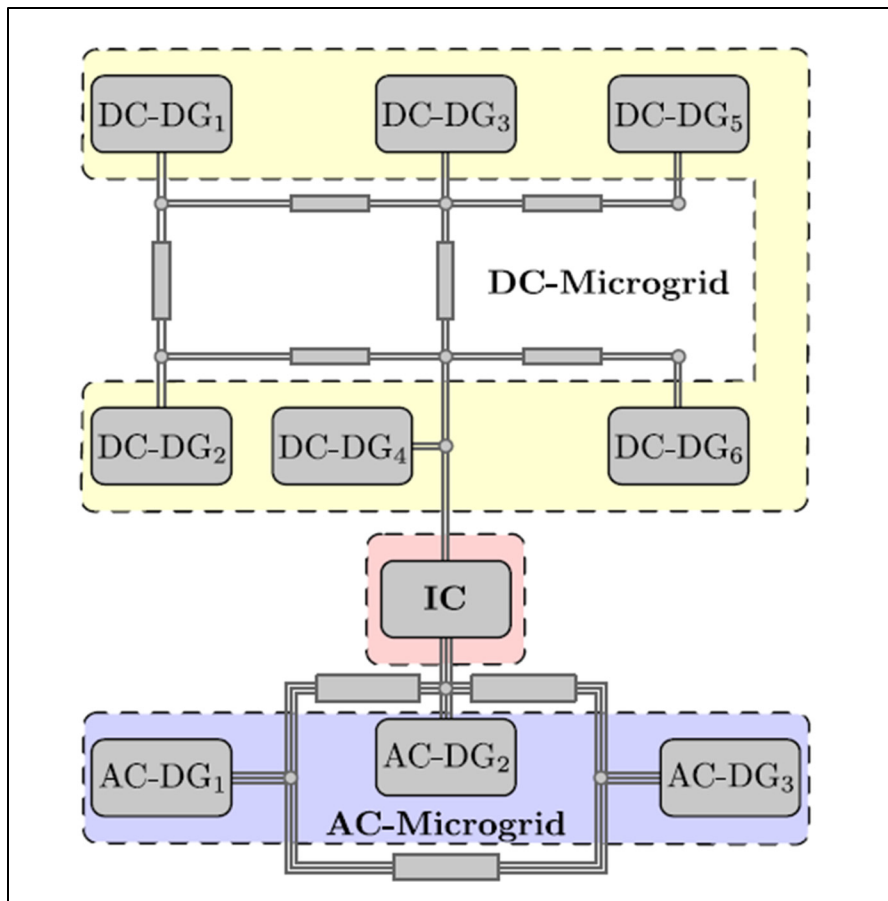


Figure 1.15 General Topology of Implemented Hybrid MG
Taken from Espina (2020)

The central control platform is implemented in the Matlab/Simulink graphical programming interface. The application of using a variety of communication protocols makes the communication between the system devices flexible, for instance, motor drivers and programmable loads acclimate Modbus protocols by connecting to the CAN bus. In the process of multiple tests, communication issues caused by various protocols have gradually emerged, such as intermittent communication failures, communication delays on different devices, and communication congestion during reading and writing data operations. To solve the latency problem, a delay is introduced in each communication path.

After conducting individual operational tests in AC-MG and DC-MG, optimal dispatch and congestion management tests are performed using three local loads and three power lines. The distributed control strategy successfully regulates the system frequency within an acceptable range and it is also able to rapidly eliminate the congestion, restoring line current from overload level within three mins (Espina, 2020). The test results confirm the economic prediction strategy, where DG2 generates more real power than DG1 and DG2 since its capacity cost is much lower.

In general, the main advantage of this experimental platform lies in the design and implementation of the control system. Compared with C/C++ programming languages, the choice of graphical programming interface of MATLAB/Simulink greatly reduces the complexity of the program and also facilitates collecting measurements.

1.4 Motivation & Research Objectives

The internal structure of the MG is complex and its control implementation is cumbersome. As a very important research direction in electrical engineering, MG technology faces certain difficulties in theoretical development and experimental test bench setup, such as the development of programming languages, the update of the software operating environments, advancements in equipment communication protocols, and the initial capital investment requirements. The design and simulation of the ÉTS AC-MG introduced in this thesis have advanced through the efforts of several graduate students and Ph.D. students, and there is an urgent need to build an experimental platform to verify the functionality of the entire system. The construction of this test platform also provides future students with an opportunity to intuitively understand the composition of MG, its operation mode, the optimization algorithm, and economic prediction control.

This thesis presents the design of a LabVIEW-based MG economic operation experimental test bench, which uses a flexible load control strategy combined with an improved neural network algorithm. LabVIEW is utilized as the host computer software to write the display interface and the operation module of each device, while Python is used to implement the

optimized algorithm and equipment profiles. It is worth mentioning that the original prototype and simulation module of this MG was constructed by Nicolas Mary (Mary, 2016) through MATLAB/Simulink, and complementary by Yohann Geli (Geli, 2021). The test bench has two working modes: Simulation and RT with equipment. In the simulation model, the forecast data such as perfect prediction can be written into the Python file, which is then read by the host computer and run-in sequence. In the RT model, the parameters and measurements collected by devices have been optimized in LabVIEW and become new commands that are returned to the devices. The operation curve is displayed in the monitoring interface and the data are saved into the SQLite database simultaneously.

1.5 Concluding Remarks

This chapter summarizes the background of MG and the research status of the MG experimental test bench. It also introduces the ÉTS experimental test bench.

CHAPTER 2

OVERALL STRUCTURE AND HARDWARE ARCHITECTURE OF THE MICROGRID TEST BENCH

2.1 Introduction

According to various standards, microgrids can be classified into many categories. For example, based on different application objectives, it can be categorized as campus MG, military MG, household MG, commercial MG, and industrial MG. In light of MG scope, it can be considered as small-scale MG, medium-scale MG, and large-scale MG. Additionally, taking account of the utilisation, it can be classified as resilience-oriented MG, bills and losses reduction MG. Moreover, based on voltage and current types, it also can be identified into AC MG, DC MG, and hybrid MG.

Furthermore, MGs can operate in two ways: off-grid and grid-connected. Off-grid MGs are capable of accomplishing energy self-regulation, while grid-connected MGs work via the process of self-generating and self-consuming, and any surplus can be adjusted by the grid. The experimental grid-connected AC MG platform studied in this thesis is modeled on ÉTS campus focusing on curtailing the invoices and is located in a laboratory in building A, with only AC loads.

Through the control system block diagram and overall structure block diagram, this chapter introduces the design framework and hardware selection of the AC-MG experimental test bench. Specifically, it covers controllers, inverters, energy storage equipment, programmable loads, protection equipment, communication units, and more. Besides, this chapter also describes the controller operation process and the hardware communication protocol settings.

2.2 Overall Structure of the Test Bench

Figure 2.1 shows the overall structure of the MG laboratory. This MG experimental economic operation test bench is built on the basis of the scientific and technological research project of

the Power Electronics and Industrial Control Research Group (GRÉPCI) of ÉTS. Currently, the laboratory is equipped with a 15.2kWh Lithium Ferro Phosphate (LFP) battery bank, a 6.8kW energy storage bidirectional converter system, a 13.5kW AC/DC Electronic Load pack, a 60A/150V MPPT, and a power and energy meter. Since the photovoltaic system hasn't been installed, the MPPT will be used in the near future.

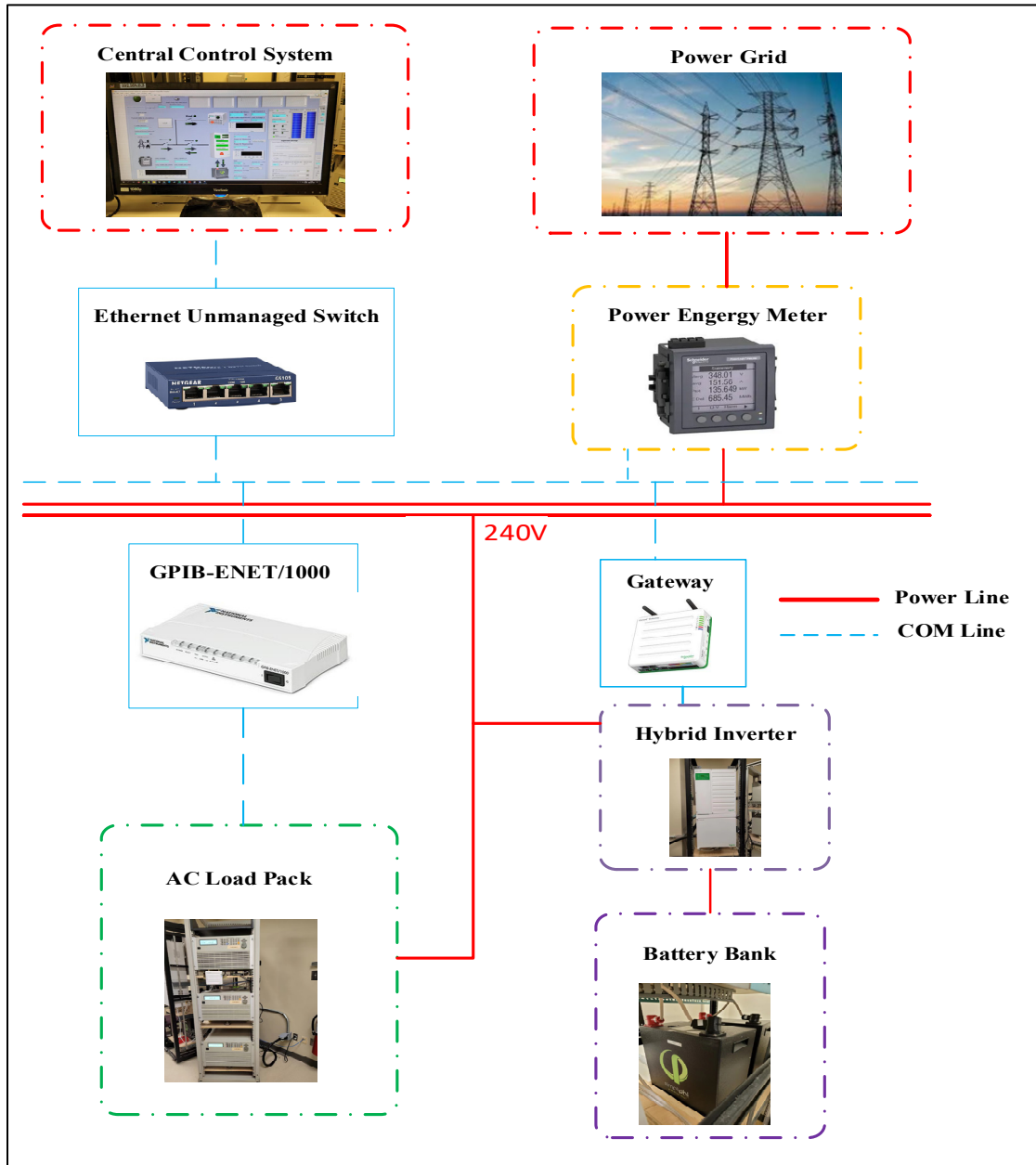


Figure 2.1 Overall Structure Diagram of MG in Laboratory of ÉTS

Regarding distribution lines, for the sake of engineering installation convenience and the protection of the whole circuit, one end of the line is directly connected to the 240V campus AC bus, while the other end is connected to MG equipment located in the laboratory. These two ends are merged through a control cabinet containing an industrial level heavy duty switch protected by two 100A fuses. There is also an electric power and energy meter on the left side of this cabinet, which can monitor the frequency, current, voltage, energy, harmonics, and wages of grid input.

The main functions of MG of monitoring and control system are:

- 1) Real-time monitoring: the system is capable of collecting various power parameter measurements from the devices with very short delay. Figure 2.2 depicts the communication topology of MG.
- 2) Intelligent analysis and decision-making: by analyzing the power consumption of the load during the peak and valley period, the energy storage system can be charged and discharged in a predicted manner, thereby adjusting and optimizing the power set point. Figure 2.3 shows the functional architecture diagram of the microgrid monitoring and control system.

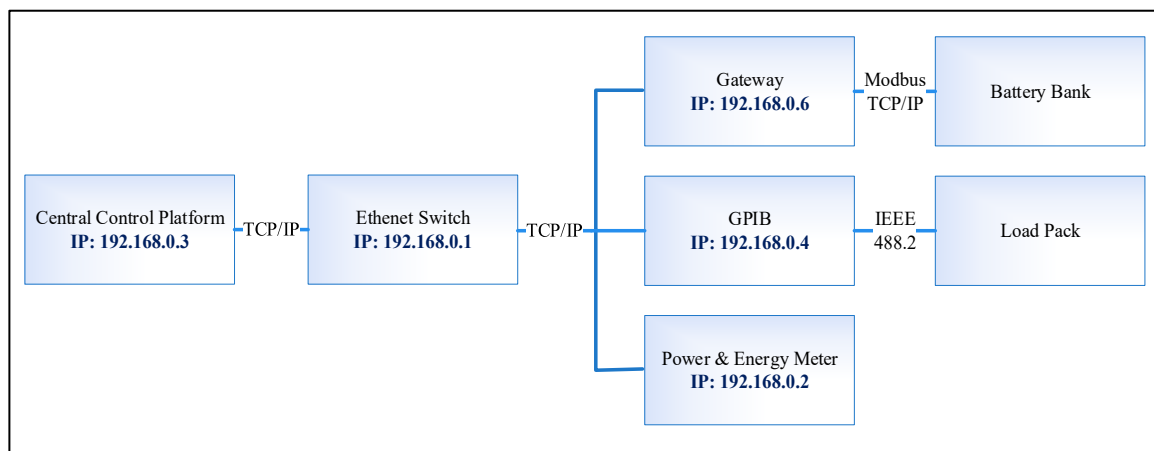


Figure 2.2 Communication Topology Diagram

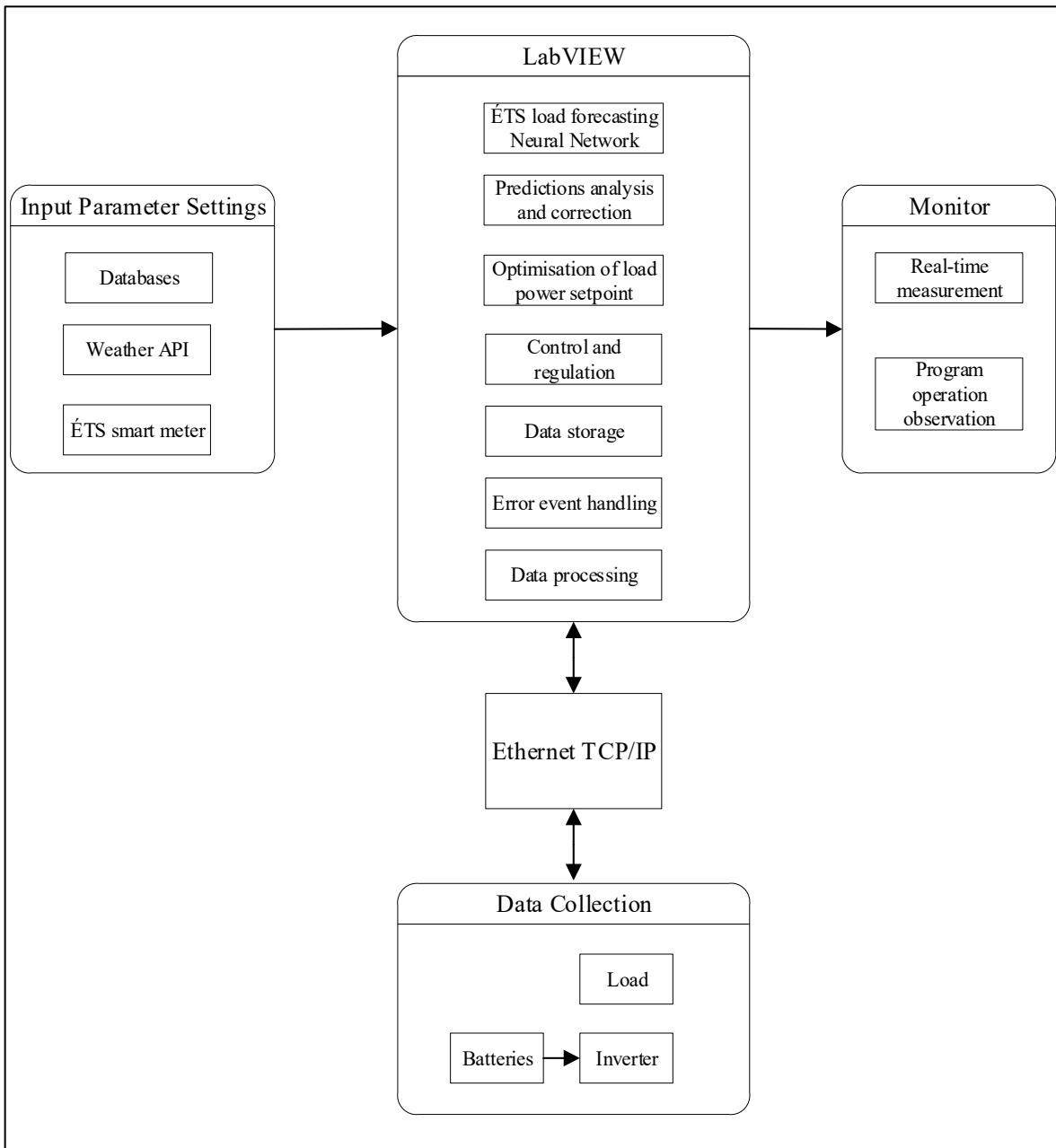


Figure 2.3 Functional Architecture Diagram

2.3 Hardware Implementation

The hardware of the MG test bench includes a grid-connected interface cabinet, power meter, load, energy storage equipment, inverter and protection equipment. Hardware selection should not only consider whether the performance, work reliability, flexibility, developability and wiring convenience can meet the work requirements, but also consider the cost and safety issues.

2.3.1 MG Gateway Cabinet

MG gateway cabinet is also known as a grid-connected interface cabinet, as shown in Figure 2.4. This cabinet, with model SIEMENS ID363, is an Industrial Duty Single Throw Disconnect Safety Switch and is installed at the grid-connected point between the MG and the low-voltage power distribution system of the large grid. It has a voltage rating of 600V and a current rating of 100A.

This switch has two main functions. For the test bench that has been installed on the site, the main research direction at this stage is to reduce the electricity costs by accomplishing load peak shaving optimisation. Therefore, the test bench will always operate in a grid-connected state, and this MG gateway cabinet is used to prevent laboratory personnel from short hazard. In the near future, this MG test bench will be equipped with rooftop solar panels, photovoltaic emulator, and critical loads, and the research direction may be extended to islanded operation. this cabinet can be considered as a quick switch for on-grid and off-grid scenarios, analyzing power outages or grid resilience.

For a 240VAC MG test bench, the setting version with two poles, two fuses, and solid neutral has been selected. This switch, which fulfills Canadian Securities Administrators (CSA) Standard C22.2 No.4, has a steel enclosure that strictly adheres to Standard 250 type 1 of National Electrical Manufacturers Association (NEMA). Furthermore, it is equipped two CDS100 fuses, which are certified under Class H, type D of CSA.



Figure 2.4 MG Gateway Cabinet

2.3.2 Power Meter Selection and Setting

Before the establishment of the MG test bench studied in this thesis, there was already an existing test platform called Testbed No.1. This Schneider PM5340 power and energy meter (ANNEX I) was originally used in this testbed. However, due to the ongoing construction of the laboratory, the testbed 1 project is currently on hold. In order to quickly put the test bench studied in this thesis (also referred to as test bench 2) into and at the same time to reduce the initial investment to the greatest extent, it is a wise choice to adapt the device from testbed 1.

As shown in the Figure 2.5, PM5340 Power meter has a 128mm x 128mm Monochrome Graphics LCD display with four buttons, which allow the operator to perform local control level operations such as manual intervention. At this research stage, this meter is primarily used to measure the grid voltage, grid current, grid power consumption, frequency and power factor. In the next phase of MG study, its multi-tariff function as well as the graphical representation of harmonics may be enabled.



Figure 2.5 Schneider PM5340 Power and Energy Meter

2.3.3 Load Selection and Setting

In the testbed No.1, there were six Chroma 63480 programmable AC/DC loads. However, due to the limitation of the laboratory size for Test bench 2, if all six loads are activated at the same time, the ventilation in the laboratory would not function quickly enough, and the room temperature would rise. This may cause the loads stop working due to their over temperature protection. Therefore, Test bench 2 has a load pack of three Chroma loads (Figure 2.6).

Chroma 63804 has a rated power of 4.5kW and 500V peak voltage, and more specification are shown in table 2.1. Unlike the separate control method using in Testbed No.1, Test bench 2 adopts a parallel connection with RJ45 communication cables. This load pack is set as one master and two slaves. The master load is connected to GPIB-ENET controller, which means that the host computer only needs to communicate with the master load to complete the simultaneous control of the three loads.



Figure 2.6 Chroma Programmable AC/DC Electronic Load

Table 2.1 Chroma 63804 Specification

Taken from Chroma 63800 Series Operation & Programming Manual (2020)

Model	63802	63803	63804
Power	1,800W	3,600W	4,500W
Current	0 ~ 18A _{rms} (54 A _{peak})	0 ~ 36A _{rms} (108 A _{peak})	0 ~ 45A _{rms} (135 A _{peak})
Voltage	50 ~ 350V _{rms} (500 V _{peak})	50 ~ 350V _{rms} (500 V _{peak})	50 ~ 350V _{rms} (500 V _{peak})
Frequency	45 ~ 440Hz, DC	45 ~ 440Hz, DC	45 ~ 440Hz, DC
AC Section			
Constant Current Mode			
Range	0 ~ 18A _{rms} , Programmable	0 ~ 36A _{rms} , Programmable	0 ~ 45A _{rms} , Programmable
Accuracy ¹	0.1% + 0.2%F.S.	0.1% + 0.2%F.S.	0.1% + 0.2%F.S.
Resolution	2mA	5mA	5mA
Constant Resistance Mode			
Range	2.77Ω ~ 2.5kΩ, Programmable	1.39Ω ~ 2.5kΩ, Programmable	1.11Ω ~ 2.5kΩ, Programmable
Accuracy	0.5% + 0.5%F.S.	0.5% + 0.5%F.S.	0.5% + 0.5%F.S.
Resolution ⁴	20μS	50μS	50μS
Constant Power Mode			
Range	1,800W, Programmable	3,600W, Programmable	4,500W, Programmable
Accuracy	0.2% + 0.3%F.S.	0.2% + 0.3%F.S.	0.2% + 0.3%F.S.
Resolution	0.375W	1.125W	1.125W
Crest Factor (under CC, CP modes)			
Range ²	1.414 ~ 5.0, Programmable	1.414 ~ 5.0, Programmable	1.414 ~ 5.0, Programmable
Accuracy	(0.5% / I _{rms}) + 1% F.S.	(0.5% / I _{rms}) + 1% F.S.	(0.5% / I _{rms}) + 1% F.S.
Resolution	0.005	0.005	0.005
Power Factor			
Range	0 ~ 1 lead or lag, Programmable	0 ~ 1 lead or lag, Programmable	0 ~ 1 lead or lag, Programmable
Accuracy	1%F.S.	1%F.S.	1%F.S.
Resolution	0.001	0.001	0.001
Rectified Load Mode			
Operating Frequency	45Hz ~ 70Hz		
RLC mode	Parameter: I _p (max), R _s , L _s , C, R _L		
Constant Power Mode	Parameter: I _p (max), Power setting = 200W ~ 1,800W, PF = 0.4 ~ 0.75	Parameter: I _p (max), Power setting = 200W ~ 3,600W, PF = 0.4 ~ 0.75	Parameter: I _p (max), Power setting = 200W ~ 4,500W, PF = 0.4 ~ 0.75
Inrush Current Mode	Parameter: I _p (max), R _s , L _s , C, R _L , Phase		
	80A (peak current)	160A (peak current)	200A (peak current)
R _s Range	0 ~ 9.999Ω	0 ~ 9.999Ω	0 ~ 9.999Ω
L _s Range	0 ~ 9999μH	0 ~ 9999μH	0 ~ 9999μH
C Range	100 ~ 9999μF	100 ~ 9999μF	100 ~ 9999μF
R _L Range	2.77 ~ 9999.99Ω	1.39 ~ 9999.99Ω	1.11 ~ 9999.99Ω
DC Section			
Voltage Range	7.5V ~ 500V	7.5V ~ 500V	7.5V ~ 500V
Current Range	0A ~ 18A	0A ~ 36A	0A ~ 45A

2.3.4 Energy storage unit selection and setting

According to the requirements, this test bench is equipped with a 6.8kW energy storage inverter (ANNEX II), and four LFP batteries for energy storage with a storage capacity of 15.2 kWh (ANNEX III), as shown in Figure 2.8 and Figure 2.9.

For the convenience of installation and additional circuit protection, an XW mini power distribution panel with three 60A circuit breakers has been added to the inverter (Figure 2.7).

In this MG test bench, the energy storage device is connected to the grid through the inverter, which acts as an intermediate medium to facilitate the exchange of energy information between the grid and MG. The battery bank can also be used as a backup power source to critical loads. However, in this thesis, since there is no critical load presented, the battery is mainly used to reduce the electricity invoice by compensating for peak power consumption that occurs during the high electricity consumption on campus. The batteries are generally charged during periods of low consumption.

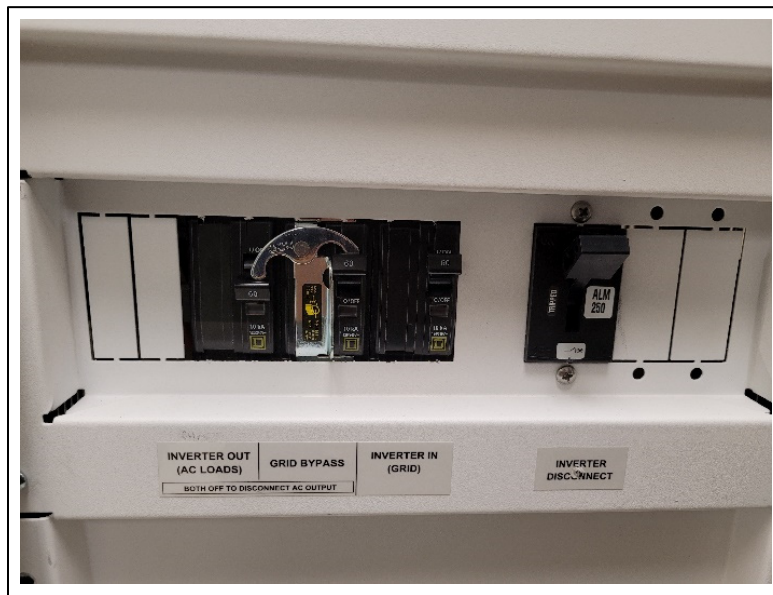


Figure 2.7 XW Mini Distribution Panel



Figure 2.8 Schneider XW Pro 6848 hybrid Inverter

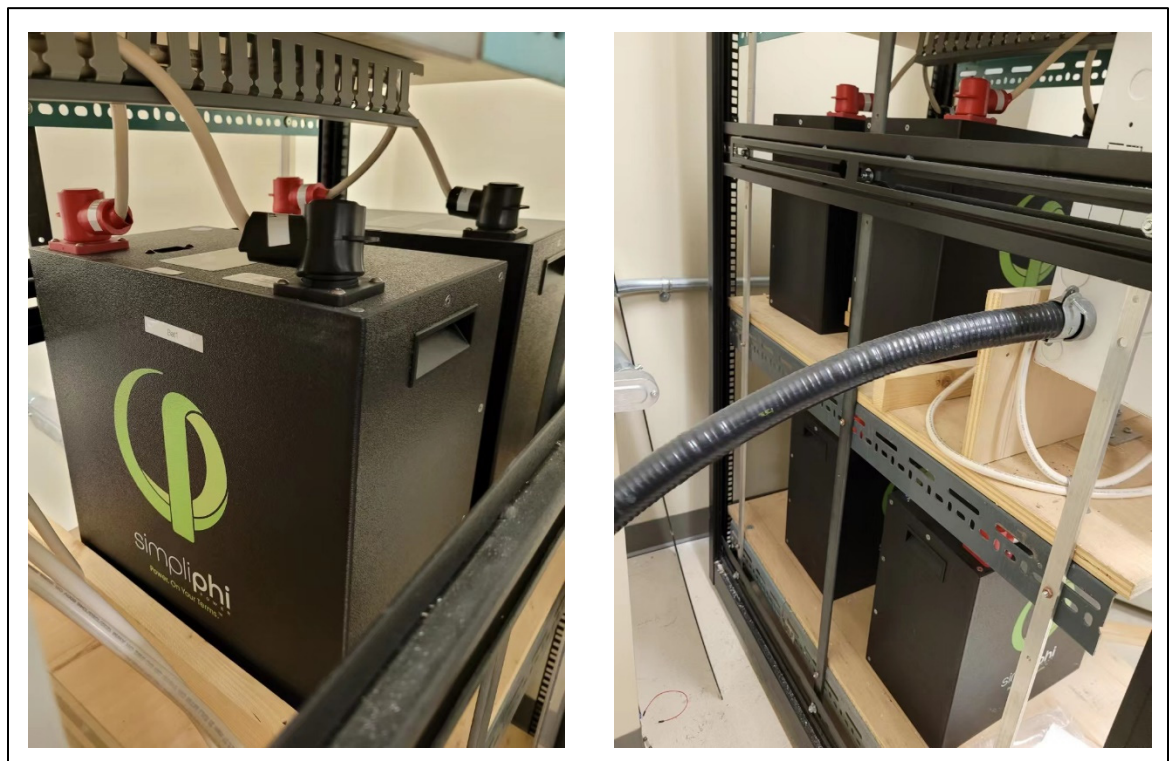


Figure 2.9 Simpliphi PHI 3.8 Battery

2.4 Communication Method and Communication Protocol Selection

2.4.1 Communication Method

Industrial control communication refers to the process of exchanging data between different devices through communication lines. The primary objective is to transfer data from one device to another in a specific way to achieve data transmission and sharing. In this thesis, the hardware devices are connected together through a local area network (LAN) to exchange data with the host computer. Parallel communication, serial communication and Ethernet communication are currently the most prevalent forms of industrial communication.

Schneider PM5340 power meter offers two communication methods such as RS-485 serial communication and Ethernet communication. RS485 is half-duplex word mode, and its communication signal is obtained by the difference between the transmission voltage values of the two lines, which are needed more cables for installation. However, the Ethernet communication connection only needs one CAT 5 cable, which greatly reduces the installation work and also save wiring costs.

Chroma 63804 programmable load provides two communication methods for remote control: GPIB and RS-232C. RS-232 is a typical serial communication with full-duplex work mode. It is similar to RS485, its signal is obtained from the voltage difference. However, it cannot connect to predefined LAN. Therefore, GPIB is the best choice. GPIB is parallel communication, which can transfer data to the receiving end in a bit-parallel arrangement at a time, and comparing with serial communication, its data transfer speed is faster. Although GPIB cannot directly access the LAN, the National Instrument GPIB-ENET/1000 controller enables GPIB devices connect to an Ethernet-based network such as LAN.

XW Pro hybrid inverter uses Xanbus network communication protocol. However, it provides a solution that applies Conext Gateway (ANNEX IV) between a network Xanbus enabled devices and Modbus devices on the network. The Gateway is also able to connect with a LAN.

2.4.2 Communication Protocol

The PM5340 power meter uses the Modbus TCP protocol to transmits data through its Ethernet communications connector, with the data transmission speeds are up to 100 Mbps.

The Conext Gateway follows IEEE2030.5 protocol, and the host computer can control and monitor the inverter by Modbus TCP protocol.

The Chroma 63804 load uses GPIB communication method and follows the IEEE 488.2 protocol. Through GPIB-ENET-1000, The host computer can program and troubleshoot the load pack by NI VISA application in LabVIEW.

2.5 Chapter Summary

This chapter provides a detailed introduction to the overall design idea, operating characteristics and functions of the MG test bench. It illustrates the structure of the test bench and the composition of the control system, and describes the energy storage system used for economic operation. Additionally, the Ethernet communication method and Modbus TCP protocol are selected to accomplish the programming and monitoring operation by the host computer.

CHAPTER 3

TEST BENCH SOFTWARE SYSTEM IMPROVEMENT

3.1 Real-Time System Implementation

The research work on microgrids requires the support of an efficient simulation system and experimental test bench. In this chapter, the control and monitoring system of this test bench has been improved by modeling and developing each hardware device in the MG.

Based on the needs of the subject and various considerations, such as the efforts made by other students and researchers before this test bench was built, the central control platform adopts LabVIEW as the development software. LabVIEW is a development software by National Instruments Corporation of the United States. It offers a wide range of hardware drivers, powerful graphics display capabilities, and an extensive library of advanced mathematical analysis tools. Its programming process is fast and convenient, and has rich extended functions that are oriented to data acquisition, data analysis, data display and data storage, etc. LabVIEW comprises a block diagram panel and a front panel with icon connectors. The LabVIEW program design is relatively simple, and virtual components can be easily modified or updated through programming. This allows developers to create new virtual experiment platform according to specific production or demonstration needs.

In addition to the functions mentioned above, LabVIEW can also call Python program files through components to obtain economic optimization algorithms, and realize the neural network prediction from the collected data.

The target MGCCP in this thesis is configured on a computer with Intel Xeon CPU 3.3GHz 64-bit processor, 16GB memory, 2 Ethernet ports, and it is running under Windows 10 operation system, shown in Figure 3.1. The Modbus module has benefit from a third party add-on, Modbus Master, which is free and well adapted to the by 64-bit version of LabVIEW 20, shown in Figure 3.2.

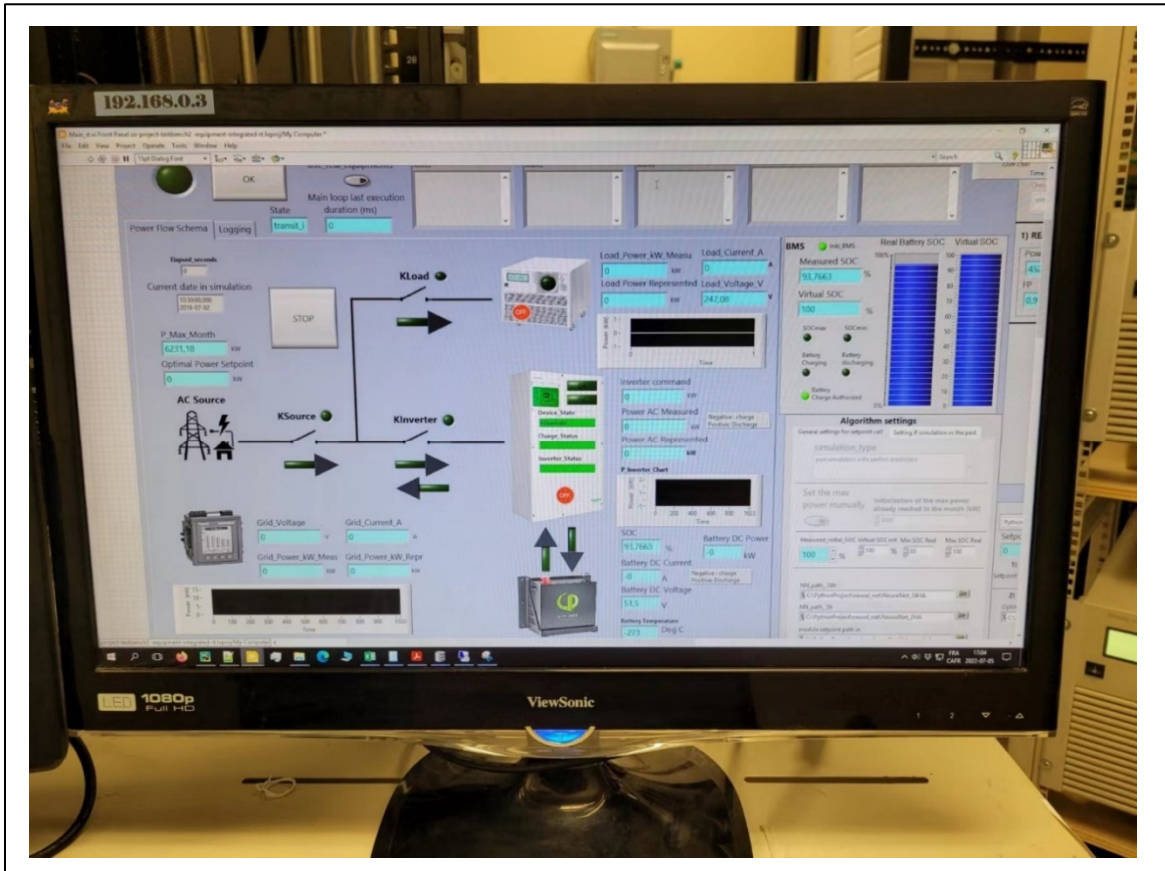


Figure 3.1 MGCCP Host Computer

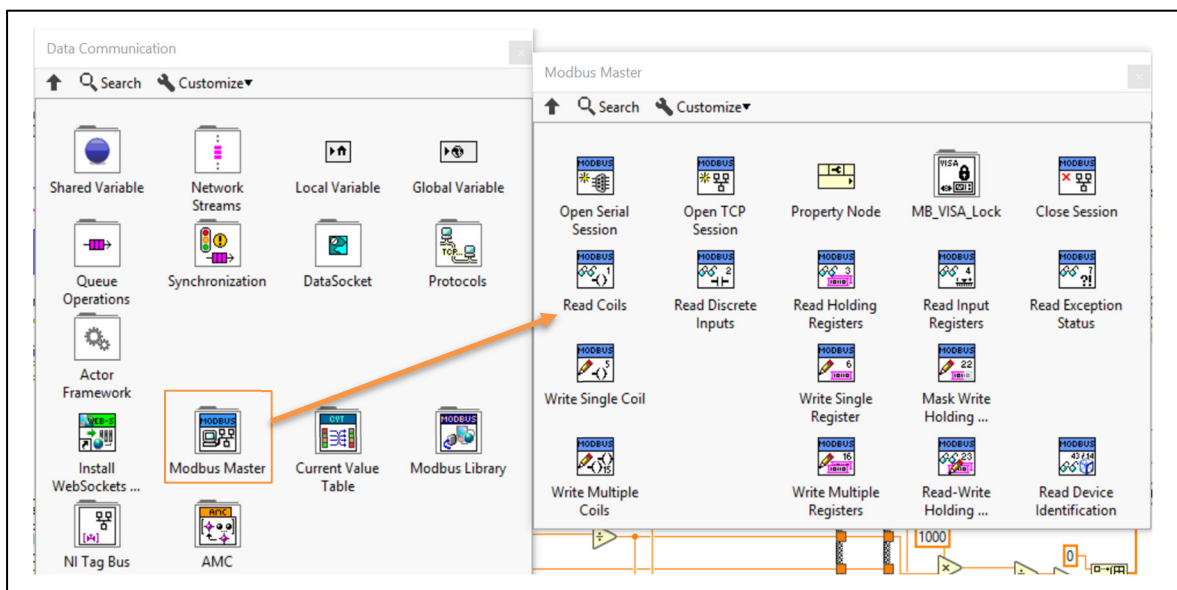


Figure 3.2 Modbus Master by Plasmionique Inc.

3.1.1 Inverter Control Module Development

Inverters are essential for connecting the battery bank with grid or generation units. As mentioned in the chapter 2.3.4, the Schneider XW Pro 6848 is selected, and its control module design starts from two aspects: data collection, which is referred to as “read” in programming, and the other hand, sending instructions to adjust parameters, which is often called “write”.

3.1.1.1 Communication

Before programming begins, it is necessary to understand the communication protocol and establish the connection between the host computer and the inverter. Since this inverter is connected to the Schneider Conext Gateway, which communicates to the host computer with Modbus TCP protocol, the Modbus map of the Conext Gateway is applied to the selection of registers.

Modbus is an implementation-level protocol which communicate between master device, such as an HMI or a host computer, and a slave device, such as PLC, gateway or sensor through predefined functions. It follows the request-response rule, where all contact is initiated by the master who is also in charge of making requests that the slave must comply with. In other words, the target device must reply to each request sent. Every request receives a single response. Additionally, queries usually come from one source and are directed at just one device (Application Development with Modbus, 2022).

In LabVIEW, the “Open TCP Session” function is used and indicated in Figure 3.3. There are four important elements that need to be correctly configured: Slave IP Address, Slave ID, Communication Port and Timeout.

- Slave IP Address: In the LAN, the Conext Gateway is assigned a fixed IP address of 192.168.0.6;
- Slave ID: The Slave ID is predefined by the manufacture and is set to 10;

- Communication Port: Generally, port 502 is setting as default communication port in most devices. However, this port is reserved for Sunspec devices in the gateway. Thus, port 503 is selected;
- Time out: The timeout value is kept at its default value, which is 10 seconds.

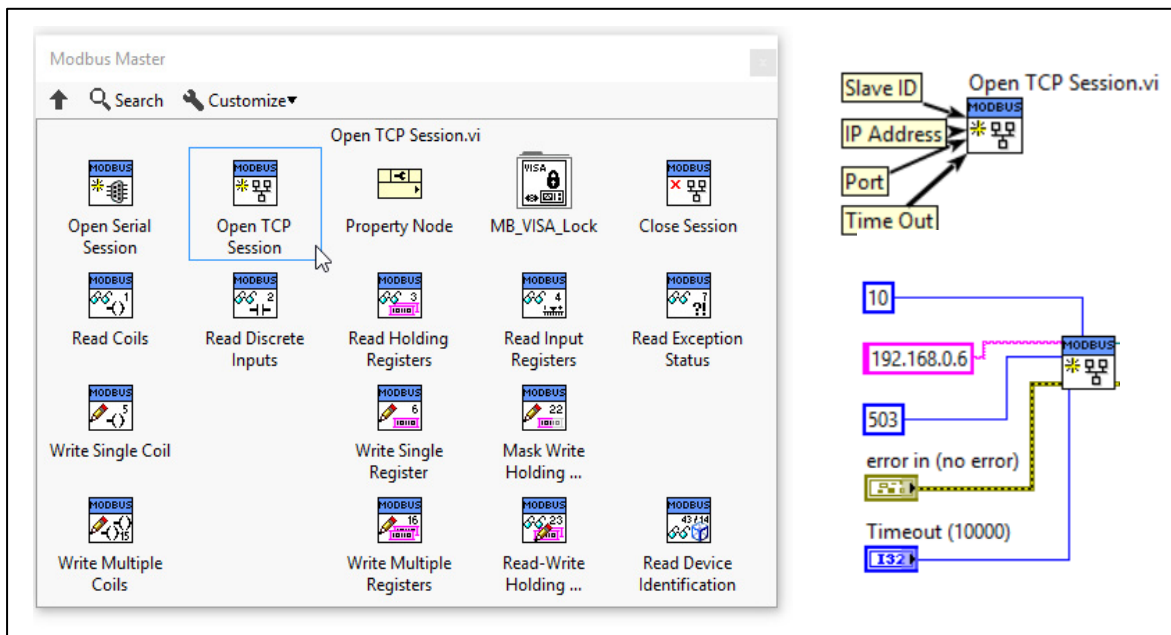


Figure 3.3 Open TCP Session

3.1.1.2 Inverter Monitoring System

In the XW Pro 6848 monitoring system, the collected data is mainly used to evaluate the operating state of the inverter. At the same time, it provides a data basis for the execution of optimization algorithms. According to the requirements of control strategies, in the grid side, this control module tracks the grid voltage, current, frequency and power. In the battery side, the inverter DC voltage, current and power are measured. Moreover, the charge status and inverter status are two important indicators to explicitly show the grid quality and inverter working mode.

The data in the inverter is stored in the corresponding registers. To access those registers, the Read Holding Register function should be used, as shown in Figure 3.4. It has two factors that need to be set properly. One is the register's address, which can be found in the Modbus map provided by the instrument manufacturer. According to this map, the quantity of registers used can be calculated. For instance, a register can store a 16-bit integer, such as grid frequency (Figure 3.5). If the target parameter is 32-bit integers, two registers are required, such as grid voltage, and current (Figure 3.6 and Figure 3.7).

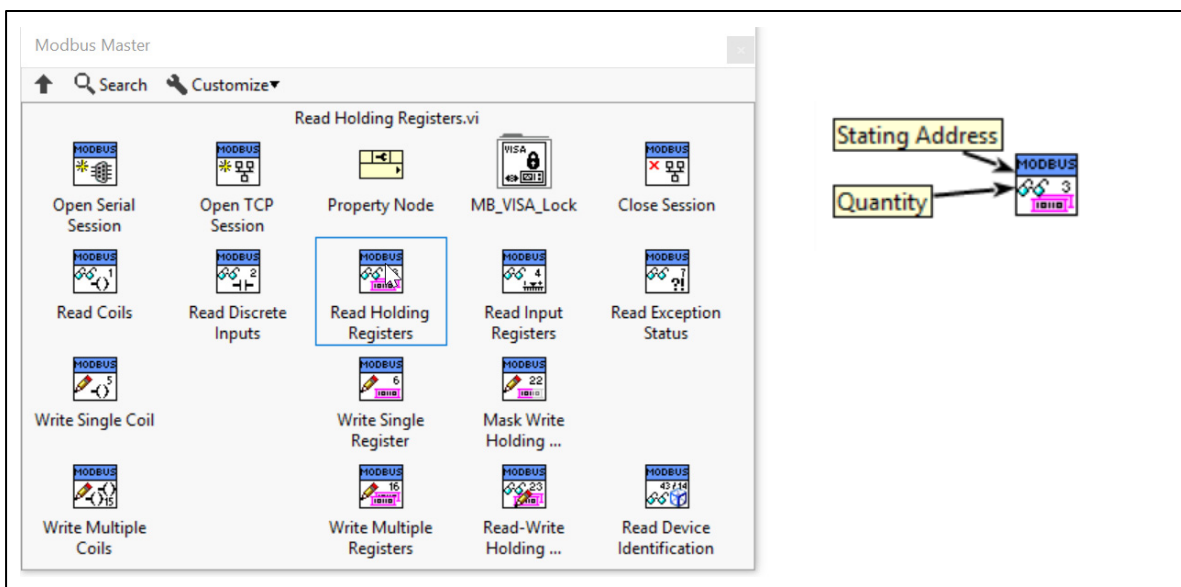


Figure 3.4 Read Holding Registers

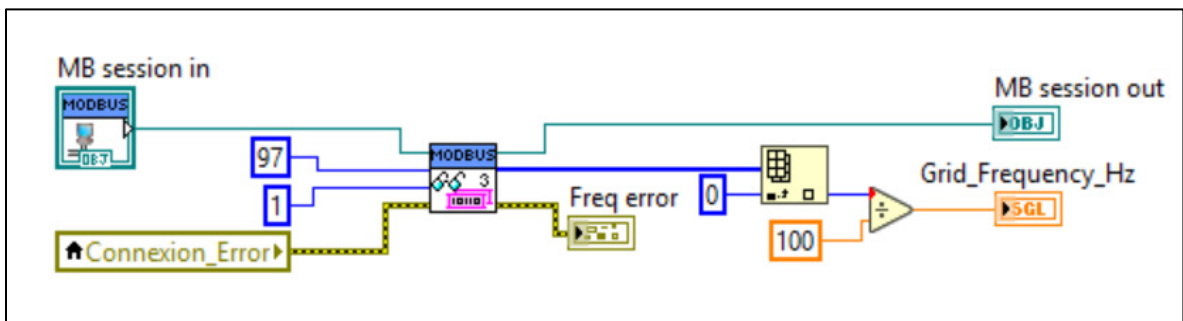


Figure 3.5 Source Block Diagram Code of Reading Grid Frequency

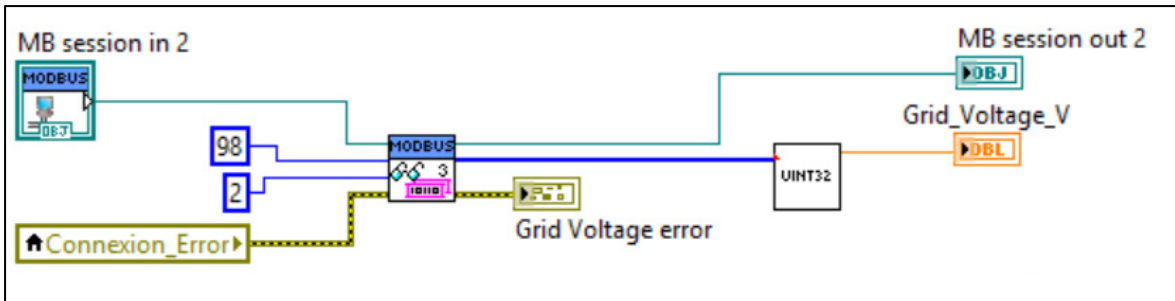


Figure 3.6 Source Block Diagram Code of Reading Grid Voltage

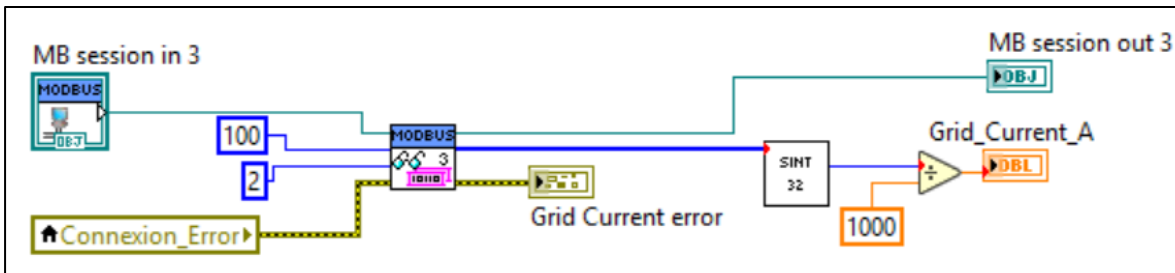


Figure 3.7 Source Block Diagram Code of Reading Grid Current

The output value of the Read Holding Register function is hexadecimal by default, and a conversion program is required if the measurement results are to be represented in decimal. Therefore, a SubVI named UINT32 or SINT32 is created for data type conversion and registers' values combination. Figure 3.8 demonstrates that the output register values are presented as a hexadecimal array. The conversion program is used to split the array into the values of their respective registers and concatenate them in the correct order and convert to decimal values. The converted number has a scale of 0.001, which represents by dividing 1000.

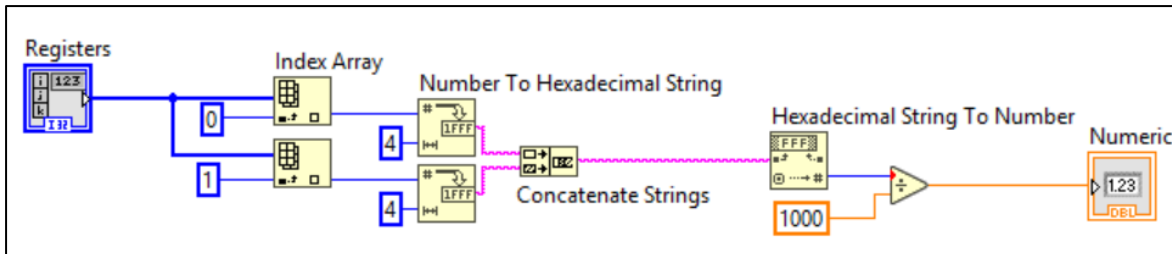


Figure 3.8 Conversion program of Hexadecimal to Decimal

3.1.1.3 Inverter Control System

The purpose of the control system design is to effectively implement the optimization algorithm to achieve peak load shaving or peak power compensation operation. According to Nicolas's optimization algorithm, whether the setpoint value is greater than zero determines whether to disable charger mode and active the mode of selling energy to the grid. Once the selling to grid mode is active, it is necessary to indicate how much power the inverter needs to pull out from the battery bank. Since there is no register representing the selling power, the maximum sell current register should be assigned. The maximum allowable selling current can be obtained by dividing the required power by the grid voltage. The power sent to the battery is calculated using Equation 3-1.

$$P_{bat_set_point} = \frac{C_{bat} \times P_{inverter} \times R_{power} \times R_t}{C_{bat_rep}} \quad (3.1)$$

$$R_{power} = \frac{P_{\acute{E}TS}}{P_{Chroma}} \quad (3.2)$$

$$R_t = \frac{T_{real}}{T_{acc}} \quad (3.3)$$

Where,

- C_{bat} is the total capacity of the battery bank consisting of four 3.8 kWh PHI batteries.
- $P_{inverter}$ is the power of inverter XW Pro.
- R_{power} is the power ratio used to calculate the scale of laboratory microgrid volumes based on representative $\acute{E}TS$ campus, calculated in Equation 3.2.
- R_t is the time ratio, which is applied to accelerate the verification experiment running on a past date to save actual test time.
- C_{bat_rep} is the represented battery bank capacity, which is essential to construct the $\acute{E}TS$ campus microgrid.
- $P_{\acute{E}TS}$ is the $\acute{E}TS$ campus power consumption in real-time.

- P_{Chroma} is the test bench load in laboratory, approximated to the ÉTS campus.
- T_{real} is real test time, and the stamped time is coordinated with the actual time.
- T_{acc} is the accelerated test time, proportional to the real test time (Equation 3.3).

In LabVIEW, the Write Single Register or Write Multiple Registers functions are applied to set values (Figure 3.10). Similar to the method mentioned above, taking Write Single Register as an example shown in Figure 3.11 (a), the first step is to find the required register address in the Modbus map, and then enter the desired value. It is worth noting that when writing to multiple registers, since the data type should be 32 bits or more, the input value needs to be represented in an array. For instance, in Figure 3.11 (b), the maximum sell current is a 32-bit unsigned integer, and two registers need to be set in the inverter. Thus, the current value should be set in the last 16-bit register, and the first 16 bits is set to 0.

Different from the output value, the input value is not in hexadecimal, but in decimal. Hence, no data type conversion is required, and the desired value can be directly put in. The previous students exploited double precision data type throughout the entirety of the LabVIEW source code. Consequently, it is necessitated to convert all output data to double precision before introducing the new section of the programme in order to avoid errors brought on by incompatibilities between data types. Simply right-click the numerical output and select representation to switch among different data precision (Figure 3.9).

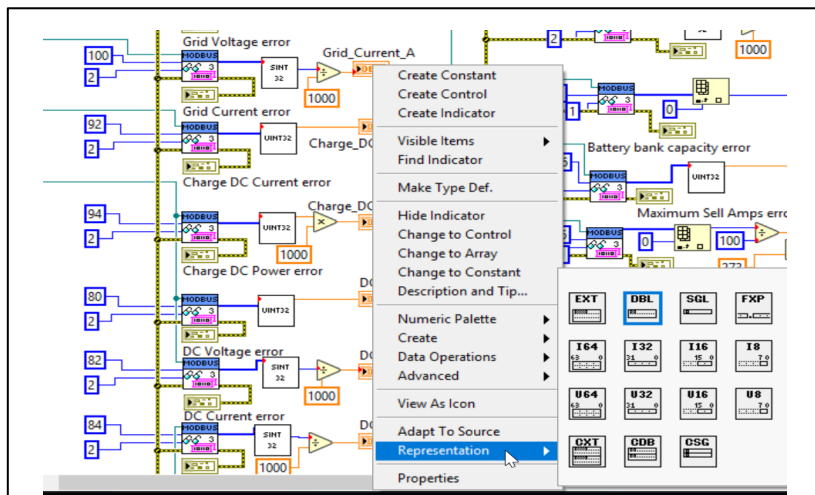


Figure 3.9 Data Precision Selection

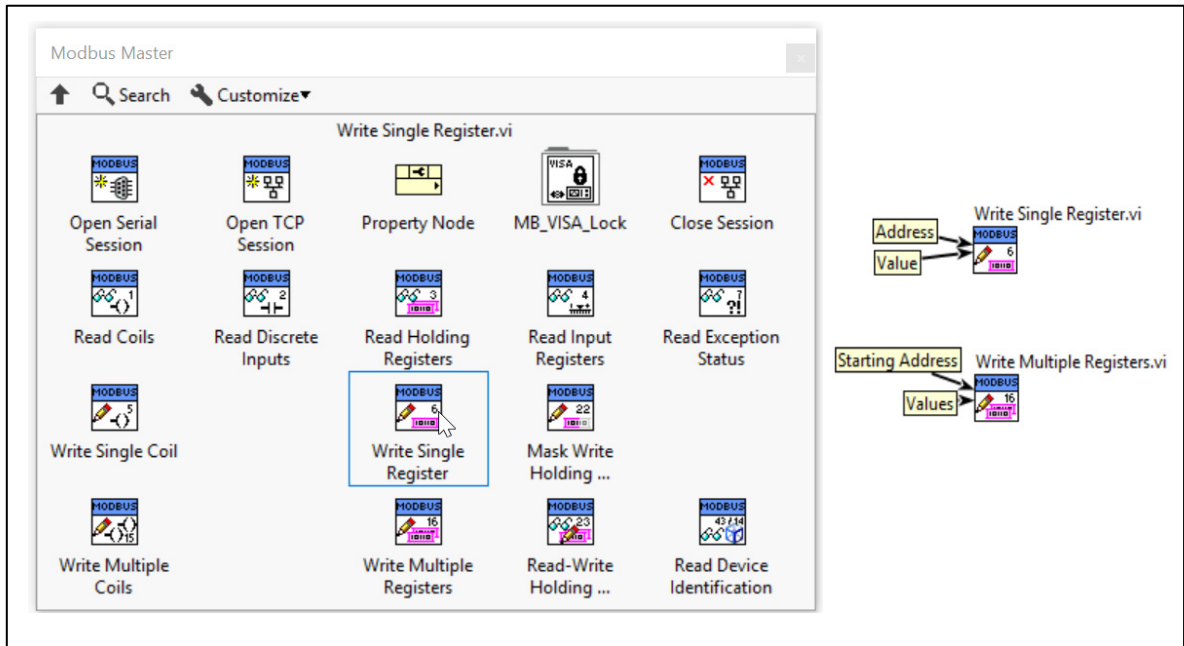


Figure 3.10 Write Single/ Multiple Registers

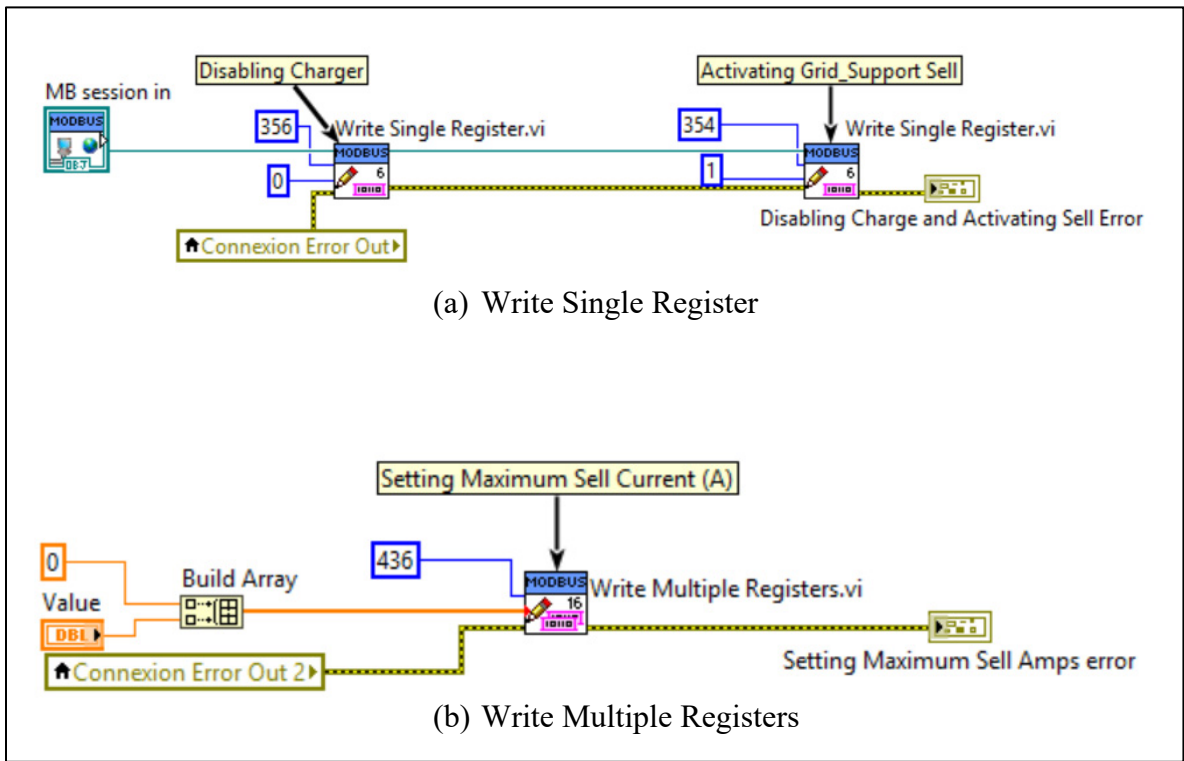


Figure 3.11 Source block diagram code of writing operation

Table 3.1, Table 3.2, Table 3.3, and Table 3.4 shows the Modbus map containing addresses and specific information corresponding to selected registers in the inverter. (Schneider Electric, 2020)

Table 3.1 Modbus Map in Gateway for XW Pro Inverter Grid Side Measurement
Taken from Schneider Electric (2020)

Reg.Addr. (Dec)	Name	Type	R/W	Units	Scale	Offset	Notes
97	Grid Frequency	uint16	r	Hz	0.01	0.0	
98	Grid Voltage	uint32	r	V	0.001	0.0	
100	Grid Current	sint32	r	A	0.001	0.0	
102	Grid Power	sint32	r	W	1.0	0.0	

Table 3.2 Modbus Map in Gateway for XW Pro Inverter Battery Side Measurement
Taken from Schneider Electric (2020)

Reg.Addr. (Dec)	Name	Type	R/W	Units	Scale	Offset	Notes
80	Battery Voltage	uint32	r	V	0.001	0.0	
82	Battery Current	sint32	r	A	0.001	0.0	
84	Battery Power	sint32	r	W	1.0	0.0	
86	Battery Temperature	uint16	r	degC	0.01	-273.0	
88	Invert Battery Current	uint32	r	A	0.001	0.0	
90	Invert Battery Power	uint32	r	W	1.0	0.0	
92	Charge Battery Current	uint32	r	A	0.001	0.0	
94	Charge Battery Power	uint32	r	W	1.0	0.0	
96	Charge Battery Power Percentage	uint16	r	%	1.0	0.0	

Table 3.3 Modbus Map in Gateway for XW Pro Inverter Mode and Status Surveillance
Taken from Schneider Electric (2020)

Reg.Addr. (Dec)	Name	Type	R/W	Units	Scale	Offset	Notes
71	Inverter Enabled Status	uint16	r		1.0	0.0	0 = Disabled 1 = Enabled
72	Charger Enabled Status	uint16	r		1.0	0.0	0 = Disabled 1 = Enabled
73	Sell Enabled Status	uint16	r		1.0	0.0	0 = Disabled 1 = Enabled
64	Device State	uint16	r		1.0	0.0	
123	Charger Status	uint16	r		1.0	0.0	
122	Inverter Status	uint16	r		1.0	0.0	

Table 3.4 Modbus Map in Gateway for XW Pro Inverter Sending Instruction Registers
Taken from Schneider Electric (2020)

Reg.Addr. (Dec)	Name	Type	R/W	Scale	Offset	Notes
354	Grid Support Sell Enable/Disable	uint16	rw	1.0	0.0	0 = Disabled 1 = Enabled
356	Charger Enable/Disable	uint16	rw	1.0	0.0	0 = Disabled 1 = Enabled
357	Force Charger State	uint16	rw	1.0	0.0	1 = Bulk 2 = Float 3 = No Float
367	Maximum Charge Rate (%)	uint16	rw	1.0	0.0	
436	Maximum Sell Amps	uint32	rw	0.001	0.0	

Since the output values of the Device State Register, Charger Status Register, and Inverter Status Register are all integers, in other words, specific information is not displayed in string type. In order to facilitate reading and monitoring the operation of the inverter, a display program is designed, as shown in Figure 3.12. Additionally, Table 3.6 lists the specific working states and ongoing operations corresponding to the output value.

Table 3.5 Device, Charger, Inverter Status Details
Taken from Schneider Electric (2020)

Device State	Charger Status	Inverter Status
0=Hibernate	768=Not Charging	1024=Invert
1=Power Save	769=Bulk	1025=AC Pass Through
2=Safe Mode	770=Absorption	1026=APS Only
3=Operating	771=Overcharge	1027=Load Sense
4=Diagnostic Mode	772=Equalize	1028=Inverter Disabled
5=Remote Power Off	773=Float	1029=Load Sense Ready
255=Data Not Available	774=No Float	1030=Engaging Inverter
	775=Constant VI	1031=Invert Fault
	776=Charger Disabled	1032=Inverter Standby
	777=Qualifying AC	1033=Grid-Tied
	778=Qualifying APS	1034=Grid Support
	779=Engaging Charger	1035=Gen Support
	780=Charge Fault	1036=Sell-to-Grid
	781=Charger Suspend	1037=Load Shaving
	782=AC Good	1038=Grid Frequency Stabilization
	783=APS Good	
	Charger Status	
	784=AC Fault	
	785=Charge	
	786=Absorption Exit Pending	
	787=Ground Fault	
788=AC Good Pending		

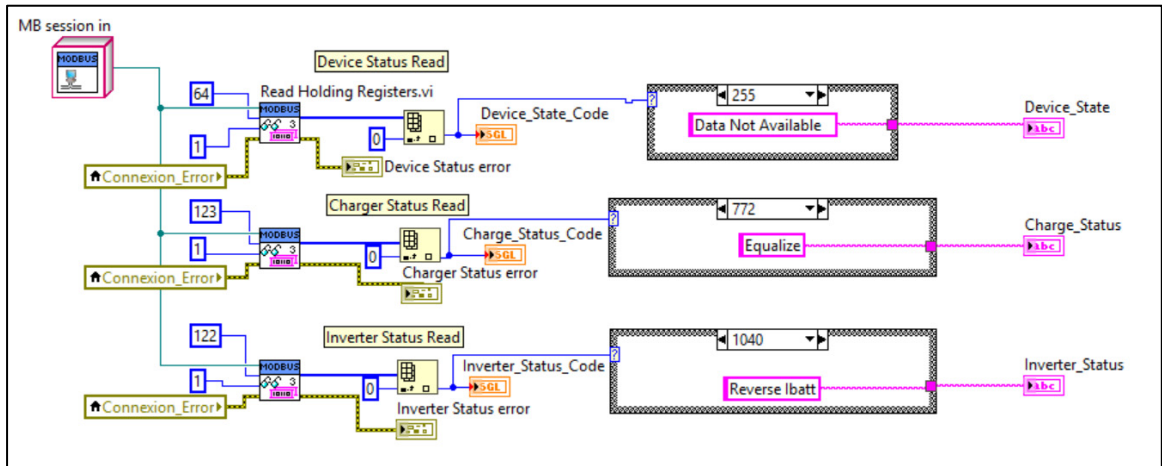


Figure 3.12 Source Block Diagram Code of Converting Code to String

The full read and write program of the inverter, including its front panels and block diagram codes, are detailed in ANNEX V.

3.1.1.4 Inverter protection setup

In order to ensure the normal operation and protection of the inverter, certain parameters need to be constrained under the instruction provided by the battery manufacturer – Simpliphi. The specification requirement is shown in Table 3.7. A file called “Inverter Initialization” is built to set the listed settings mentioned in Table 3.7. The corresponding Modbus Map is shown in Table 3.8 and a partial program is presented in Figure 3.13. The full-size program is detailed in ANNEX VI.

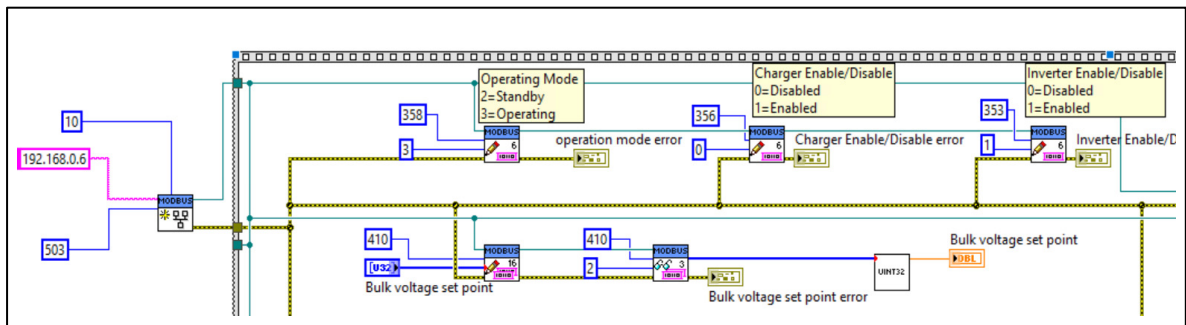


Figure 3.13 Inverter Initialization Program Segment

Table 3.6 Settings for SimpliPhi PHI 3.8 kWh 48V Battery with Schneider Conext XW Pro & XW+ Inverters

Taken from SIMPLIPHI POWER (2020)

Conext XW+ & XW Pro Settings	
Advanced Settings > Inverter Settings	
Low Battery Cut Out Voltage ¹	48
LBCO Hysteresis	2.0V
LBCO Delay	10 Sec
High Batt Cut Out	60V
Search Watts	Default
Search Delay	Default
Charger Settings > Custom Settings	
Batt Type	Custom
Lithium Ion	
Control	2StgNoFloat
Bulk Voltage	56V
MaxBulkCurrent (C/2) ²	37.5A (per PHI 3.8)
DisChgImax ²	80A (per PHI 3.8) (up to 500A per bank)
DisChgImax Timer	300 sec
Batt Capacity ²	75Ah (per PHI 3.8)
Max Charge Rate (C/2) ^{2,3}	37.5A (per PHI 3.8)
Default Batt Temp	Warm
Recharge Volts	50.4V
Absorb Time	.1 Hour (6 minutes)
Chg Block Start	Default
Chg Block Stop	Default

Table 3.7 Modbus Map for Inverter Protection

Taken from Schneider Electric (2020)

Reg.Addr. (Dec)	Name	Type	R/W	Units	Scale	Offset	Notes
410	Bulk/Boost Voltage Set Point	uint32	rw	V	0.001	0.0	
378	Recharge Voltage	uint32	rw	V	0.001	0.0	
498	Low Battery Cut Out Hysteresis	uint32	rw	V	0.001	0.0	
394	High Battery Cut Out	uint32	rw	V	0.001	0.0	
374	Battery Bank Capacity	uint16	rw	Ah	1.0	0.0	
414	Absorption Time	uint16	rw	s	1.0	0.0	
380	Low battery Cut Out	uint32	rw	V	0.001	0.0	
382	Low Battery Cut Out Delay	uint16	rw	s	0.01	0.0	
468	Maximum Discharge Current	uint16	rw	A	1.0	0.0	
376	Grid Support Voltage	uint32	rw	V	0.001	0.0	

3.1.2 Electrical Load Control Module Improvement

Test bench No.2 not only adopts the three Chroma 63804 AC/DC Loads from testbed No.1, but also includes its software control module. Nonetheless, the module has communication problem, which means the host computer cannot communicate with the loads to achieve remote control. In addition, since the test bench No. 2 chooses a parallel connection mode, the data collection module has to be modified.

In testbed No.1, six Chroma loads are connected together through the GPIB buses, and the host computer can control all six loads simultaneously through the GPIB-ENET controller. Regardless of the mode of operation (Constant Power or Constant Current), setpoint value commands are sent to the entire load pack, which is then mathematically performed by the control program, such as dividing by the number of detected loads connected to the system, to evenly distribute the setpoint value to each load. It is difficult to control a single load from existing program prototype. Besides, this program uses the cluster array to display the real-time data changes of each load at the same time, as a consequence, it makes inconvenient to extract any data from each cluster of loads and integrate them together for use.

The phase parallel mode is actualized by connecting CAT 5 cables into the system buses (RJ45) and one GPIB connector has been used to associate the controller and load pack. The Chroma load with primary address 1 is selected as the master, and the other two, with primary address 4 and 5, respectively, are slaves. the software program can control the entire load pack only by realizing the control of the master load, as the distribution of power consumption within the load pack is managed by the master load itself. This greatly simplifies the difficulty of controlling the load pack.

3.1.2.1 Communication

Chroma loads provides multiple communication methods, and GPIB is the best choice for connecting to LAN with GPIB-ENET. In LabVIEW, the NI-VISA driver is used to accomplish the communication between host computer and GPIB-ENET controller. VISA is implemented by the NI instrument company for configuring, programming, and troubleshooting the GPIB, Serial (RS232/RS485), Ethernet and USB interfaces of instrumentation systems.

To install the communication by VISA, the VISA Write function is selected, and there are four important elements need to be properly setup:

- GPIB-ENET IP Address: 192.168.0.4;
- Chroma Master Load ID: Chroma.63804.0.1.41, where 63804 is the model, 0 is the serial number, and 1.41 is the firmware version;
- VISA Resource Name: GPIB0::1::INSTR, where 1 is the primary address of the load;
- GPIB address: 8, configured by the manufacture.

An example of connecting to the target load by its VISA resource name is shown in Figure 3.14 and Figure 3.15. The command syntax follows the IEEE488.2 standard. or example, ‘CURR?’ stands for getting the real current measurement, ‘VOLT?’ is for voltage value, ‘POW?’ is for power, and ‘MEAS:POW:PFAC’ is for power factor.

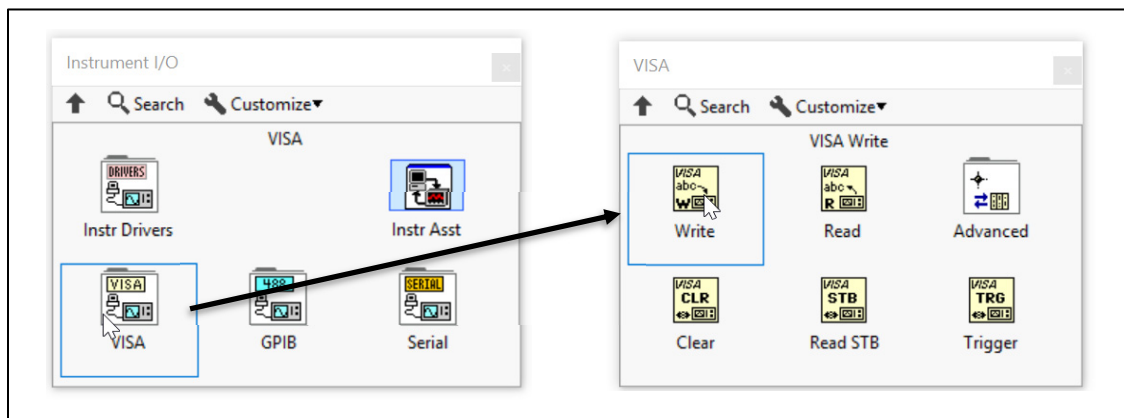


Figure 3.14 Open Selected Load by VISA Write Function

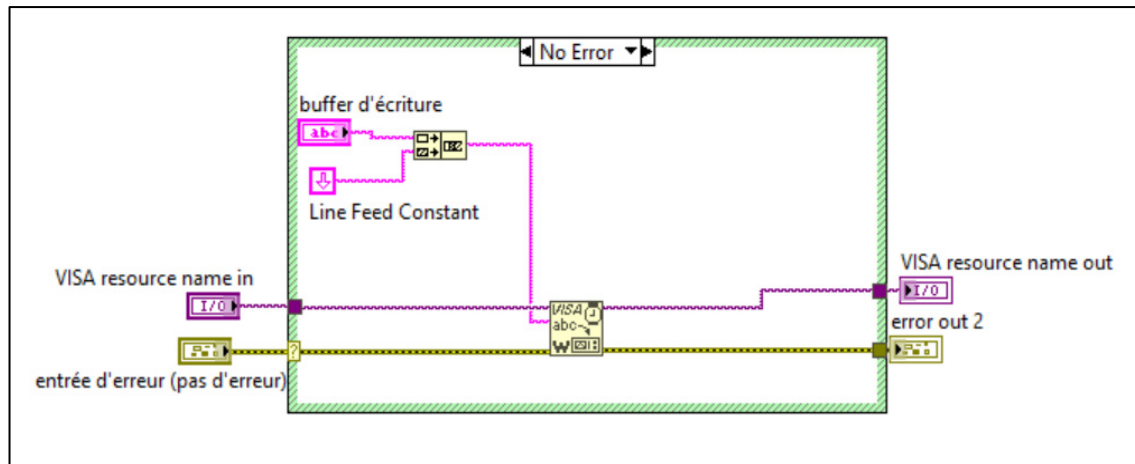


Figure 3.15 Block Diagram of VISA Write Function

3.1.2.2 Data Extraction

The optimization algorithm needs to access the real-time power consumption of the load pack, which has to extract this measurement from the corresponding cluster function. The “Unbundle By Name” function has been used, and the source code is showing in Figure 3.16 and Figure 3.17. The full-size program for Chroma Load is given in ANNEX VII.

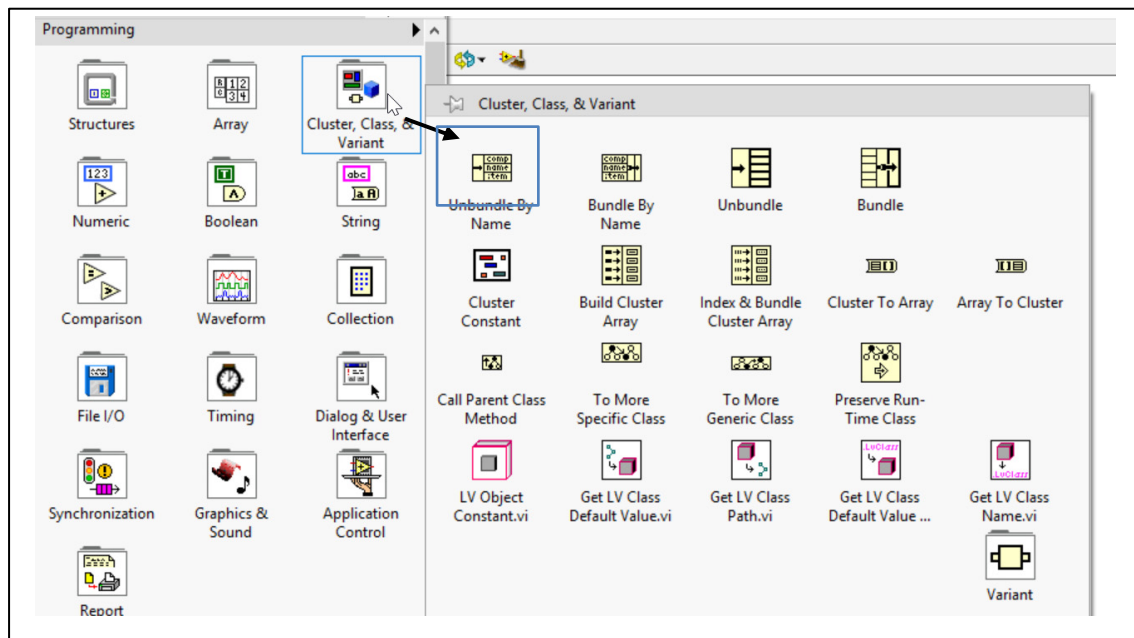


Figure 3.16 Data extraction program

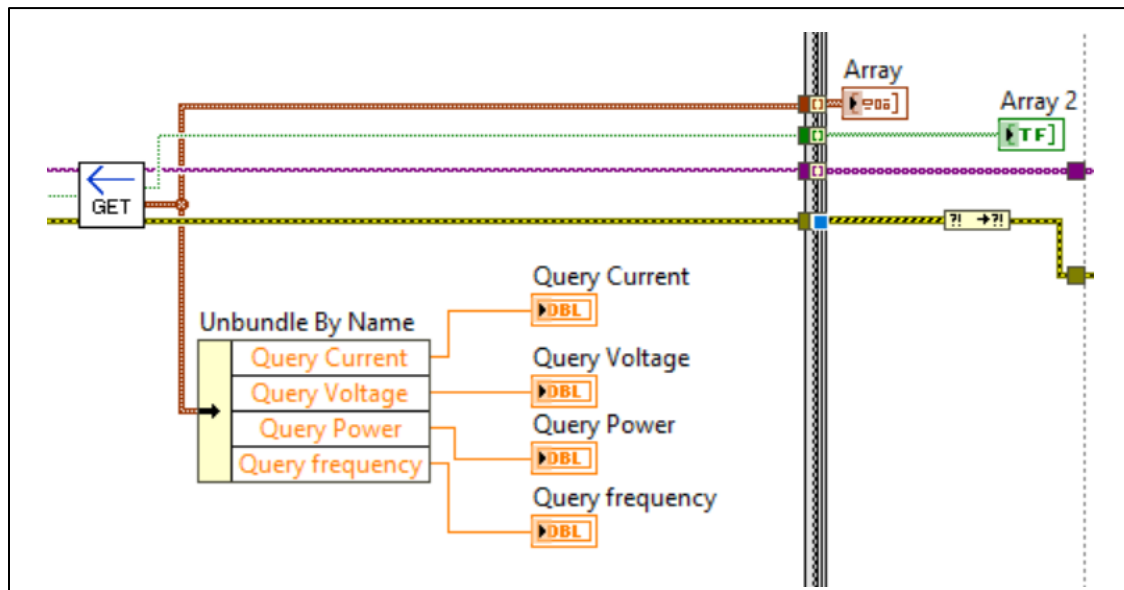


Figure 3.17 Data extraction Block Diagram

3.1.3 Power Meter Monitoring Module Design

Recalling from the chapter 2.3.2, the Schneider PM5340 Power and Energy meter has been adopted from the Testbed No. 1. This meter is mainly used to measure the power obtained by the Testbench No.2 or the simulated MG from the large grid. Its role is also equivalent to the electricity meter used by Hydro Quebec for billing. Although there are many parameters or registers that can be set in this meter, only the function of reading the parameters' measurement is used in this testbench.

3.1.3.1 Communication

The PM5430 meter is also adapted the Modbus TCP protocol, so the communication configuration is the same as the XW Pro inverter. Its Open TCP Session function is set as follows

- Slave IP Address: a fixed IP address: 192.168.0.2;
- Slave ID: 255, as default;
- Communication Port: port 502, as default;

- Time out: 10 seconds, as default.

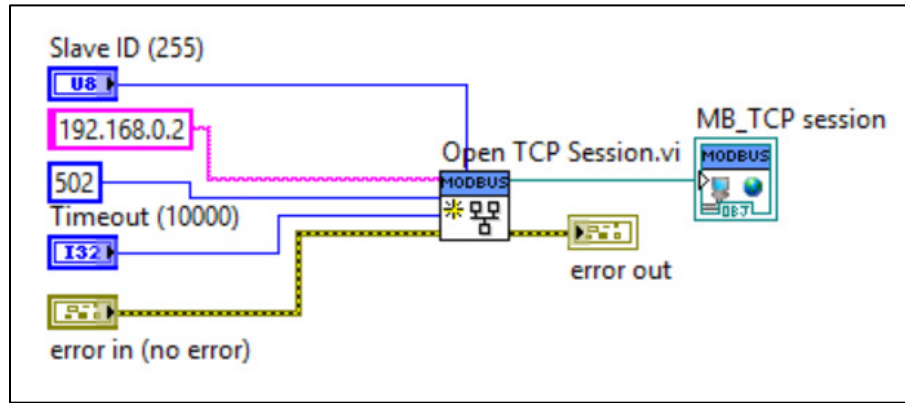


Figure 3.18 Source Block Diagram of PM5340 Communication

3.1.3.2 Measurement

At this stage, according to the actual test requirements, grid voltage, grid current, grid frequency, power, and power factor are measured (the partial program is shown in Figure 3.19). Like the delivered energy, the billing function may be applied in the next research phase. In this meter, energy-related parameters have a type of 64-bit integers, so that those values could be stored in at least four registers, as shown in Figure 3.20. The complete source code is attached in ANNEX VIII.

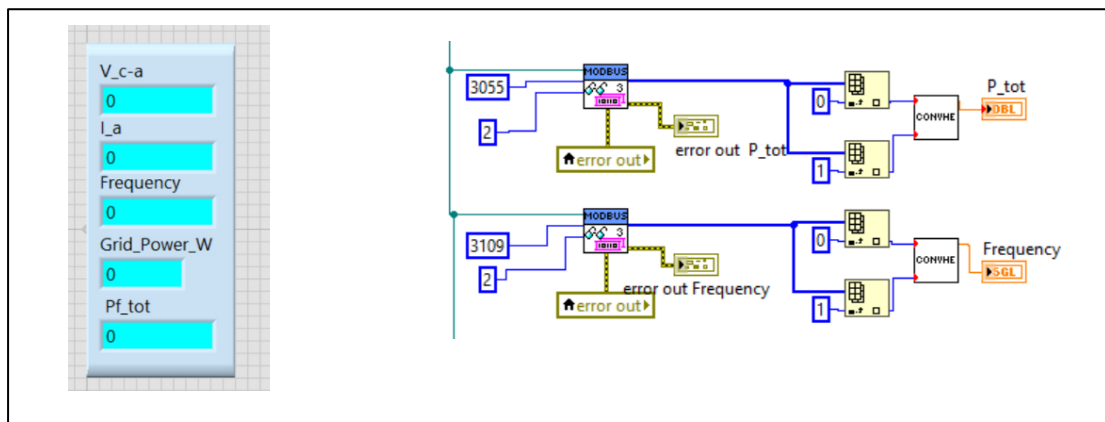


Figure 3.19 Measurement system of PM5340

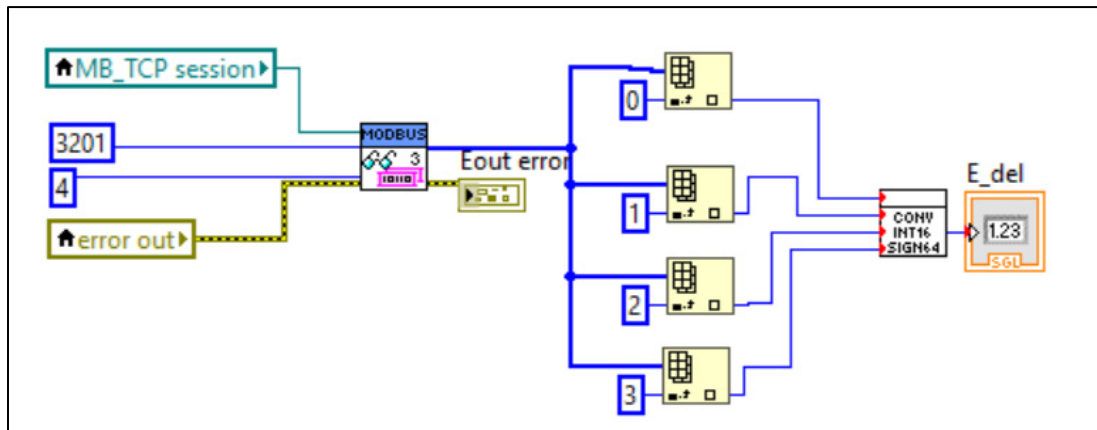


Figure 3.20 Measurement of Energy Delivered to Load

3.2 Test Bench Device Software Modules Integration

Thanks to the research project of the Testbed No. 1, the simulation part of the MGCCP has been completed and tested under various conditions. The work of this thesis, is to integrate the program of each actual devices on the basis of the original simulation system to realize the smart control of the operation of the equipment through the MGCCP.

3.2.1 Terminals Assignment and Icons definition

The first thing to do before integrating these programs is to assign front panel controls and indicators to corresponding terminals in the connector pane. Some terminal patterns have been pre-set in LabVIEW. If there is no suitable pattern to choose from, connector pane terminal patterns can also be customized. It is important that even if some terminals are not used in the global programs, all input and output still need to be considered to have terminals. In the future, when the global program needs to access certain data, the terminals that have been set can be used directly without redefining the connector pane.

Besides, the icon name can help users to quickly understand the functions of those SubVIs, and the name should be kept simple, such as ‘XW PRO’ is for the inverter program, ‘PM5340’ is for the power meter, and ‘Load’ is for load pack.

3.2.2 Integration

A new operation case has been added to distinguish between simulation mode (Case Init) and real-time with equipment mode (Case Step 1). In order to better serve Nicolas’ control strategies, certain modification has been performed in the integrated program.

3.2.2.1 XW Pro Inverter integration

As shown in Figure 3.21, three input terminals have been applied: Time ratio, Power ratio, and Battery power setpoint, with unit of kW. Moreover, there are two output terminals have been used for optimisation algorithm. Besides, to avoid data transfer congestion, the program reading part and writing part have been split into two separate programs named XW PRO Write, and XW PRO Read. The integration program of XW PRO read is described in ANNEX IX.

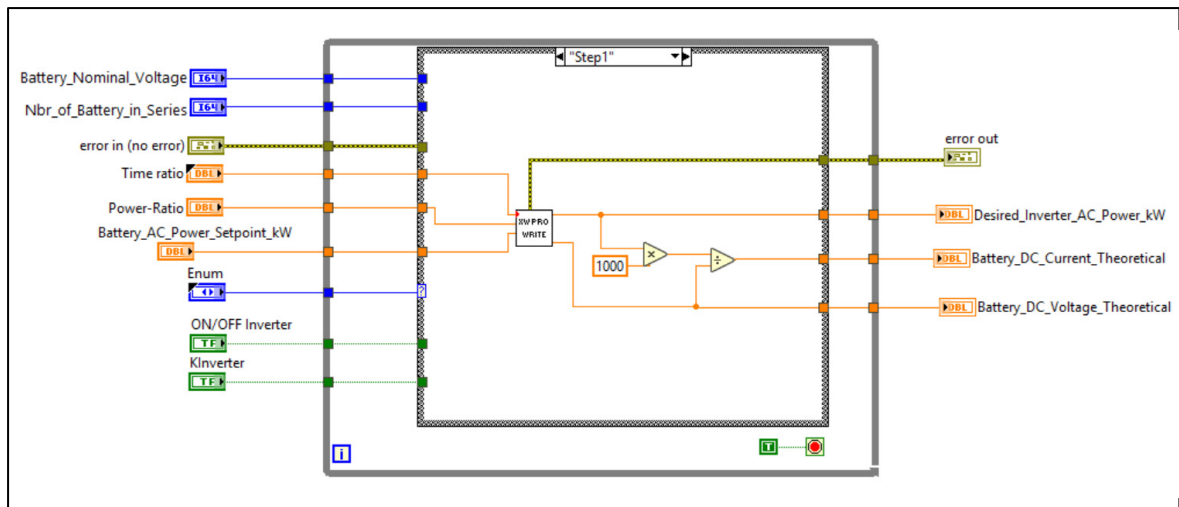


Figure 3.21 XW Pro Inverter Write Program Integration Block Diagram

3.2.2.2 Chroma Load integration

Before running the load pack, it is necessary to set the working mode, such as CP mode, as well as the maximum current value and the required power value. As mentioned earlier, all data using in Chroma load program are grouped in clusters, so that Bundle function is used to rebind those three parameters. As the same reason with the inverter, the Chroma load program is also divided into two SubVIs. The program is showing in Figure 3.22.

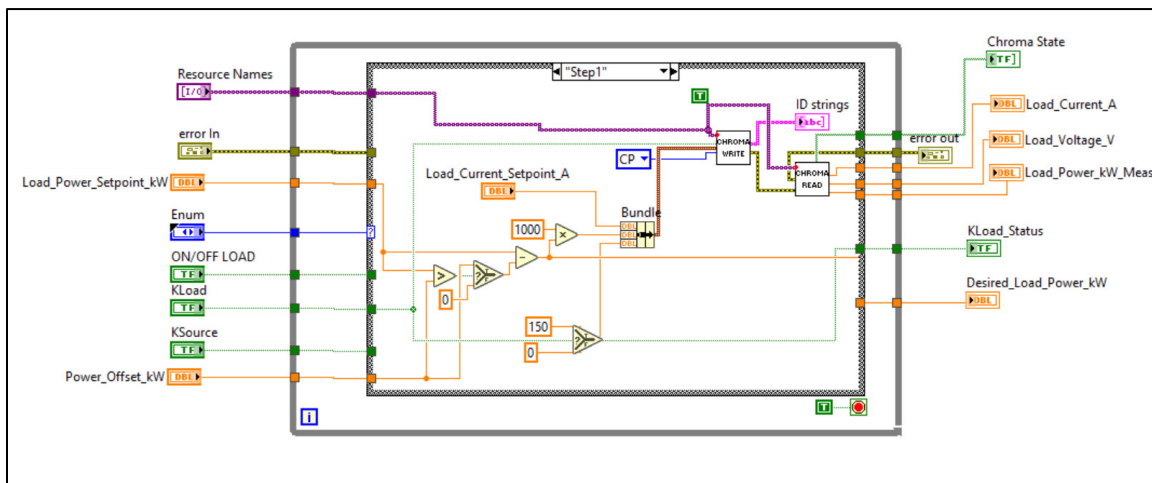


Figure 3.22 Chroma Load Integration Program

3.2.2.3 PM5340 Power Meter integration

The integration of the PM5340 power meter is much simpler than the other two devices, since this program has no input, only measurements. Thus, the integration is to display the output data in the main program, as shown in Figure 3.23.

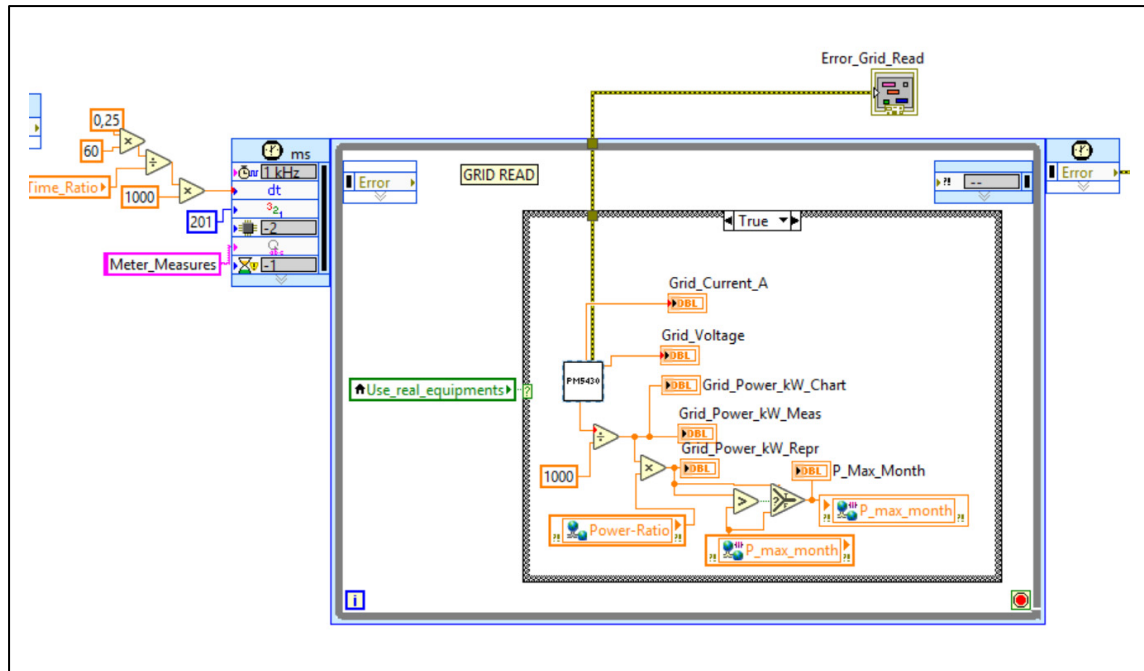


Figure 3.23 PM5340 Power Meter Integration Program

3.3 Test Bench Virtual Interface Improvement

The test bench virtual Interface is implemented using LabVIEW, and it illustrates the output of the power demand in real-time and executes the optimization algorithm. In the operational mode, the MGCCP receives the data and performs calculations, while the computer starts collecting new data once the previous data has been processed. The setting of equipment parameters, test results and display functions are all realized by LabVIEW programming. Therefore, the interface of the system software is required to be simple and directly equipped with relevant operation and display controls, making it convenient for users to operate and observe the working status of the entire system.

The prototype of this MGCCP was designed for the testbed 1. Due to the limitation of the non-zoom of the LabVIEW software, the original control interface lacks both readability and scalability. In addition, since the system has experienced the joint efforts of several groups of students and researchers, there are problems of incoherence and redundancy. The interface front panel and main program need to be reorganized and updated. The criteria for interface

improvement were simplicity and clarity, which the program should try to focus on one monitor size style. The Figure 3.24 depicts the overall layout of the updated MGCCP interface.

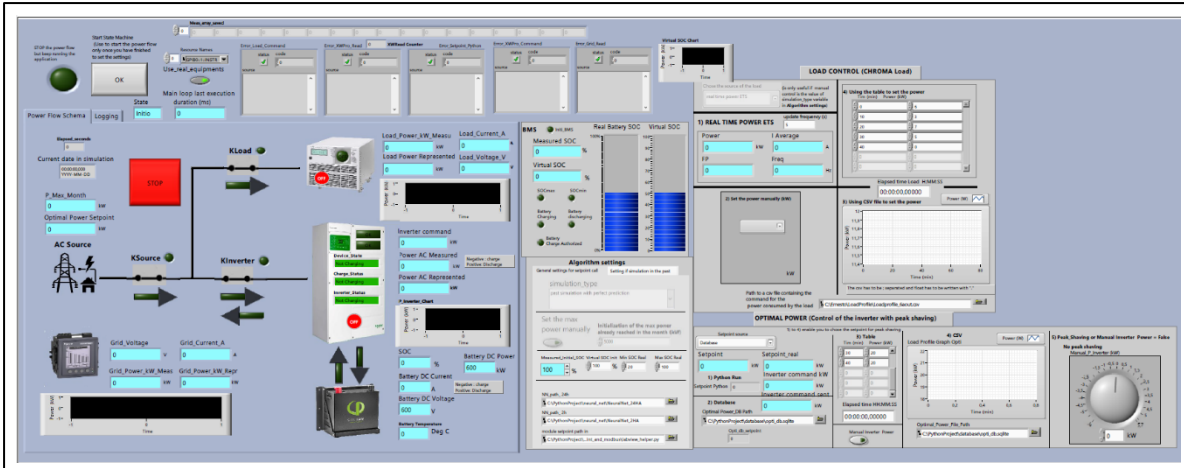


Figure 3.24 Microgrid Central Control Platform

3.3.1 MGCCP Main Interface

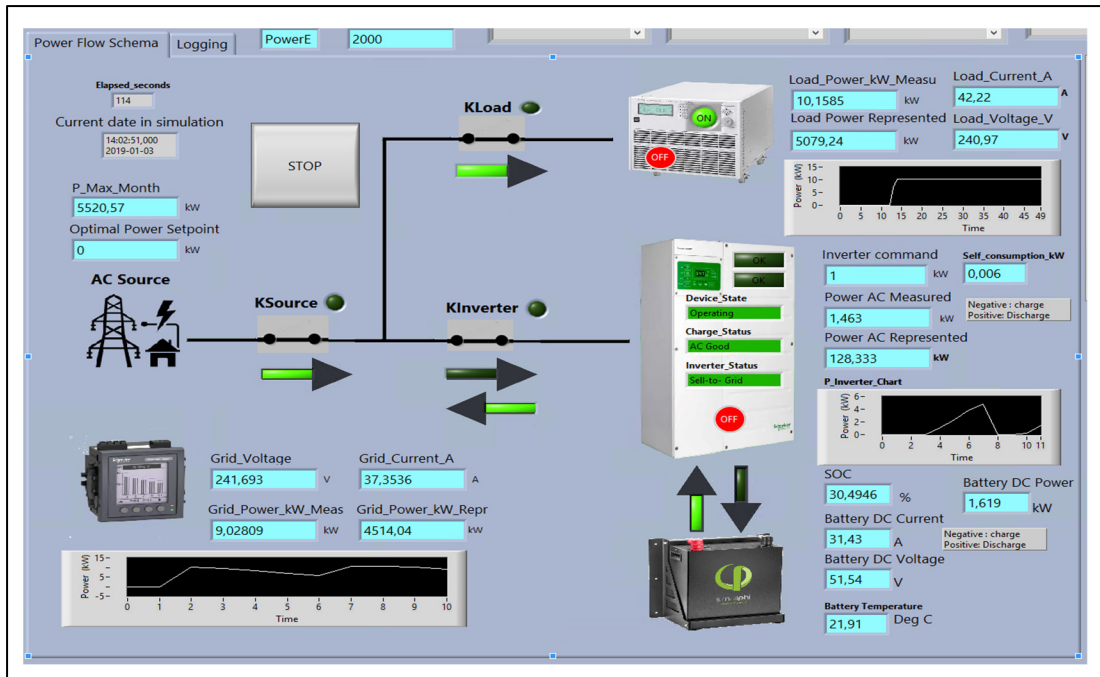


Figure 3.25 MGCCP Main Interface

The entire architecture of the MGCCP can be conceptualized through the system's primary interface, as illustrated in Figure 3.25, which presents the two main circuits of battery energy storage system and load. Simultaneously, the main interface features the voltage, current, and power information of the power grid as well as each individual circuit, and is equipped with an RT curve display. Additionally, it is also able to demonstrate the information of test date and running time. On this interface, closing and opening operations can be performed to connect and disconnect loads and energy storage devices. Moreover, the logging interface (Figure 3.26) can be accessed by clicking on the upper tab; this interface is where the log name and path are initially edited.

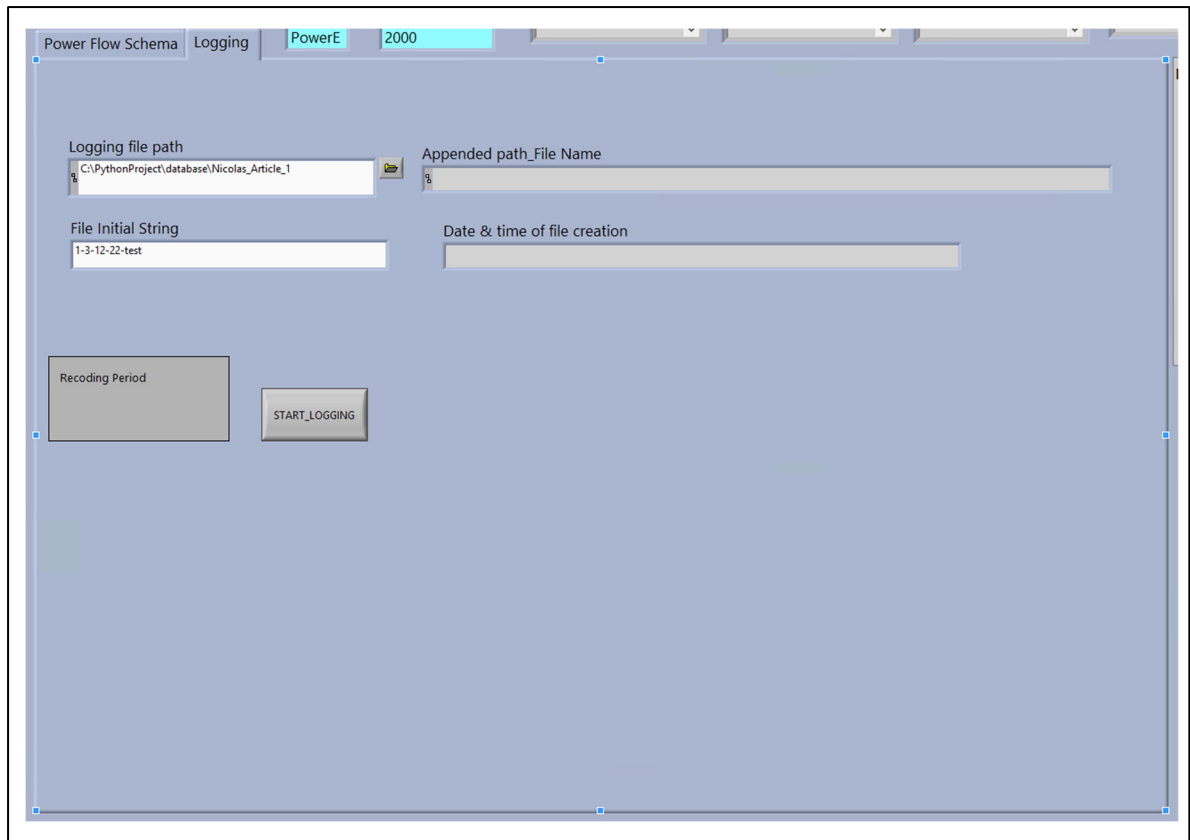


Figure 3.26 Logging Interface

3.3.2 BMS Interface

Figure 3.27 shows the BMS interface which is divided into two sections. On the left side, there are setting and status indicators for the battery and the virtual battery used for accelerated testing (the concept of virtual battery will be explained in the following chapter), as well as the real-time SOC and virtual SOC values. On the right side, there are bar charts displaying the SOC and virtual SOC values, allowing for a visual observation of the battery's state. As shown in the following figure, the real SOC is 22.0531% and virtual SOC is 2.5664%, indicating that the battery bank is currently in a charging state.

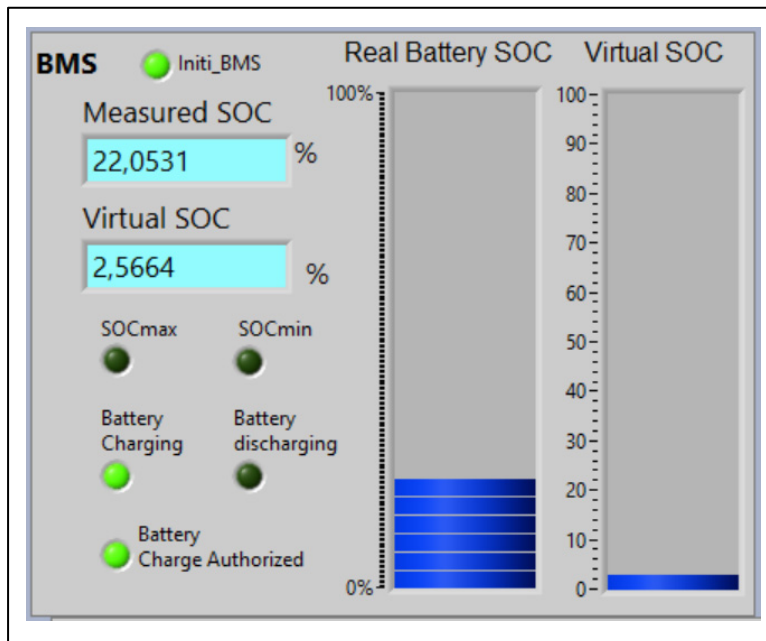


Figure 3.27 BMS Interface

3.3.3 Test Parameters Configuration Interface

This interface has two-tab pages that are primarily used to configure testing parameters. On Tab1, shown in Figure 3.28, the test date, time and power and time ratios are determined. This page is only for validation experiments with past dates. Tab 2, shown in Figure 3.29 is used to select the algorithm type for testing and the battery bank SOC limiting requirements. The

“NN_path_24H” or “NN_path_2H” is used to select the neural network load prediction algorithm during the simulation or tests via Python. In addition, the “Module setpoint in” allow other users to apply their own algorithms writing with Python during simulation and tests.

Figure 3.28 Tab 1 of Parameter Setting Interface

Measured_Initial_SOC	Virtual SOC init	Min SOC Real	Max SOC Real
30,748. %	100 %	20	100

Figure 3.29 Tab2 of Parameters Setting Interface

3.3.4 Load Control Panel

Load control panel (Figure 3.30) is divided into 4 sections. The first section displays the real-time power consumption information of ÉTS, which is updated every five seconds and is obtained from its main power meter with an IP address of 10.168.9.62. The second section allows the user or operator to manually enter load power to match their specific requirements. The third section is employed a CSV file to supply the load's power. The fourth section enables the user to enter the load power using a tabular format.

In previous testing, section 1 was used to optimize load prediction, while section 3 served as a historical load database for validation tests.

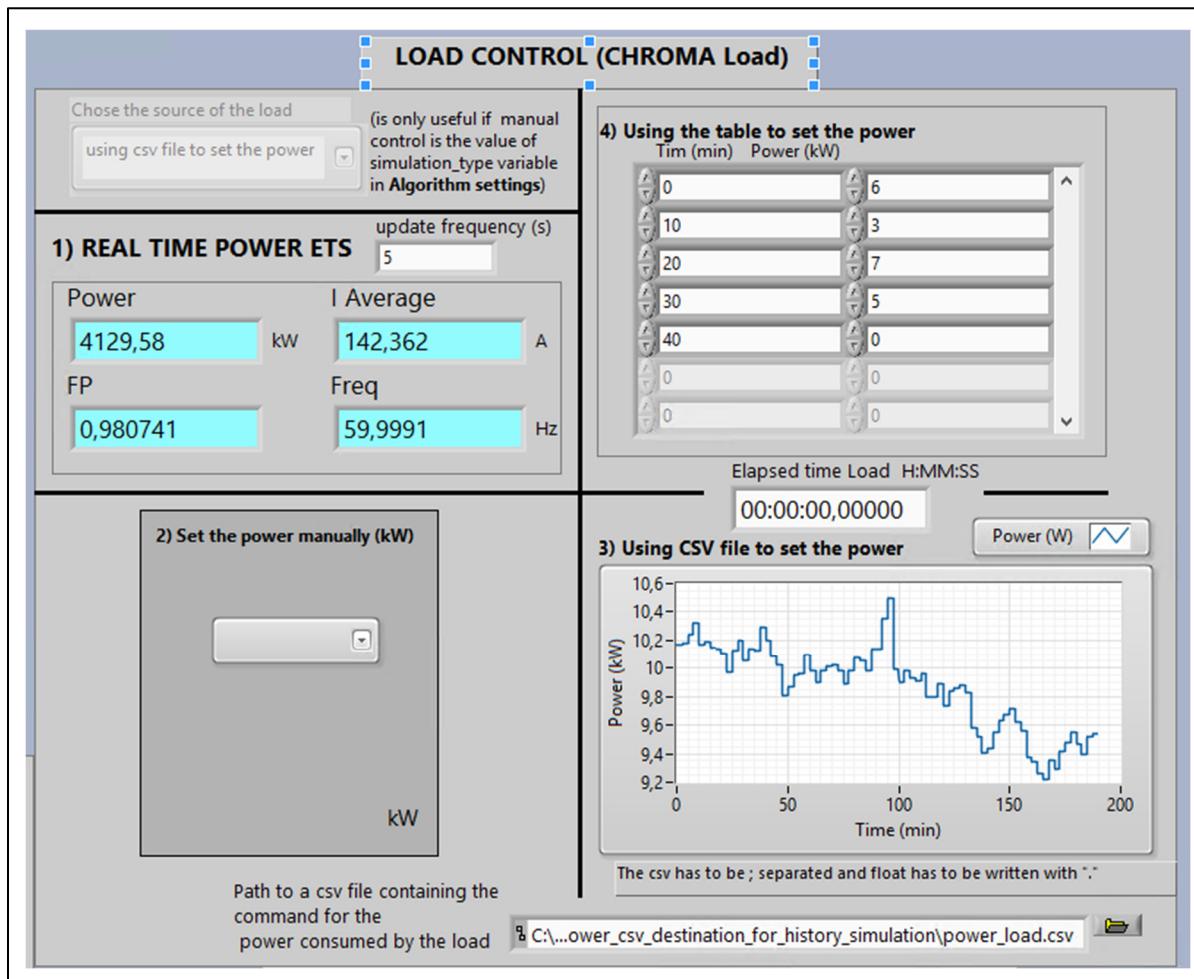


Figure 3.30 Load Control Panel

3.3.5 Optimal Power Control Panel

This panel resembles the division of the load control panel described above. The user or operator can select the optimal power setpoint from various sources, such as Python, a database, a table, and a CSV file. The fifth section keeps the ability to configure the inverter power for peak shaving. In the running test shown in Figure 3.31, the power setpoint is calculated by Python.

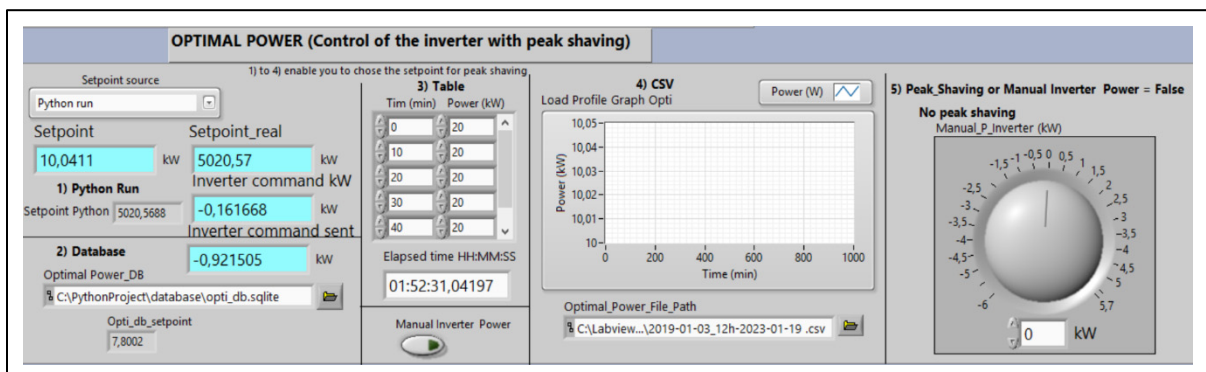


Figure 3.31 Optimal Power Control Panel

3.4 Chapter Summary

This chapter provides an overview of the design and improvement of control system of each device in the LabVIEW programming environment. By using the Modbus protocol and GPIB standard, the data can be transported between host computer and equipment. In this AC MG system, voltage, current, and power are important indicators for evaluating the success of the optimization algorithm. The monitoring system enables the storage and processing of collected data, and supports various protection and control programming for the MGCCP.

CHAPTER 4

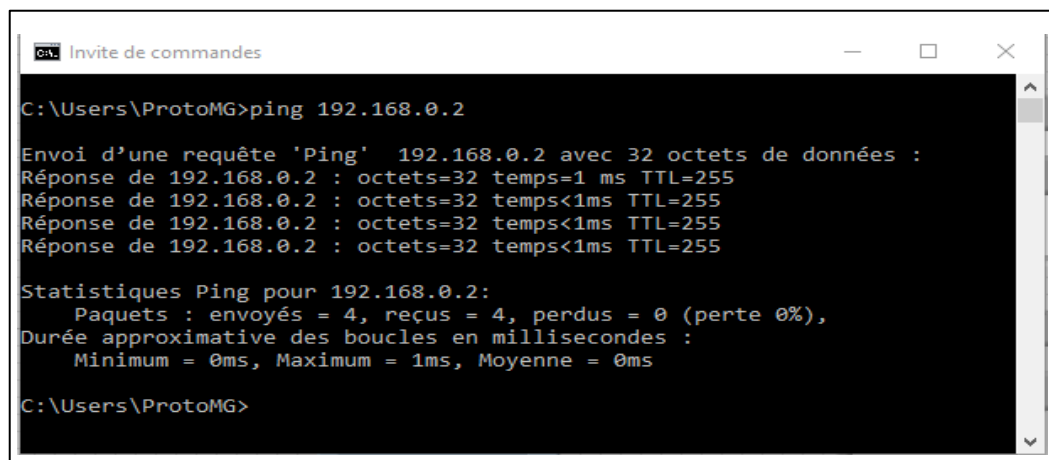
TEST BENCH PERFORMANCE TEST

Before the experimental test bench is put into service, ensuring its safety and correctness of operation is crucial to achieving the expected research goals. Testing the performance of the test bench can also identify any deficiencies, which can serve as a reference for improving the design. In this chapter, the performance of the test bench is tested in combination with practical applications.

4.1 Communication Function Test

4.1.1 PM5430 Power meter Communication Test

The communication test is necessary to ensure that the MGCCP host computer can communicate with the power meter through TCP/IP protocol. First, open a command window and send data packets to the power meter's IP address 192.168.0.2 via 'ping' command. It will then show how long it took to transmit data and receive a response. As shown in Figure 4.1, the communication time between host computer and the power meter is 1ms without data losses.



```
Invite de commandes
C:\Users\ProtoMG>ping 192.168.0.2

Envoi d'une requête 'Ping' 192.168.0.2 avec 32 octets de données :
Réponse de 192.168.0.2 : octets=32 temps=1 ms TTL=255
Réponse de 192.168.0.2 : octets=32 temps<1ms TTL=255
Réponse de 192.168.0.2 : octets=32 temps<1ms TTL=255
Réponse de 192.168.0.2 : octets=32 temps<1ms TTL=255

Statistiques Ping pour 192.168.0.2:
    Paquets : envoyés = 4, reçus = 4, perdus = 0 (perte 0%),
    Durée approximative des boucles en millisecondes :
        Minimum = 0ms, Maximum = 1ms, Moyenne = 0ms

C:\Users\ProtoMG>
```

Figure 4.1 Communication Time between Host Computer and PM5430

In LabVIEW, using the “Highlight Execution” function is necessary. This allows the user to immediately see whether the communication is successful without waiting for the entire program to finish running. As indicated by the arrow in Figure 4.2, there are no error in the communication part of the program. If the communication fails, the classic 56 timeout error will appear in the message window.

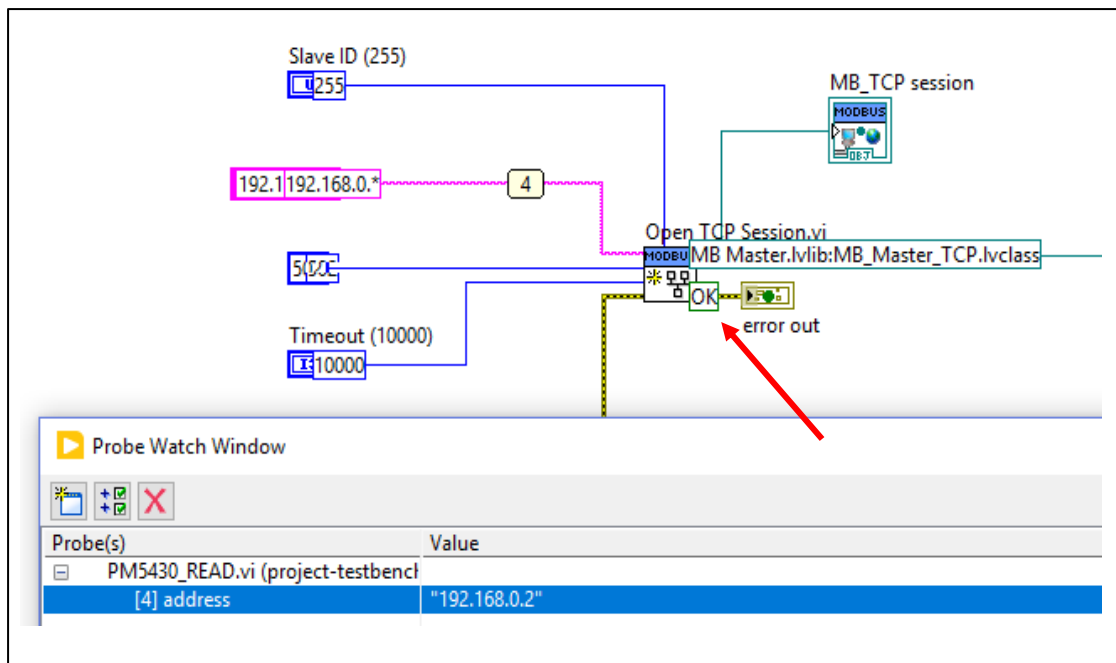


Figure 4.2 Communication Test of PM5340 Power Meter

4.1.2 Chroma 63480 AC/DC Load Communication Test

The communication test of the Chroma load 63804 follows a similar procedure to that of the power meter. The first step is to verify whether the GPIB can communicate with the host computer. The advantage of GPIB-ENET/1000 is its Web page-based configuration function. The fixed IP address has been set since testbed No.1, and to display the configuration interface (Figure 4.3), simply enter its IP address (192.168.0.4) in the browser’s address bar.

GPIB-ENET/1000 Configuration

General Settings

Changing settings may require the device to be removed and reconfigured on the host system.

Hostname: NIENET18D75BB

Static IP Configuration:

IP Address: 192.168.0.4

Subnet Mask: 255.255.255.0

Default Gateway: 192.168.0.1

Primary DNS Server:

Secondary DNS Server:

Comment

63 characters remaining

Save Revert

NATIONAL INSTRUMENTS

Details

General

Model: GPIB-ENET/1000
 Serial #: 18D75BB
 Hostname: NIENET18D75BB
 IP Address: 192.168.0.4
 MAC Address: 00:80:2F:15:5B:85

Firmware

Current Version: 1.2.0f0 | [Update](#)

Status

Device Status: Running
 User Status: You are not logged in | [Log In](#)

Figure 4.3 GPIB-ENET/1000 Configuration Web Page

Since LabVIEW communicates with GPIB via VISA application, it is necessary to know the VISA resource name, which is similar to an IP address in TCP/IP protocol. Before looking up the VISA resource name of the load pack, it is important to number the loads through their control panel in the front of the loads, which is also called primary address. Although only three loads are picked up in this test bench, in order to accommodate the other three loads in the future research, the primary address set in the testbed 1 is maintained. As aforementioned, in parallel mode, only the VISA resource name of the master device must be recognized.

LabVIEW's NI Measurement and Automation Explorer (NI MAX) Application Programming Interface (API) could retrieve this information. As illustrated by Figure 4.4, the VISA resource name of the master load is GPIB0::1::INSTR. The program should choose this name before executing. The system successfully incorporated the detailed load pack information, which can be seen in Figure 4.5.

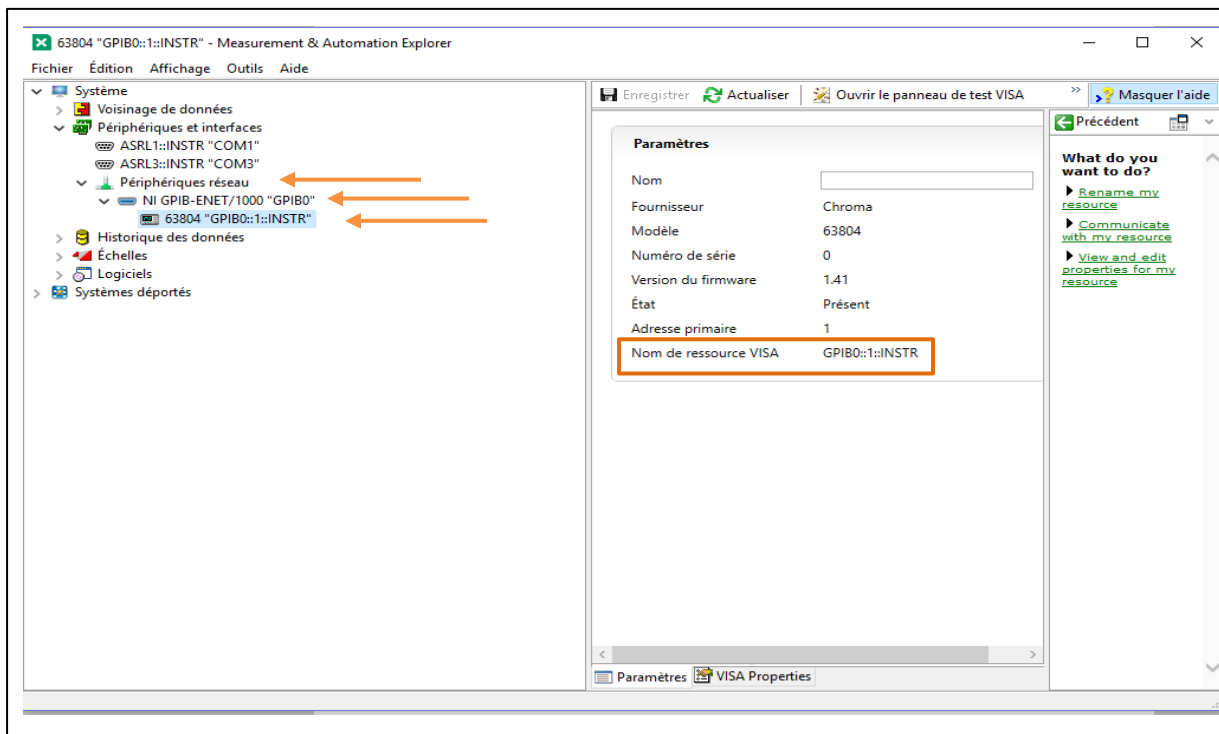


Figure 4.4 Master Chroma Load information from NI MAX

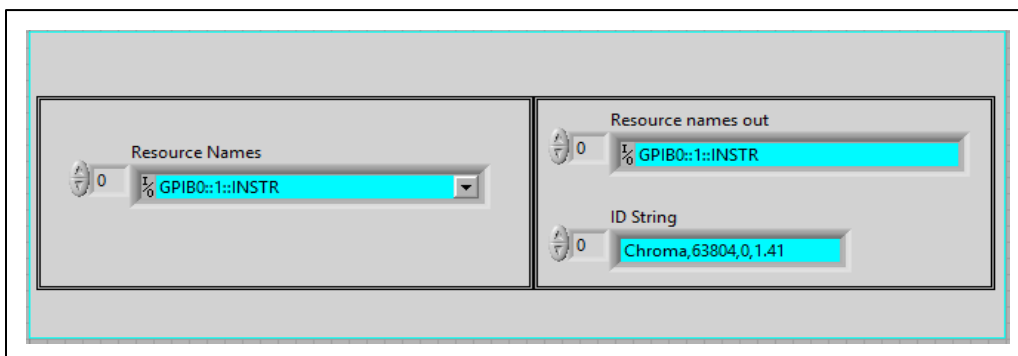
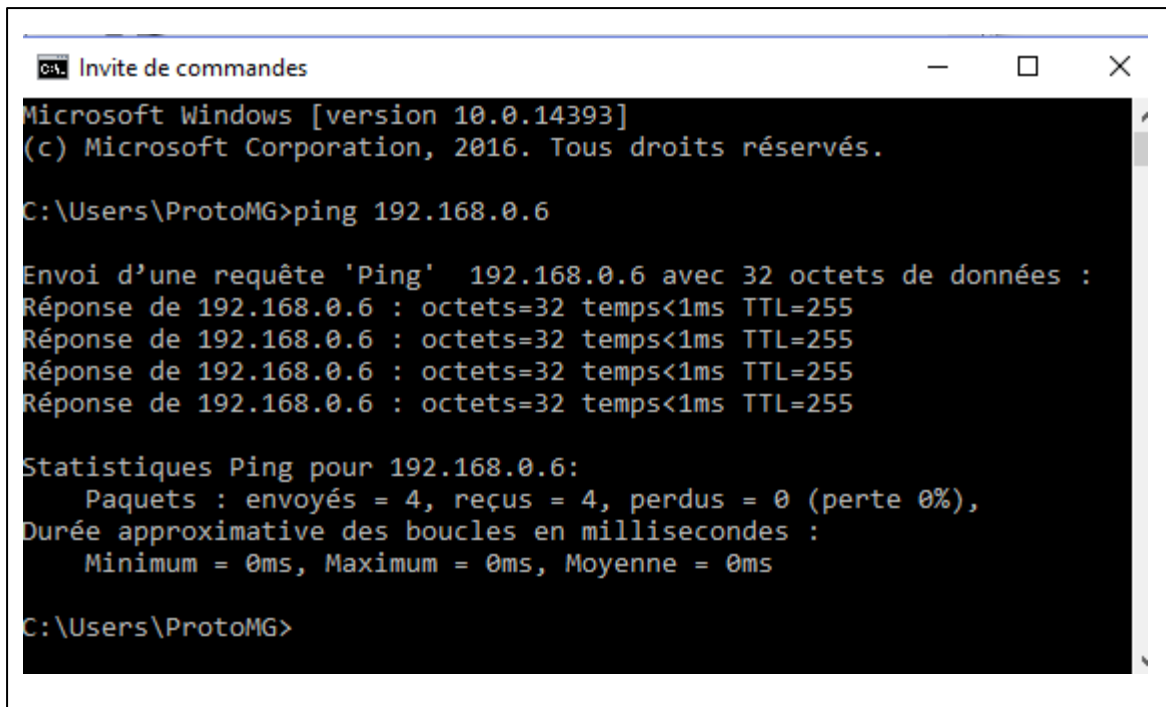


Figure 4.5 Reading load information from LabVIEW

4.1.3 XW Pro 6848 NA Inverter Communication Test

The XW Pro inverter employs the same communication method as the PM5340 power meter; hence, the same approach has been used. Using the 'ping' command to verify connectivity between both the host computer and the Conext gateway, whose IP address is 192.168.0.6, is fairly successful. As shown in Figure 4.6, the connection time is less than 1 ms with no data losses. After running the programme in LabVIEW, no connecting errors are present in Figure 4.7.



```
Invite de commandes
Microsoft Windows [version 10.0.14393]
(c) Microsoft Corporation, 2016. Tous droits réservés.

C:\Users\ProtoMG>ping 192.168.0.6

Envoi d'une requête 'Ping' 192.168.0.6 avec 32 octets de données :
Réponse de 192.168.0.6 : octets=32 temps<1ms TTL=255
Réponse de 192.168.0.6 : octets=32 temps<1ms TTL=255
Réponse de 192.168.0.6 : octets=32 temps<1ms TTL=255
Réponse de 192.168.0.6 : octets=32 temps<1ms TTL=255

Statistiques Ping pour 192.168.0.6:
    Paquets : envoyés = 4, reçus = 4, perdus = 0 (perte 0%),
Durée approximative des boucles en millisecondes :
    Minimum = 0ms, Maximum = 0ms, Moyenne = 0ms

C:\Users\ProtoMG>
```

Figure 4.6 Communication Time between Host Computer and XW Pro Inverter

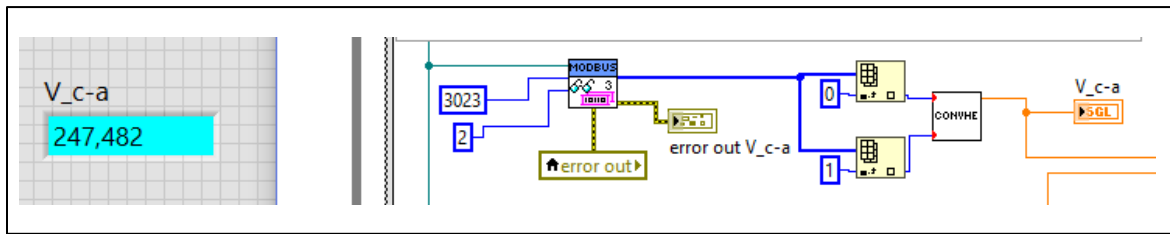


Figure 4.8 Grid Voltage Read from PM5340 in LabVIEW



Figure 4.9 Grid Voltage Read from HMI

Table 4.1 Observation results of grid voltage at HMI and LabVIEW

	LabVIEW	HMI
Grid voltage	247.482V	247.48V

Table 4.1 shows that the grid voltage collected by the LabVIEW is 247.482V, while the number on the power meter's HMI screen is 247.48V. There is a difference of 0.002V between the two readings (Figure 4.8 and Figure 4.9) due to the display precision. Obviously, LabVIEW program is able to obtain the measurements from the power meter in real-time. Another

example is shown in Figure 4.10 and Figure 4.11. The readings of frequency are both 59.99Hz (Table 4.2).

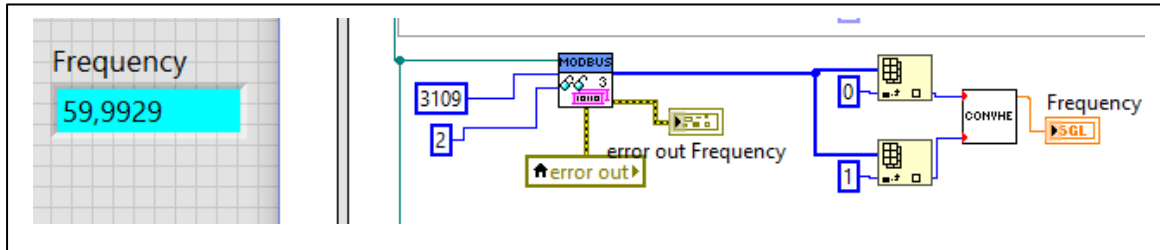


Figure 4.10 Grid Frequency Read from LabVIEW



Figure 4.11 Grid Frequency Read from HMI

Table 4.2 Grid Frequency Reading from HMI and LabVIEW

	LabVIEW	HMI
Grid Frequency	59.9929Hz	59.99Hz

4.2.2 Chroma 63804 AC/DC Load Test with Constant Power Mode

According to the research on the MG control strategy served by this test bench, the Chroma 63804 will only be used to operate in the AC mode and constant power mode. Therefore, several related parameters need to be set in advance such as AC mode, CP mode, operating power and maximum current limit value. As indicated by Figure 4.12, the required power is 1.5kW and the maximum current is limited to 10A.

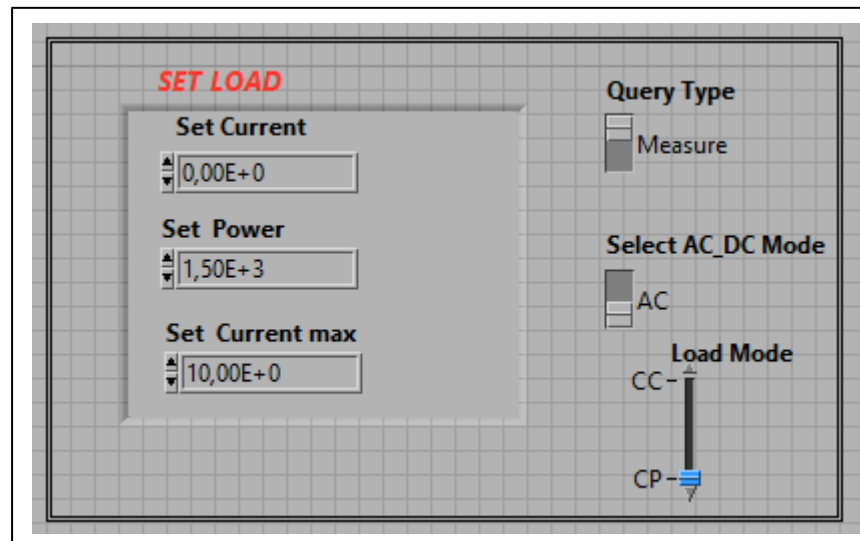


Figure 4.12 Chroma load configuration in LabVIEW

The data transmission test of the load pack still uses the same method as the previous power meter test, which is to compare the actual data of the HMI with the data obtained by LabVIEW. Three main monitoring data are shown in Figure 4.13 and Figure 4.14.

According to Table 4.3, the load voltage is 247.79V, the load current is 6.05A, and the load power is 1497.81W. The data displayed by both devices are in perfect agreement and the data transfer is successful and accurate in real time.

The power reading shows that there is a 0.146% error between the actual power output of 1497.81W and the set power of 1500W. According to the equipment manual, the accuracy of Chroma load is 0.2% +0.3% F.S. Hence, this 0.146% error is within the acceptable range.

During the equipment testing period, there were several cases where the power error was greater than 0.2%. After repeated experiments, the conclusion is that most of this situation occurs after continuous long-term testing. This device supports real-time refreshing operations, which allows users to reset the measurement of Chroma load in their program after a certain amount of testing time.

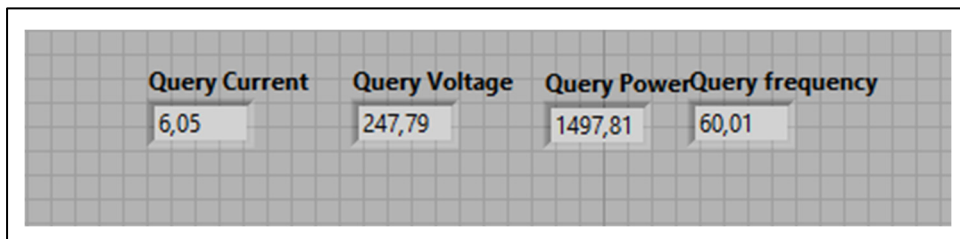


Figure 4.13 Chroma Load Pack Measurement via LabVIEW



Figure 4.14 Chroma Load Pack Measurement via Control Panel

Table 4.3 Chroma Load Pack reading from HMI and LabVIEW

	LabVIEW	HMI
Load Voltage	247.79	247.79V
Load Current	6.05A	6.05A
Load Power	1497.81W	1497.813W

4.2.3 XW Pro Inverter Test and Validation with Conext Gateway interface

The verification method for the inverter is simpler and more intuitive, thanks to the powerful Conext Gateway. This gateway has a user-friendly interface and a sophisticated control webpage via the address 192.168.100.1, which provides the possibility to configure the XW Pro 6848 inverter, manage, and monitor its behavior. Its wireless networking capability is used to exchange information with the host computer. There are two main reasons for choosing the Wi-Fi: first, the host computer is only equipped with two Ethernet cards - one is used to connecting to the external network, and the other is applied to build the MG LAN. Secondly, there is only one Ethernet port on the gateway side, which is already occupied to access the LAN. If this connection is also employed to open the control page, it will cause unpredictable communication congestion. When the MGCCP is in the process of running and debugging, there might be some doubts about whether the inverter is functioning properly. At this time, it is necessary to confirm the status of the converter and eliminate the possible error sources through the control system of the gateway. In addition, it is vital to recognize that this gateway is also compatible with Conext MPPT 60, which will be significant for upcoming research once MPPT has been implemented.

As discussed in the preceding chapter 3.1.1.4, the initial setting file is executed and goes into effect when the control system reaches the initial state during start-up. It is possible to directly observe whether the parameter values were satisfactorily written into their corresponding registers. An instruction to read the assignment of this register is added after each write

command in the initial configuration program. The written values are on the left, while the read results are on the right, as depicted in Figure 4.15. Furthermore, these preferences can be displayed through the gateway interface in order to carry out double verification. The data selected by the boxes in Figure 4.16 are completely consistent with the results obtained in the LabVIEW program, and it can be determined that the static data exchange test between the inverter and the host computer is successful.

INPUT	OUTPUT
Bulk voltage set point 0 60000	Bulk voltage set point 60 V
Recharge Voltage 0 50400	Recharge Voltage 50,4 V
Low battery cut out 0 48000	Low battery cut out 48 V
Low Battery Cut Out Hysteresis 0 2000	Low battery cut out hysteresis 2 V
High battery cut out voltage 0 60000	High battery cut out voltage 60 V
Grid Support Voltage 0 51000	Grid Support Voltage 51 V

Figure 4.15 XW Pro Inverter Initial Configuration in LabVIEW

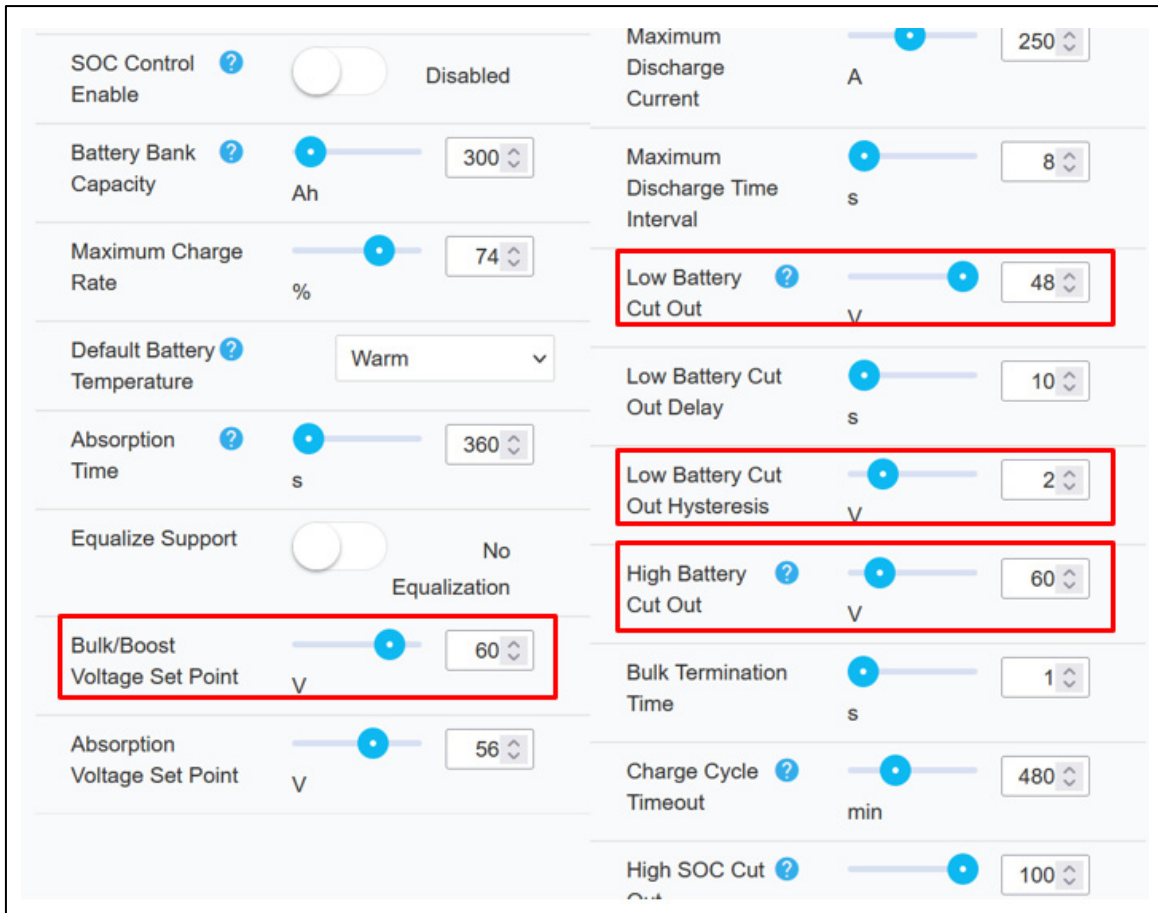


Figure 4.16 XW Pro Inverter Initial configuration displayed in Gateway Interface

To conduct the dynamical data transfer test, the XW Pro Read-Write program in LabVIEW should be started under the battery sell-to-grid mode and run at full strength, which is 6.4kW. Figure 4.17 represents the discharging graphical dashboard and the real-time discharging power in the Gateway webpage. More detailed information is exemplified in Figure 4.19. Additionally, Figure 4.18 shows the data provided in LabVIEW, which is consistent with the results obtained from Gateway.

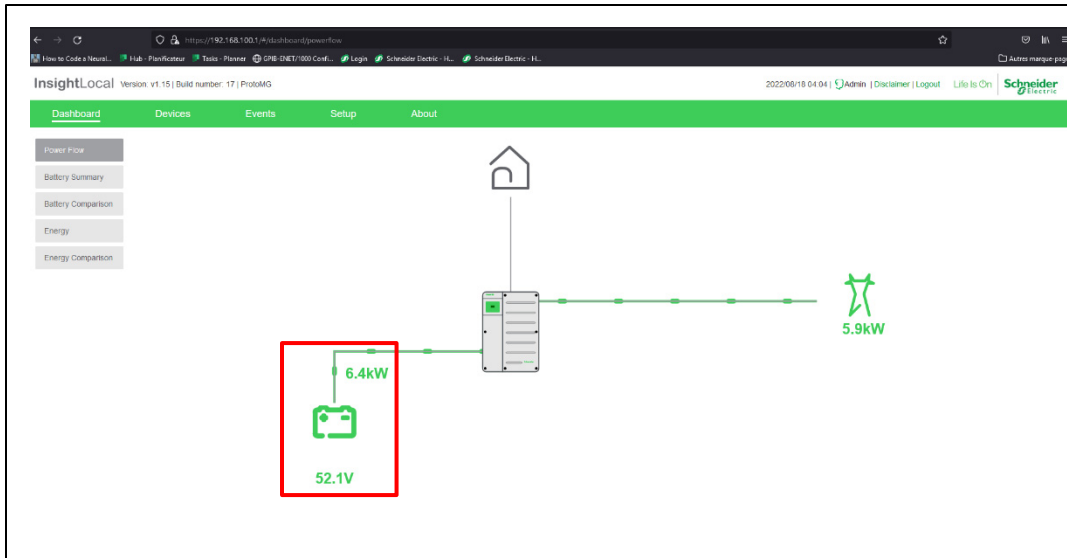


Figure 4.17 XW Pro Inverter Sell-to-Grid with 6.4kW showing in Gateway

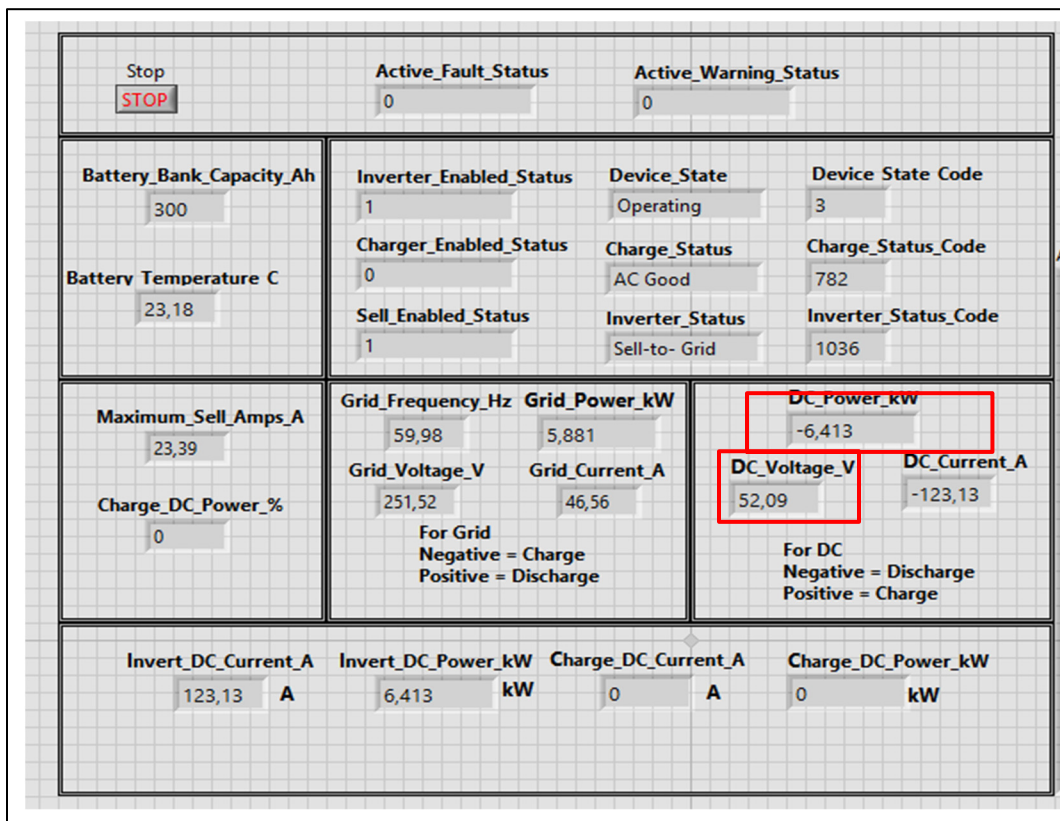


Figure 4.18 XW Pro Inverter Sell-to-Grid with 6.4kW showing in LabVIEW

	Modbus Slave Address
(Port 502)	10
Device Present	Active (data valid)
Modbus Slave Address (Port 503)	10
Inverter Enabled Status	Enabled
Charger Enabled Status	Disabled
Sell Enabled Status	Enabled
Device State	Operating
Inverter Status	Sell-to-Grid
Charger Status	AC Good
Active Faults	No Faults
Active Warnings	No Warnings
Battery Association	House Battery Bank 1
DC Voltage	52.1 V
DC Current	-123.1 A
DC Power	-6413 W
Battery Temperature	23.20 °C
Charge Mode Status	Primary
AC1 Association (Grid)	Grid 1
AC1 Active Power	5876 W
AC1 Frequency	60 Hz
AC1 Voltage	251.4 V

Figure 4.19 XW Pro Inverter Sell-to-Grid with more information showing in Gateway

Table 4.4 Comparison of battery pack voltage and discharge power in both LabVIEW and Gateway interface

	LabVIEW	Gateway
Battery Pack Voltage	52.09V	52.1V
Discharge Power	6.413kW	6.4kW

4.3 System Operation Test

After several trials of each hardware devices, test bench No. 2 is ready to launch the overall debugging test. In furtherance of verifying the correctness of the improved peak load shaving optimization algorithm, which is written in Python separately and called by LabVIEW Python Integration Toolkit.

Hence, the configuration of this test is listed below:

- Mode: Past simulation with perfect prediction
- Date: 2019-09-08
- Time slot: 10h11mins - 12h19mins
- Time ratio: 1.5
- Power ratio: 500
- SOC_min: 82%
- SOC_max: 100%
- SOC_virtual_int: 100%
- Power set point: 5000kW

4.3.1 Test Condition and Set Up

The system test has two primary goals: to determine whether the MGCCP can behave correctly and whether the devices can coordinate the required operation. Therefore, the test conditions should be simplified as much as possible to minimize the interference factors and facilitate faster problem identification after the test.

4.3.1.1 Test mode selection

In this system test, the same operating modes are used as in the simulation. At this stage, there are seven test modes, namely: past simulation with perfect prediction, past simulation with 24h and 2h neural network prediction, past simulation with 24h and 2h neural network prediction

and correction, real time simulation with 24h and 2h neural network prediction, real-time simulation with 24h and 2h neural network prediction and correction, and manual control. Currently, the past simulation with perfect prediction mode is active since a fixed value of 5000 kW has been assigned to ETS power consumption forecasting setpoint, which is the minimum billing demand for large-power customers by Hydro Québec.

4.3.1.2 Test Date selection

As Covid-19 is expected to have a significant effect on ÉTS power consumption post-2020, with consumption levels anticipated to be lower than in previous years, 2019 will serve as the test year. It is essential to maintain a focus on minimalism during the early phases of system testing and to ensure that the power usage on the selected test date is below 5000 kW. The actual test has been administered on September 8, 2022, and as September 8, 2019, was a Sunday, it satisfies the test requirements.

4.3.1.3 Power ratio determination

In this study, the mini-power MG testbed is reduced by a factor of 500 compared to the ÉTS campus, which is also frequently alluded to as the power ratio. This parameter plays a crucial role in the selection of equipment, including battery size, inverter rating power, and the potential installation of solar panels. When conducting experiments, the actual amount of power being measured is known as “real power” with the unit of kW. Represented power reflects the ÉTS consumption power in a real situation. For the purpose of testing, a power ratio of 500 is used to step down a 6750kW ÉTS power to 13.5kW, which is the total power of three Chroma loads. The mathematical expression for this can be found in Equation 3.2 in Chapter 3.

4.3.1.4 Time ratio determination

The time ratio is solely used for the purpose of shortening the amount of time required for experimental tests by making use of historical data. Its general form has been clarified in Equation 3.3, and will not be restated here. The primary focus is on developing a method for determining the appropriate time ratio to be utilized in various test scenarios. In practise, the amount of time that the energy storage system can discharge at full power can be estimated by dividing the battery bank's capacity by the represented inverter power (Equation 4.2). Due to the limitation of the rated characteristics of the battery bank and the inverter on the experimental platform, the discharge time that the battery bank may be discharged sustainably while the inverter is operating at full capacity is shown in Equation 4.3. By dividing the two, the time ratio that can be applied to accelerate the test is obtained in Equation 4.1:

$$R_t = \frac{T_{real}}{T_{test_bench}} = \frac{C_{BESS_ETS}}{P_{inv_rep}} \cdot \frac{P_{inv_max}}{C_{bat_test_bench}} \quad (4.1)$$

Where,

$$T_{real} = \frac{C_{BESS_ETS}}{P_{inv_rep}} \quad (4.2)$$

$$T_{test_bench} = \frac{C_{bat_test_bench}}{P_{inv_max}} \quad (4.3)$$

The BESS has a capacity of 2000 kWh, and the battery bank has a capacity of 15.2 kWh. Besides, the maximum operation power and the represented power are 6 kW and 500 kW, respectively. Inserting these values into Equation 4.1 yields a time ratio of 1.57895, rounded up to 1.5 for the accelerated test.

4.3.1.5 SOC associated parameter identification

It is typically necessary to take into consideration the charge-discharge SOC of the battery as well as the limit of the charge-discharge power in order to make confident that the battery will function in the most efficient and cost-effective manner possible. In practical application, charging and discharging the battery is often prohibited when the SOC approaches the critical limit. When the SOC does not reach the critical limit, the charge and discharge power is restricted to a range determined by the battery's rated capacity and the inverter's rated power. As a result, in order to satisfy both the power fluctuation needs of the grid-connected system and the SOC requirements of the BESS, the power restriction must be determined in line with the battery charging and discharging requirements.

Excessive charging or discharging can permanently damage the BESS, especially for lithium batteries, which could seriously affect their service life. Therefore, it is necessary to quickly determine the SOC of the BESS device.

According to the charge voltage vs SOC chart (Figure 4.20) from the Solacity company website (Beckers, 2022), when the percentage of SOC of the LPF battery is somewhere between 20% and 90%, the power characteristic is at its optimum and the battery's internal resistance is at its lowest level. When the SOC falls below 20%, the open circuit voltage decreases, the working voltage drops below the rated voltage value, and the internal resistance is relatively high. Lithium deposition is a common occurrence inside the battery. The discharge voltage vs SOC chart of the SimpliPhi battery bank is listed in Figure 4.21 (SimpliPhi Power, 2021).

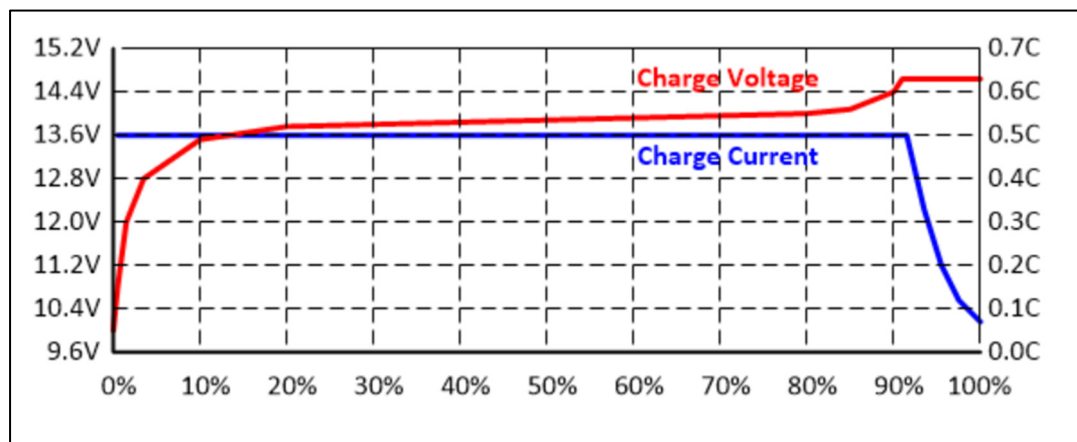


Figure 4.20 LiFePO4 Charge Voltage vs. SOC
Taken from Beckers (2022)

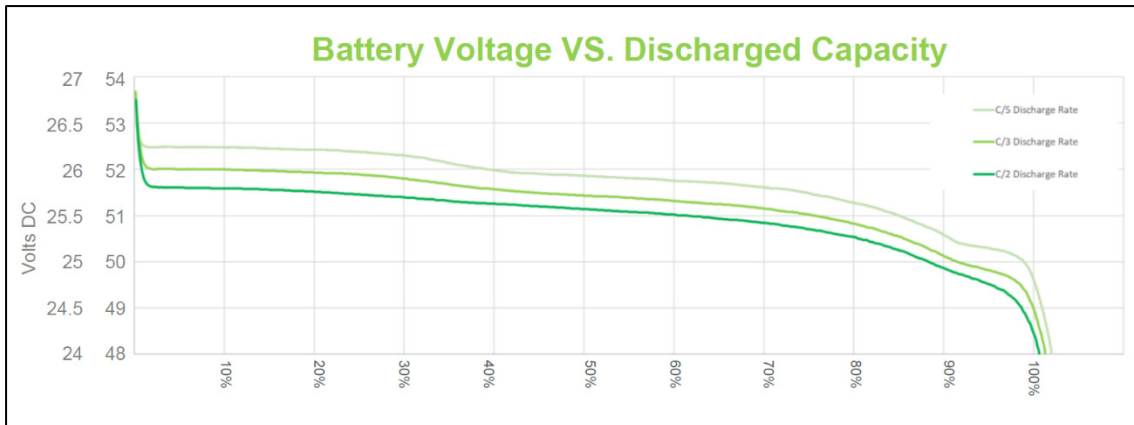


Figure 4.21 SimpliPhi Battery Discharge Voltage vs SOC
Taken from SimpliPhi Power (2021)

The SOC of the LFP battery can be split into five sections due to the powerful function of the inverter: the forbidden charging area, the SOC start delay area (the charging warning area), the normal working area, the SOC stop delay area (the discharging warning area), and the forbidden discharging area. In the current testbed, only three non-delay areas are employed. In the future, when BMS monitoring device is installed, all five areas can be implemented.

The discharge power setpoint must be changed when the battery pack is allowed to discharge but the SOC is in the restricted discharge region (less than or equal to 20%):

$$P'_{dis_inv} = P_{dis_inv} \cdot \max\{0, SOC_{bat} - SOC_{min}\} \quad (4.4)$$

Here, SOC_{min} is equal to 0.2 and SOC_{bat} is less than 0.2, so that the discharge power setpoint becomes 0.

The same procedure is applied to the charge power setpoint:

$$P'_{cha_inv} = P_{cha_inv} \cdot \max\{0, SOC_{max} - SOC_{bat}\} \quad (4.5)$$

Due to the time-accelerated nature of certain tests, a virtual SOC must be implemented here. From a programming perspective, it is feasible to accelerate the program's operation. However, none of the experimental equipment on the test bench can pass the accelerated test in normal operation conditions, as the power required for this kind of operation is considerably more than their rated power. The portion of the power that exceeds the rated power of the test bench could be transferred to the higher consumption of the BESS's SOC. In other words, the test bench is operating normally, and the virtual SOC will decrease more than the actual measured battery bank SOC during the acceleration test. The calculation equation of the virtual SOC is developed by Nicolas Mary in 2022:

$$SOC_{virtual} = SOC_{max} + \frac{SOC_{bat} - SOC_{max}}{SOC_{max} - SOC_{min}} \quad (4.6)$$

Where,

$$SOC_{min} = SOC_{max} - \frac{C_{Bess_ETS}}{C_{bat_test_bench}} \quad (4.7)$$

Normally, ÉTS doesn't have a significant nighttime need for electricity. The battery bank can be fully charged overnight, as evidenced by past statistics on energy use; hence SOC has initially been set to 1, which means:

$$SOC_{Max} = SOC_{virtual_int} = 1 = 100\% \quad (4.8)$$

Under the assumption that the time ratio is 1.5 and the power ratio is 500, the usable portion of the SOC during the accelerated test can be determined using the following equation:

$$SOC_{available} = \frac{C_{BESS}}{R_t \cdot R_p} = 17.5439\% \tag{4.9}$$

Therefore, from Equation 4.7:

$$SOC_{min} = 82.4561\% \tag{4.10}$$

4.3.2 Test result

The test was carried out on last September 8th last year. The actual running time of this test was one and a half hours, during which a total of 9785 pieces of data were collected. Due to the overwhelming amount of data, it is difficult to observe and analyze the full data graph. Thus, only the power change within the first 20 minutes is illustrated in Figure 4.22.

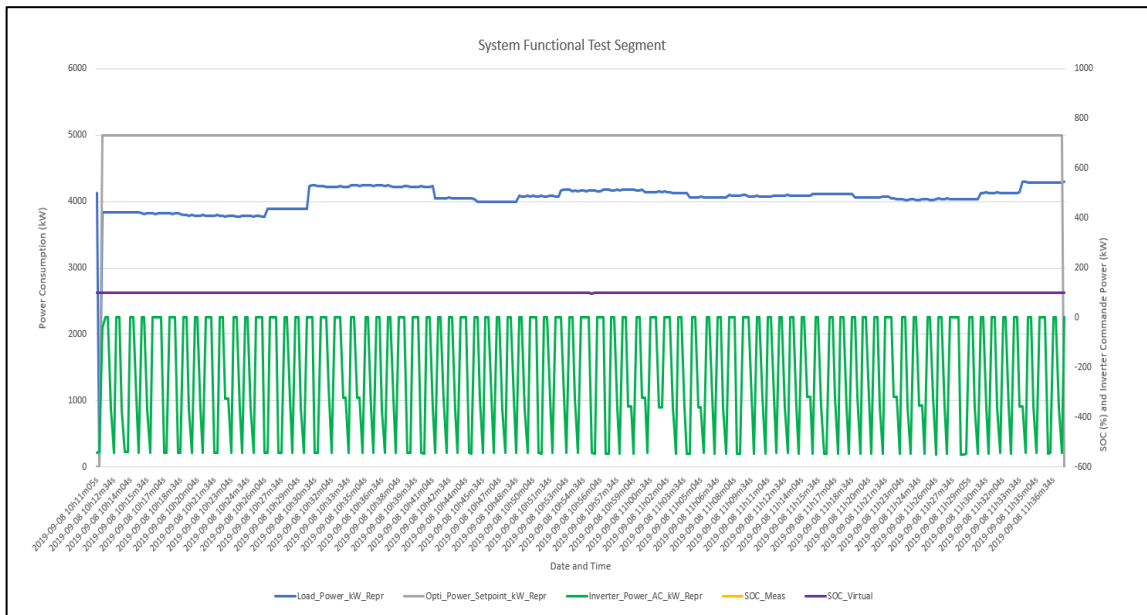


Figure 4.22 System Functional Test Result Segment

4.3.2.1 Load Power and Grid Power Consumption

The yellow curve represents the load power. It is evident from the graph that the load achieves the required 3840kW during the first 30 seconds of the system operation, which are the initial and transitional stage. The Chroma load pack is able to remain the required power, and the accuracy is 99.9%, as demonstrated by the straight line in the graph. This also proves that the load pack is functioning as expected.

The grid power, depicted in the figure as a small triangular wavy form, is represented by the pink curve. It is noticeable that the grid power increases while battery charging and drops in battery discharge. The grid power is the sum of the load power and the battery power, as shown in Equation 4.11, and the mean power red curve indicates that the power usage is remaining in the 4000kW level.

$$P_{grid_power} = P_{inverter} + P_{load} \quad (4.11)$$

4.3.2.2 Battery Bank Charging and Discharging Oscillation

The light green curve, the khaki curve, and the light blue curve represent AC command power of the inverter, SOC_{bat} , and $SOC_{virtual}$, respectively. Negative values indicate the discharge process, while positive value indicate the charging process.

The experimental results exhibit obvious data oscillations, which is mostly manifested primarily in the inverter-controlled battery pack's continuously switching between its charging state and grid support state. The main cause for this phenomenon is that the battery bank has the authorization to charge since the load power consumption throughout the test period was less than the minimum billing demand of 5000kW, which means that the load power is less than the power setpoint. When the system is first turned on, the SOC_{max} is set to 100%, which is that the battery is fully charged. Given that the inverter is currently configured for grid support mode, the battery bank is slowly draining. Then, the control center would issue an

instruction to charge the battery when the program detects that the SOC is less than 100% so that the battery is permitted to charge. Since the battery was only depleted by a fraction of 1%, the SOC quickly returns to 100%, and the battery is once again completely charged. The consequence of this repeated process is the oscillations in the grid power.

A possible solution to this problem is to increase the robustness of charging SOC in the optimization algorithm strategy. This means that, according to the discharge cycle of the battery in grid support mode, the time required to reach a specific battery voltage can be estimated and it can be converted into SOC, which becomes the new condition for allowing charging. Another option is to specify a qualifying time interval to allow the battery pack to charge. This approach can considerably minimize the oscillation of the power waveform while simultaneously ensuring that the inverter doesn't become overburden. However, this method requires a more sophisticated optimization algorithm and more accurate SOC measurement.

There have been many attempts to improve the situation, but the outcomes have not been particularly successful. Even though certain tests have the potential to effectively lower the oscillation amplitude, this does not alter the inverter's constantly switch from two status. Finally, there is a way to limit charging and discharging based on the voltage range, which also successfully flattened the curve and eliminated oscillation. Since the battery bank and inverter were installed, a number of charging and discharging tests have shown that the battery does not require charging and can constantly provide energy into the grid with litter power consumption in grid support mode while the battery voltage between 53 and 56 volts. As mentioned before, the normal voltage for a single battery is 53V. When the battery voltage is less than 53V, charging is permitted. 56V is the float charge setpoint, so the charging process could not be guaranteed when the battery voltage is greater than 56V. when the battery voltage is within the range of 53 and 56V, Grid support mode is active, and the battery bank starts to discharge for days. Therefore, a case structure has been added to the MGCCP. The true case and false case LabView program are shown below:

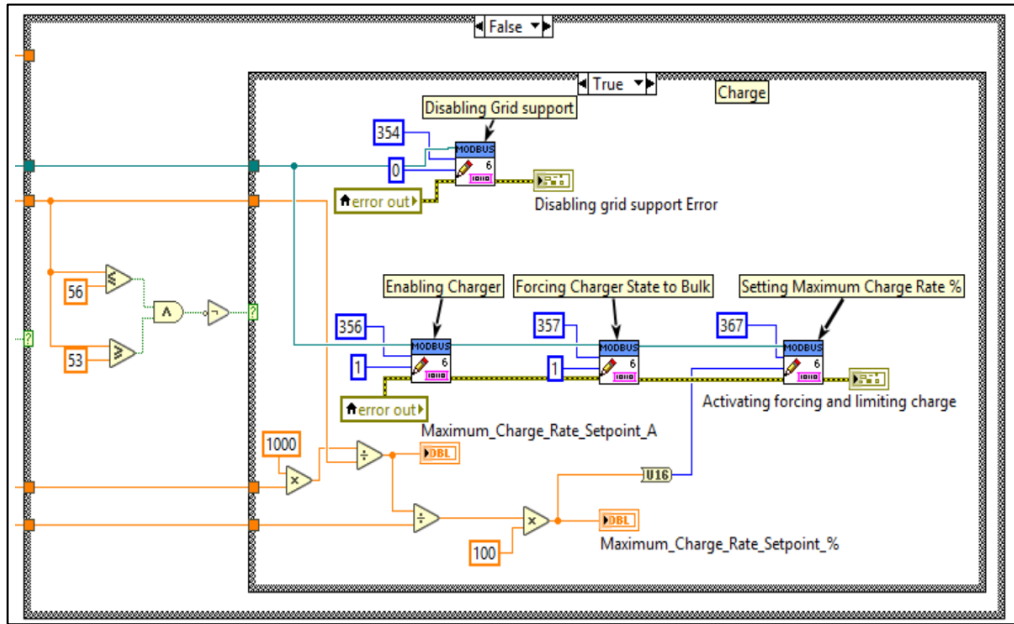


Figure 4.23 Charging when DC voltage is out of the required range

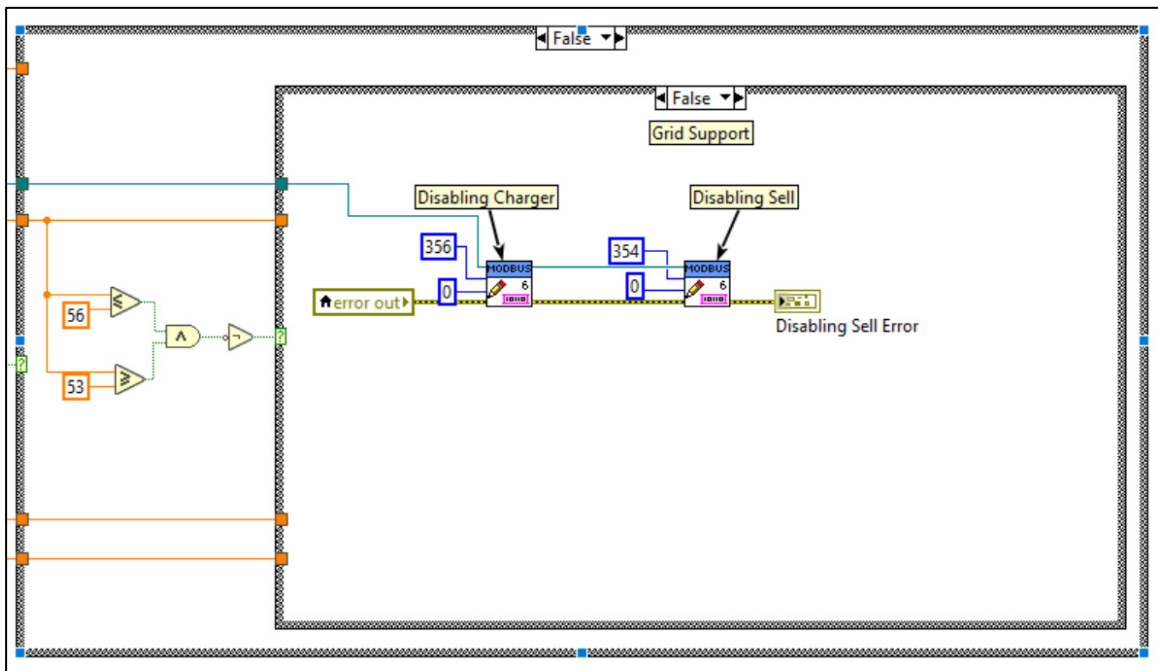


Figure 4.24 Discharge with DC voltage less than 53V

Figure 4-25 presents the results of the tests conducted on the upgraded MG system (only 20 minutes of results are shown here). Based on this figure, it is not difficult to see that the power of the inverter is constantly positive with an average value of 1.389kW. Additionally, the inverter is continuously operating in grid support mode, As the SOC decreases, there is no longer data oscillation or the inverter is not constantly cycling between charging and discharging states. The grid average curve (red), the grid power curve (violet), and the load power curve (orange) all tend to be steady straight lines.

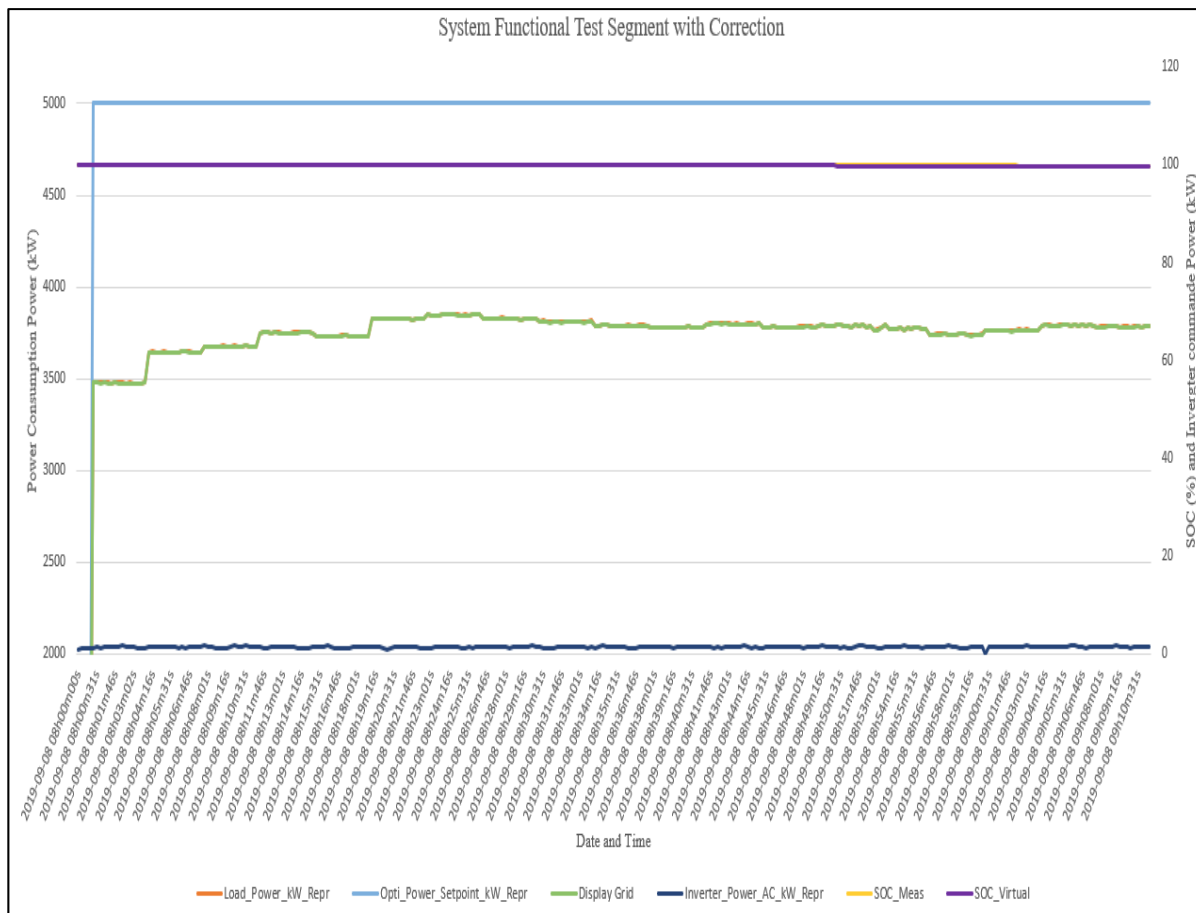


Figure 4.25 Sunday, September 8, 2019, the operating curve of the MG test bench

4.4 Chapter Summary

This chapter focuses on the functionality of each component on the experimental test bench separately, followed by an assessment of the entire system. Communication tests focus on the connectivity between the host computer and the equipment, whereas data transceiver tests examine the precision of the transmitted and received data as well as the register address validation. The outcome of the system test indicated that all devices function as expected and that this test bench and its MGCCP are completely prepared for further control strategies tests.

CHAPTER 5

VALIDATION AND VERIFICATION OF CONTROL STRATEGIES TEST RESULTS

In this chapter, a grid-connected campus MG model is established based on the constructed MG experimental test bench, and validation tests are conducted by adopting specific dates in 2019. This model is optimized using Nicolas' algorithm which combines the artificial neural network (ANN), and also an economic dispatch plan is provided to guarantee the MG's economical, secure, and stable operation. According to the energy management strategy and the establishment of the historical power consumption database, the output and load demand of batteries at each time period is determined, and the power setpoint is optimally scheduled. The objective is to verify the optimal algorithm's ability to reduce the extra cost on electricity bills.

5.1 Energy Management Control Architecture

The energy management control system shown below was originally created by Nicolas and includes four primary parts: DAS, artificial neural network forecasting, optimization algorithm, and real-time control (Mary, 2022).

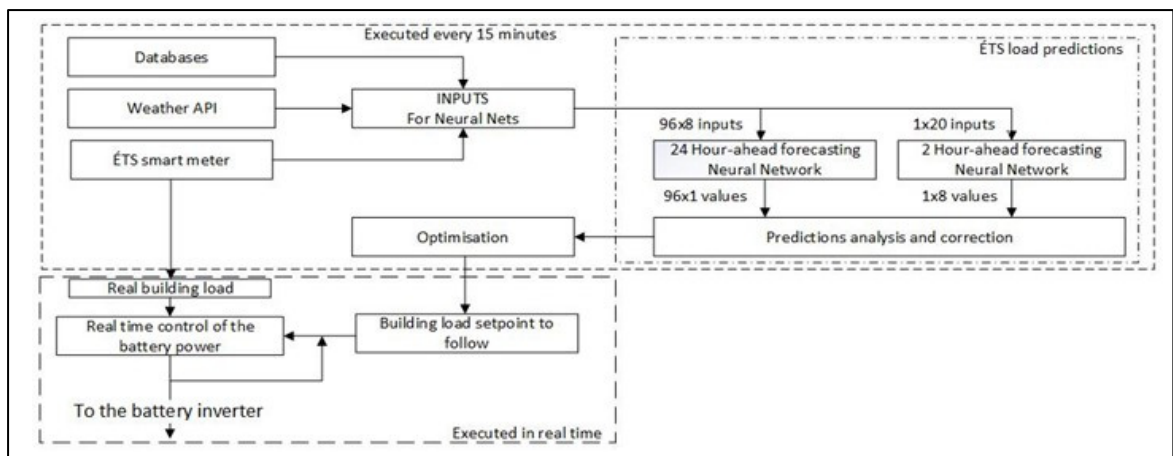


Figure 5.1 Energy Management System, Taken from (Mary, 2022)

5.1.1 Neural network input data

Meteorological conditions frequently reflect the variability of MG load predictions. The ups and downs of power consumption are also significantly impacted by climatic factors, such as seasonal shifts. Each season has distinct characteristics, extreme weather conditions like high and low temperatures, heavy rain, blizzards, etc., can cause significant fluctuations in the MG load demand, making load forecasting questionable. Therefore, accurate meteorological information, especially temperature, is essential for making correct predictions. Temperature data is obtained online at Visual Crossing API ([Historical weather data for any location | Visual Crossing](#)), as a result, users are able to create a dataset with one temperature reading per hour since January 1, 2016. This API is called once a day, and it updates the temperature database on the server with data from the previous day.

The ÉTS historical power consumption database is generated by Nicolas and supplemented by Yohann (Geli, 2021). LabVIEW's database collection is accessible via Dr. James Powel's SQLite Library, which is available for free through the VI Package Manager. The software logs data information every 10 seconds.

The Schneider Electric PM8000 meter installed at the ÉTS electrical network's main entry has been connected through Modbus to continue feeding the real-time power usage database. This meter maintains a register that provides Modbus access to the average power over the previous 5 minutes. To update the neural network predictions in real time, it is crucial for avoiding any gaps in the database.

However, external factors like signal interference, power outage, etc., during the conversion and transmission process after the power meter collects load information, may cause missing data, leading to discontinuity and affecting the accuracy of load forecast. Consequently, linear programming is required to address such situations, as mentioned in the thesis of Yohann (Geli, 2021).

5.1.2 MG Load Power Forecasting

Load forecasting is typically divided into four distinct subfields based on the varying time horizons over which predictions, as outlined by V. Y. Kondaiah in 2022:

- 1) Long-Term Load Forecasting (LTLF). LTLF predicts load five or more years into the future, and the forecast results are typically used for the construction planning of the power grid, which is largely attributed to the national energy policy and is predominantly used for the modernization of the power system.
- 2) Medium-Term Load Forecasting (MTLF). MTLF estimates the load from one month to five years in the future, and the outcomes of the forecast are mainly used to determine the operation mode of the generator set and to create maintenance schedules for the equipment.
- 3) Short-Term Load Forecasting (STLF). STLF forecasts the load one day to one week ahead, and the results of these calculations are generally used for economically efficient programming and making short-term unit start and stop plans.
- 4) Very Short-Term Load Forecasting (VSTLF). VSTLF commonly anticipates the load for a few minutes to several hours in the future, and its prediction outcomes are frequently used for real-time condition analysis.

The prediction model presented in this thesis incorporates both STLF and VSTL. Since the power requirements are tallied for 15-minute integration intervals, which matches the metering equipment that has been officially sanctioned by Hydro Québec, a time step of 15 minutes is adopted as the resolution of ANN prediction. A Feedforward Neural Network (FNN) is a traditional NN model, which consists of an input layer, one or more hidden layers, and an output layer. The input layer receives the incoming input signals such as temperature information, ÉTS meter reading, and historical power consumption data, which is then calculated and transferred to the four concealed layers. After the data has been processed in the hidden layers, it will be propagated to the output layer in order to achieve the output result. Therefore, the 24H forecast (STLF) includes 96 steps ahead prediction, which would

encompass the prediction of every 15 minutes for the subsequent 24 hours. Similarly, the 2H prediction (VSTLF) must account for the load forecast every 15 minutes for the next two hours with 8 steps ahead forecast data.

Not only the ANN but also the model predictive control (MPC) is implemented in this study, since it is a crucial area of inquiry for the advancement of control and load forecasting. The use of MPC as the foundational optimization approach in the context of microgrid energy optimization has garnered significant interest in the academic community in recent years. Due to the unpredictability of renewable energy power generation and plug-and-play load power consumption in the scheduling problem, and the necessity to solve optimization problem at each discrete time step, the discovered optimal decision value can be enforced at the subsequent discrete time step.

Mean Error (ME) is a frequently employed criterion for gauging the accuracy of forecasting models in the field of statistical applications, and it has been widely applied as an evaluation criterion for load forecasting activities. Equation 5.1 provides the calculation expressions of ME, which allows for the correction of only the amplitude of the consumption.

The ME formula is given by:

$$e_{ME} = \frac{\sum_{t=1}^m L_{predicted}(t) - L_{real}(t)}{m} \quad (5.1)$$

Here,

$L_{real}(t)$ represents the actual load power, $L_{predict}(t)$ represents the predicted load power, and m represents the amount of load forecasting data. Since correction can be applied after at least 3 times of discrete time steps (45 minutes), the value of m is 3.

Therefore, the load prediction equation for multiple rounds of iterative training is shown in Equation 5.2:

$$L_{corrected}(t + n) = L_{predicted}(t + n) - e_{ME} \quad (5.2)$$

For the 24-hour ahead (24HA) prediction, the range of t values is $1 \leq t \leq 96$. With a combined 2-hour ahead (2HA) prediction, the maximum value of t reduces to 88.

5.1.3 Power Optimization Dispatch Strategy

In a distributed energy storage system, the load forecasting and energy distribution unit determine the charging and discharging interval of the battery based on the load forecasting information, the peak-valley time-of-use price, and the battery's SOC, and then transmits charging and discharging instructions to the inverter. The control of the inverter completes the process of charging and discharging the energy storage battery and realizes the dispatching of the energy storage energy. The specific process is shown in Figure 5.1.

According to Hydro Quebec's LG rate, the peak and valley electricity prices are the same. Since the consumption of electricity in ÉTS is typically lowest during periods of the night, the energy storage system can profitably store electricity without any extra charge. During periods of peak demand, electricity is expensive. To lower the quantity of electricity purchased from the grid, the battery will release the stored energy for immediate usage. Without modifying the electricity consumption behavior of the ÉTS campus, this strategy can lower the power consumption during the high-price period, reduce the bill, and allow the customer to gain the maximum economic benefit.

5.1.3.1 Objective Function

The economics of MG operation is characterized by the minimal power consumption cost, minimum energy storage maintenance cost, and maximum system power generation revenue. The minimum cost in a single operating cycle, and the objective function is shown in Equation (5.3):

$$\min Cost = \sum_{t=0}^{n-1} (Cost_{\acute{E}TS,t} + Cost_{Degradation,t}) \quad (5.3)$$

Subject to:

$$Cost_{\acute{E}TS,t} = (P_{buildings,t} - P_{bat,t}^{Discharge} + P_{bat,t}^{Charge}) \cdot \Delta t \cdot \lambda_{grid} \quad (5.4)$$

$$Cost_{Degradation,t} = C_{degradation,t} \cdot \lambda_{degradation} \quad (5.5)$$

Where,

- $Cost_{\acute{E}TS,t}$ (\$) and $Cost_{Degradation,t}$ (\$) stand for the electricity cost of $\acute{E}TS$ and the maintenance cost of battery, respectively
- $P_{buildings,t}$ (kW) is $\acute{E}TS$ electric power consumption of all buildings at time t
- $P_{bat,t}^{Discharge}$ (kW) and $P_{bat,t}^{Charge}$ (kW) are the battery bank discharge power and charge power at time t, respectively
- λ_{grid} (\$/kWh) and $\lambda_{degradation}$ (\$/kWh) are the price of electricity purchased from the grid and the maintenance price of battery degradation, respectively
- $C_{degradation,t}$ (kWh) represents the capacity lost due to battery degradation at time t
- Δt is the time step of the simulation or the optimization
- Equation (5.4) calculates the electricity cost by multiplying the net energy demand by the electricity rate of Hydro Quebec
- Equation (5.5) calculates the battery's maintenance cost by multiplying the capacity lost due to degradation by the degradation price

As noted in the prior chapter, overcharging and over-discharging the battery will lead to issues including battery performance degradation and capacity reduction, therefore doing so repeatedly will have a negative impact on the battery's life. The SOC is usually used to evaluate the remaining energy of the battery, and its calculation equation is shown in (5.6):

$$SOC_t = \frac{E_{bess,t}}{C_{bat}} \times 100\% = \frac{P_{bess,t} \cdot \Delta t}{C_{bat}} \times 100\% \quad (5.6)$$

Where,

- $E_{bess,t}$ and C_{bat} signify, respectively, the energy stored in the battery energy storage system and the battery's rated capacity
- $P_{bess,t}$ stands for the battery's output power

5.1.3.2 Constraints

$$0 \leq P_{bat,t}^{Discharge} \leq P_{bat,max} \quad \forall t \quad (5.7)$$

$$0 \leq P_{bat,t}^{charge} \leq P_{bat,max} \quad \forall t \quad (5.8)$$

$$SOC_{min} \leq SOC_t \leq SOC_{max} \quad \forall t \quad (5.9)$$

$$SOC_{ini,t} = SOC_{end,t} \quad \forall t \quad (5.10)$$

$$E_{bess,t} = \begin{cases} C_{bess} \cdot SOC_t & , discharge. \\ 0 & , charge. \end{cases} \quad (5.11)$$

$$P_{bat,t}^{Discharge} \cdot P_{bat,t}^{Charge} = 0 \quad \forall t \quad (5.12)$$

$$0 \leq E_{bess,t} \leq C_{bess} \quad \forall t \quad (5.13)$$

Where,

- Constraint (5.7) and Equation (5.8) are charge and discharge power limitations, which means the charging and discharging power should be within the range of the rated power

- SOC_{max} and SOC_{min} represent the maximum and minimum levels of the remaining energy in the battery, respectively
- Constraint (5.9) shows that battery's SOC value should be maintained within the normal charge and discharge range to avoid the profound charging and discharging
- $SOC_{ini,t}$ is the initial SOC and $SOC_{end,t}$ is the SOC at the end of the day
- Constraint (5.10) assures that the initial SOC and final SOC are identical to assuring the next-day operation
- Constraint (5.11) and Constraint (5.12) are for prohibiting simultaneous charge and discharge events, which means at the optimal point, at least one of $P_{bat,t}^{Discharge}$ and $P_{bat,t}^{Charge}$ is always zero
- Constraint (5.13) defines that $E_{bess,t}$ is equal to the battery rated capacity when it is fully charged, and it is equal to 0 when the battery is deep discharged

5.1.3.3 Charge and Discharge Scheduling

Two conditions must be met before charging is permitted. First, the power needs of the campus must be lower than the minimum power set by Hydro Québec, which is 5000kW. The second requirement is that once programmed instructions allow charging, the power required for charging does not create a peak demand. Similarly, the prerequisites for discharge are that the power demand must exceed 5000kW and the power optimization setpoint must have a positive value.

$$Charge_{authorised,t} = \begin{cases} 1, & P_{ETS,t} - 5000 < 0 \\ 0, & \text{charge not allowed} \end{cases} \quad \forall t \quad (5.14)$$

The equation for calculating the optimal power setpoint is given below:

$$P_{setpoint} = (P_{buildings}(0 : N - 1) - P_{bess}(0 : N - 1)) \quad (5.15)$$

Where $P_{setpoint}$ is the power delivered to the program and is used to calculate actual BESS power according to the campus demand in real time. This equation is adapted from Nicolas' article (Mary, 2022)

Table 5.1 Parameter Value Configuration

No.	Symbol	Description	Value	Unit	Note
1	λ_{grid}	Electricity Price	0.03596	\$/kWh	LG Rate
2	C_{bat}	Capacity of Battery	15.2	kWh	Specification
3	SOC_{min}	Minimum SOC	20%		Configuration
4	SOC_{max}	Maximum SOC	100%		Configuration
5	$SOC_{ini,t}$	Initial SOC	100%		Configuration
6	$SOC_{end,t}$	Final SOC	100%		Configuration
7	$P_{bat,max}$	Maximum Power of battery	6	kW	Specification
8	LÉTS	Load power demand	13.5	kW	Specification

5.2 Simulation and Validation Tests on the test bench with 3rd January, 2019

January 3, 2019, was a typical winter day with a maximum power consumption of 5689kW, which is suitable for the validation test. The following simulations are based on 24 hours. Since ÉTS has fewer teaching activities in the early morning and late night, the real lift tests with equipment are based on working hours, from 7:00 am to 6:00 pm.

Again, the test bench represented all buildings of ÉTS with three programmable Chroma electrical loads and four LFP batteries as BESS controlled by XW Pro inverter. The real life test would consider the battery bank completely charged overnight and in the early morning, thus the starting SOC is 100%. The real-time tests select two distinct load forecasting techniques for comparison and validation of the peak load shaving optimal algorithm.

5.2.1 Past Time Simulation and Test with Perfect Load Prediction Algorithm

As mentioned in chapter 4, the perfect load prediction is using the power setpoint with a constant value of 5000 kW.

The configuration of the simulation is listed below:

- Mode: Past simulation with perfect prediction
- Date: 2019-01-03
- Time slot: 24 hours
- Time ratio: 1.5
- Power ratio: 500
- SOC_min: 20%
- SOC_max: 100%
- Power set point: 5000kW

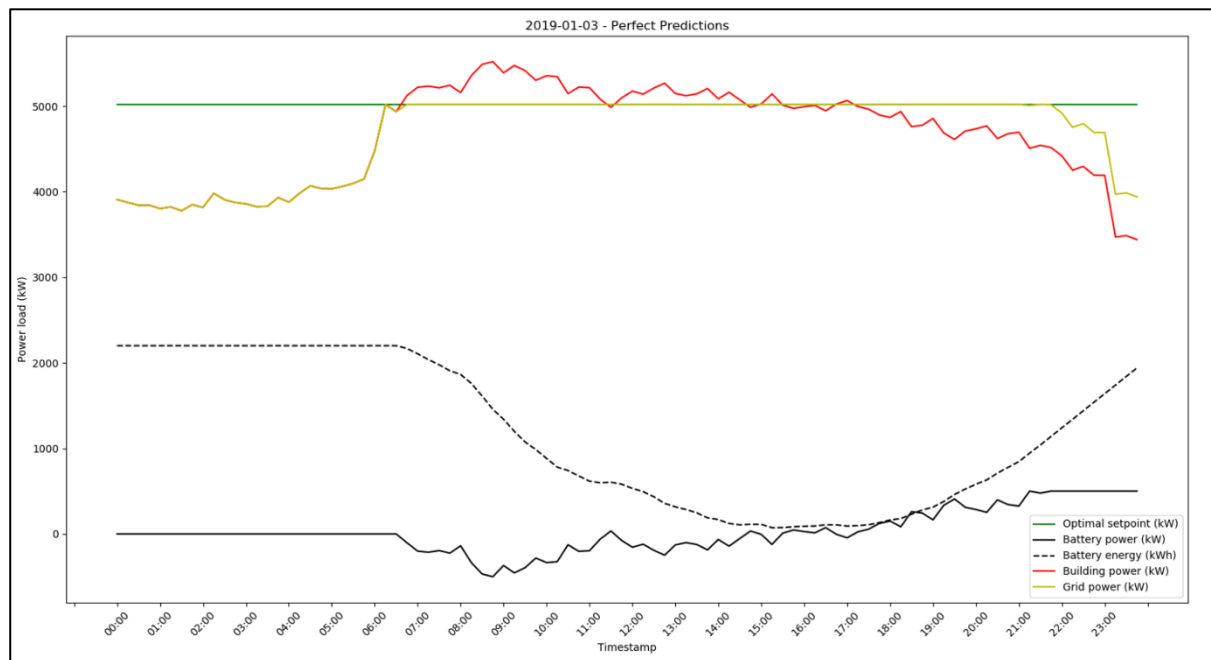


Figure 5.2 2019-01-03 Simulation Power Curve with Perfect Load Prediction

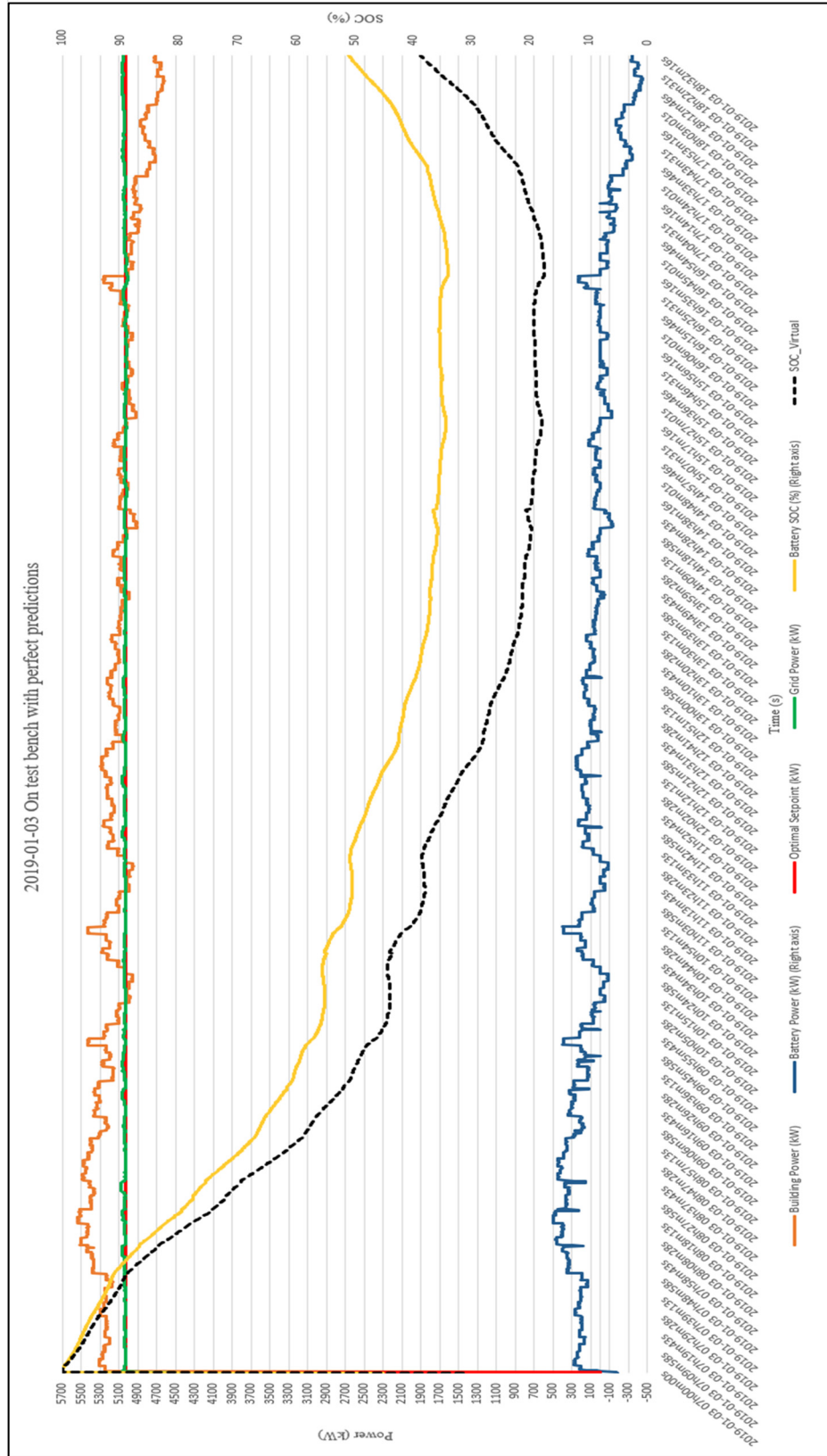


Figure 5.3 2019-01-03 on Test Bench with Perfect Load Prediction

The configuration of the real-life test is listed below:

- Mode: Past simulation with perfect prediction
- Date: 2019-01-03
- Time slot: 7:00 – 18:29
- Time ratio: 1.5
- Power ratio: 500
- SOC_min: 20%
- SOC_max: 100%

The test with an actual load for nine hours reveals that this test bench is safe and stable. Figure 5.3 illustrates that when the MG operates in those conditions, the load demand begins to increase around 7:00 a.m. and reaches 5000 kW. The inverter controls the battery bank to start discharging and track the load change. In addition, from Figure 5.3, it can also be seen that the BESS can promptly detect the load shift. At approximately 3 p.m., the load demand begins to decrease and the battery bank is close to its minimum SOC value, at which point it ceased discharging. According to the demand of the subsequent load, the battery bank proceeds to charge steadily. The variation in real SOC and virtual SOC is also depicted in Figure 5.3 with a yellow line and a black dotted line.

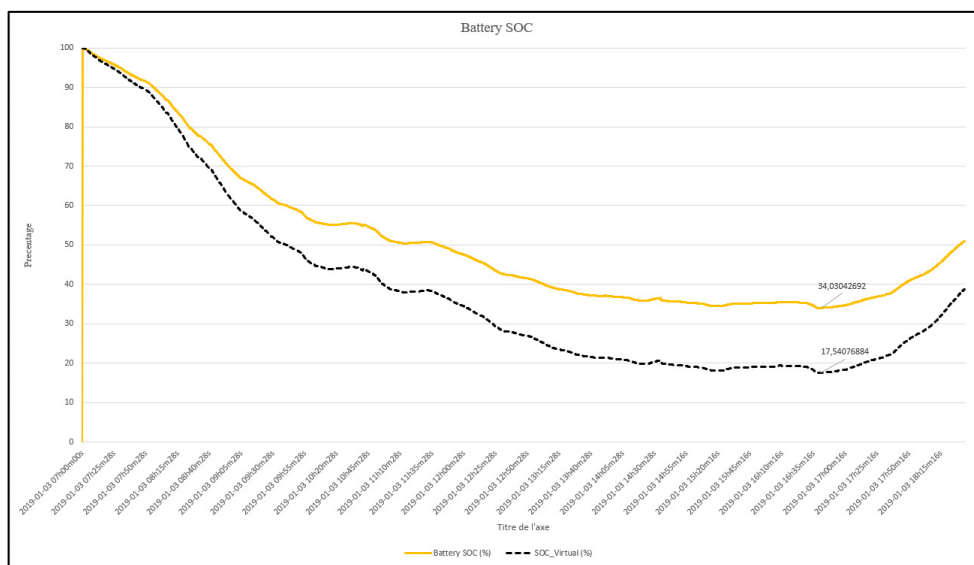


Figure 5.4 Battery SOC change during the test for 2019-01-03

According to the load demand, the batteries have not reached their minimal limit condition of 20%. At 16:38, SOC arrived its lowest value, 34.0304%. In other words, the load forecasting algorithm can be further optimized and enhanced, since the batteries have the ability to contribute more power into the grid.

The curves of the experimental results and the simulation results are highly similar. During the test run, however, it was observed that the inverter stopped intermittently or went into a hibernation state for about one or two seconds, which is causing the inverter power to suddenly drop to 0. This kind of phenomenon should be the problem of the inverter itself, and its incidence rate is between 1% and 2%. Using a suitable filter can help reduce or eliminate the occurrence of such zeros in the collected data.

5.2.2 Past Time Simulation and Test with ANN Prediction Algorithm

With ANN prediction, the power setpoint is calculated by Nicolas' algorithm described earlier in this chapter.

The configuration of the simulation is listed below:

- Mode: Past simulation with ANN prediction
- Date: 2019-01-03
- Time slot: 24 hours
- Time ratio: 1.5
- Power ratio: 500
- SOC_min: 20%
- SOC_max: 100%

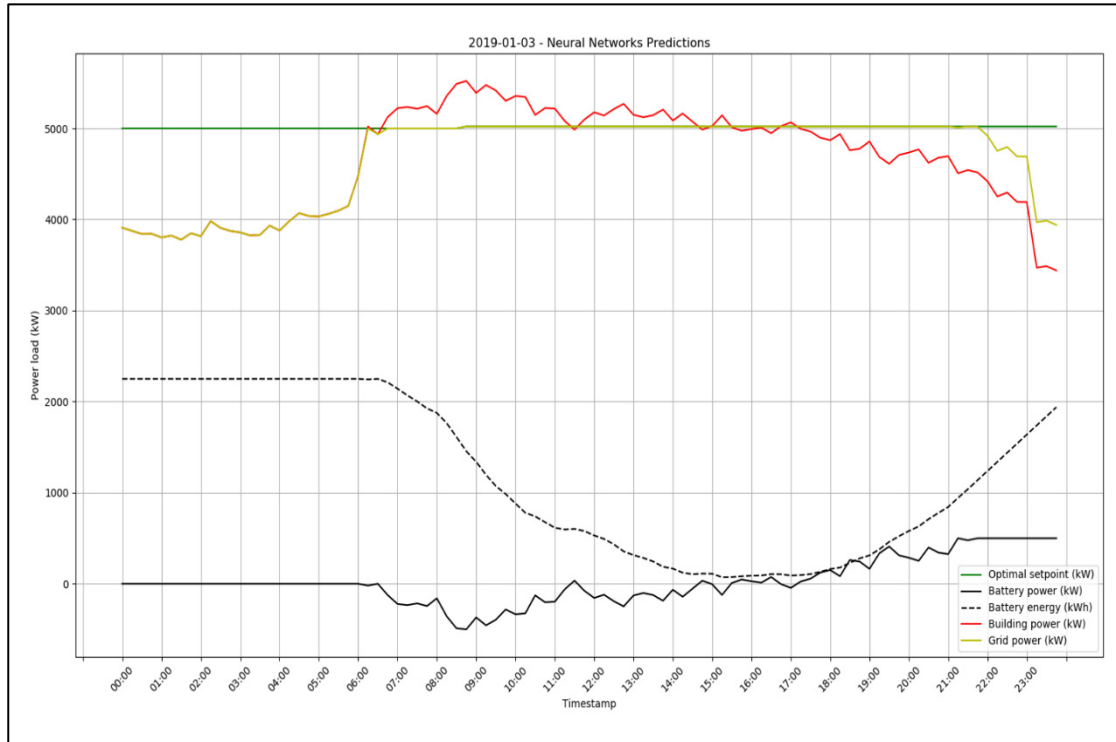


Figure 5.5 2019-01-03 Simulation Power Curve with ANN Load Forecasting

The configuration of on test bench test is listed below:

- Mode: Past simulation with ANN prediction
- Date: 2019-01-03
- Time slot: 7:00 – 17:20
- Time ratio: 1.5
- Power ratio: 500
- SOC_min: 20%
- SOC_max: 100%

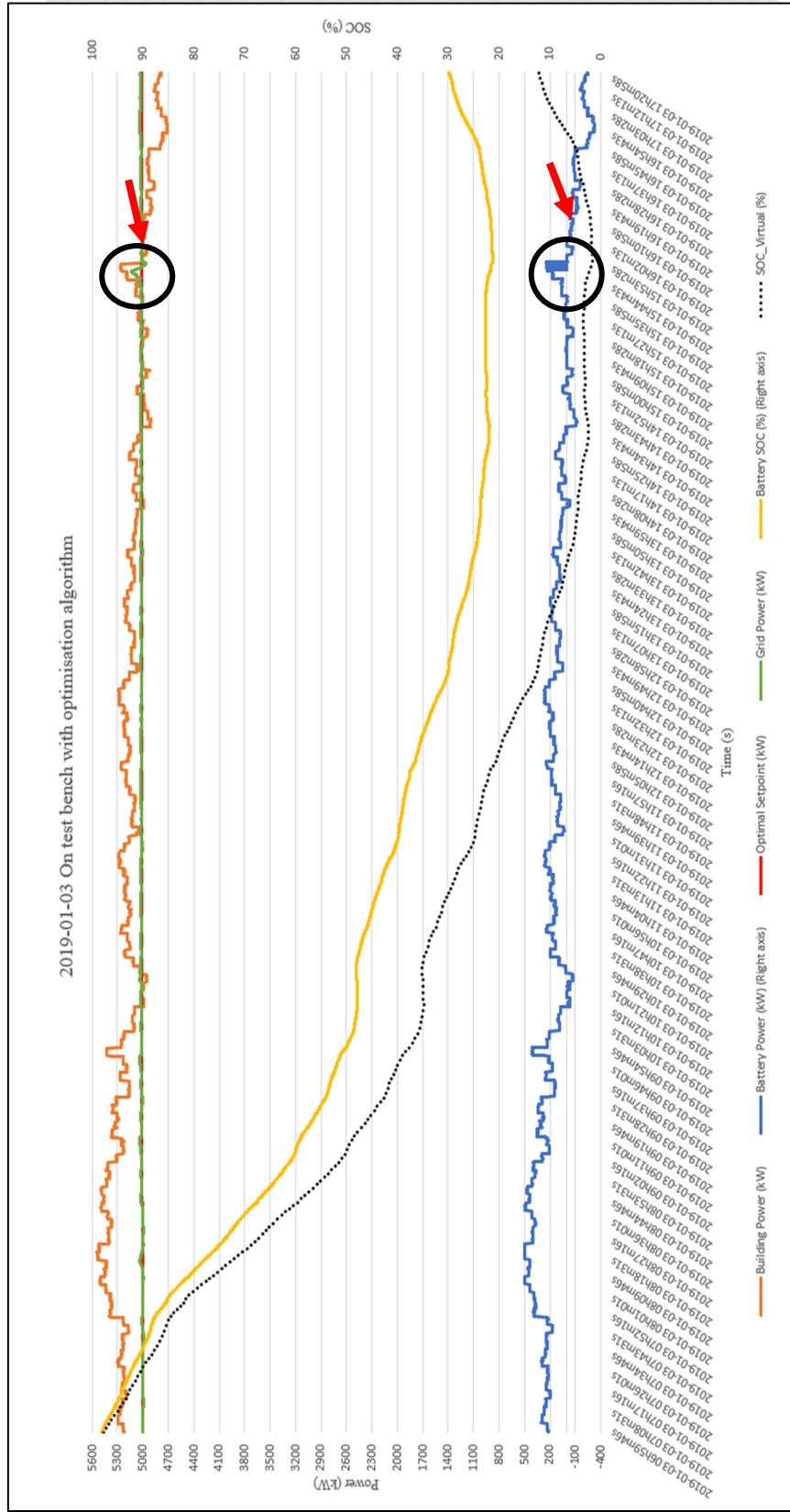


Figure 5.6 2019-01-03 On Test Bench with ANN Load Forecasting

Figure 5.5 and Figure 5.7 show the simulation results and on test bench test results after using the ANN prediction algorithm, respectively. It can be seen from the figures that the control strategy and optimization algorithm adopted can make the batteries charge during low load demand periods and discharge during peak load demand time slots, so as to achieve the effect of peak load shaving and valley filling. Affected by energy storage capacity, response characteristics and, prediction accuracy, there is a certain difference between the simulated power and the measured power, especially during the last peak load demand of the day, which occurs around 16:30 in the afternoon. From Figure 5.6, at 16:00, the batteries have been reached to the preset minimum value of 21.2813071%, and it can be considered that the battery bank’s full potential has been drained out at this point. Therefore, at 16h30, the battery cannot meet the load shaving requirements, and the program will arrange for the battery to charge. However, once the battery bank is charged a little bit, the batteries need to be discharged to serve the demand of peak load. The battery bank will then return to its minimum charge threshold again and need to be recharged. This results in the power oscillation showed with a black circle and red flash in the Figure 5.7. This problem can be solved by enhancing the robustness in the load forecasting algorithm or defining the SOC charge and discharge range more precisely in LabVIEW. In addition, the good estimation of SOC will help to calculate better power setpoints and the tracking effect of the load power.

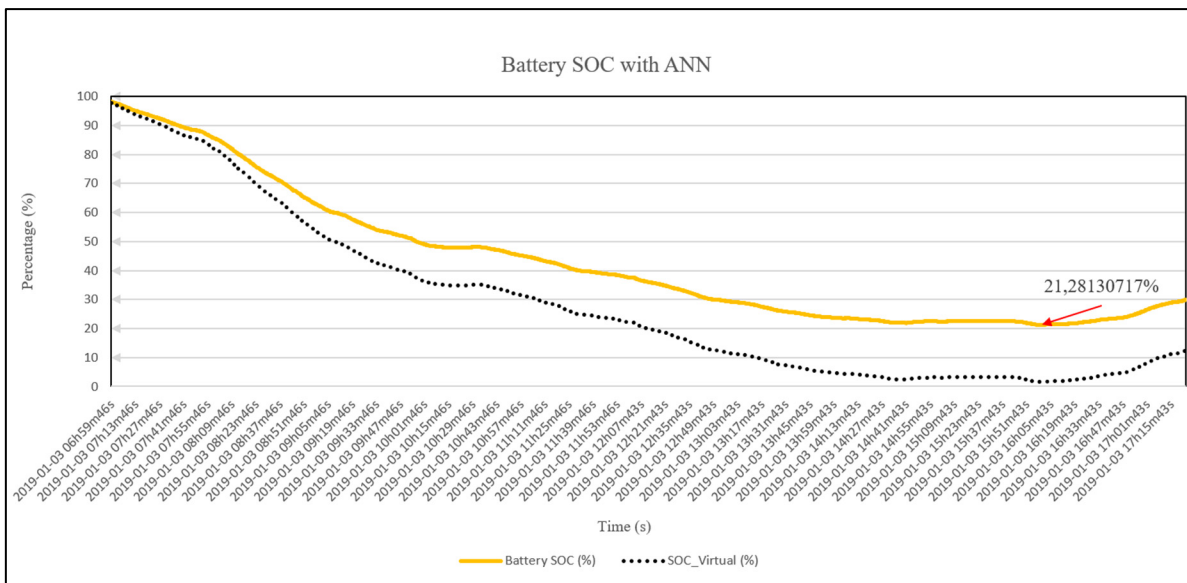


Figure 5.7 Battery SOC with ANN on 2019-01-03

5.3 Simulation and Validation Tests on test bench with 2nd July, 2019

Similar approach is adopted for the tests on 2nd July of 2019.

5.3.1 Past Time Simulation and Test with Perfect Load Prediction Algorithm

The configuration of the simulation is listed below:

- Mode: Past simulation with perfect prediction
- Date: 2019-07-02
- Time slot: 24 hours
- Time ratio: 1.5
- Power ratio: 500
- SOC_min: 20%
- SOC_max: 100%
- Power set point: 5000kW

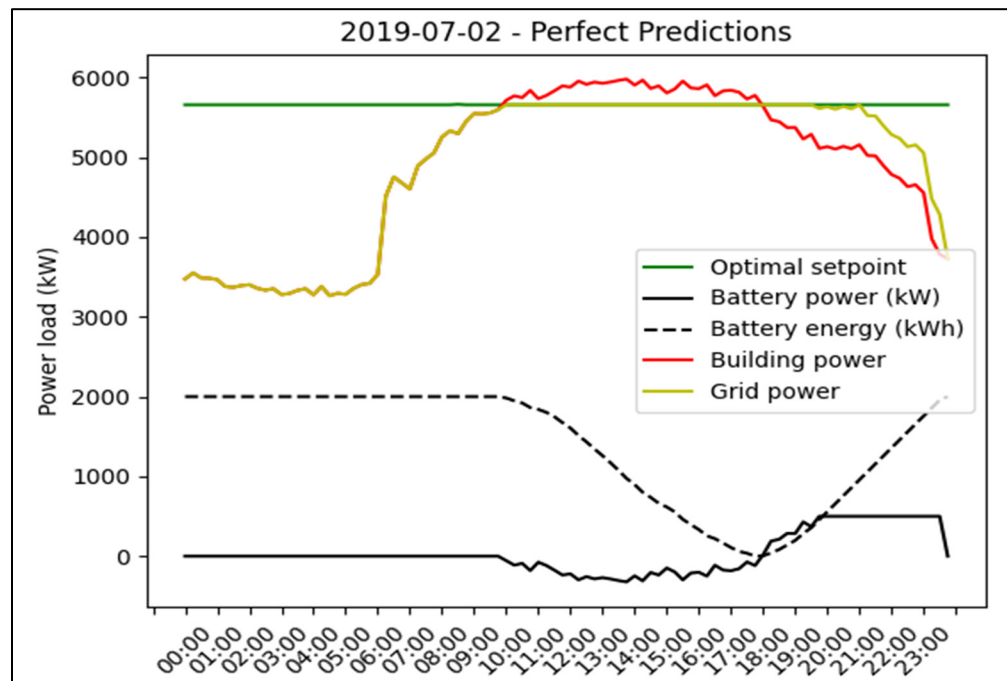


Figure 5.8 2019-07-02 Simulation Power Curve with Perfect Load Prediction

The configuration of on test bench test is listed below:

- Mode: Past simulation with perfect prediction
- Date: 2019-07-02
- Time slot: 10:00 – 17:57
- Time ratio: 1.5
- Power ratio: 500
- SOC_min: 20%
- SOC_max: 100%

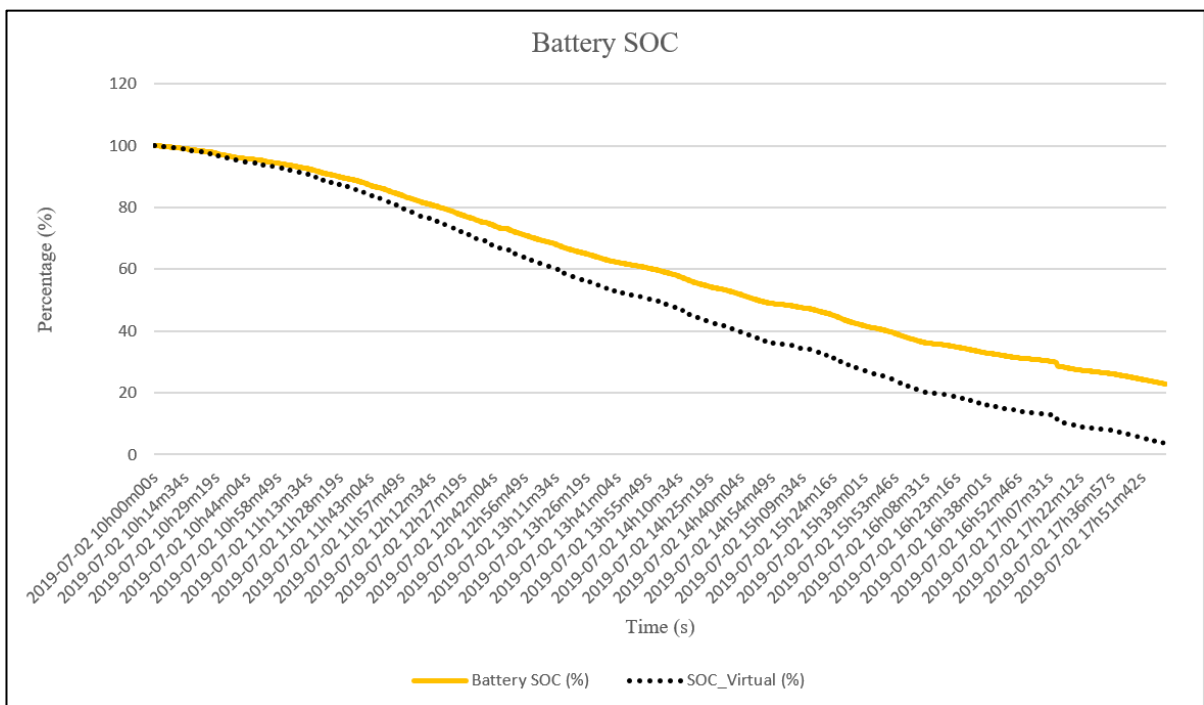


Figure 5.9 Battery SOC change during the test for 2019-07-02

In Figure 5.9, it can be seen that virtual SOC has almost reached to 0 around 18h, which is corresponding to the simulation result.

In the following picture, it will show the entire test result.

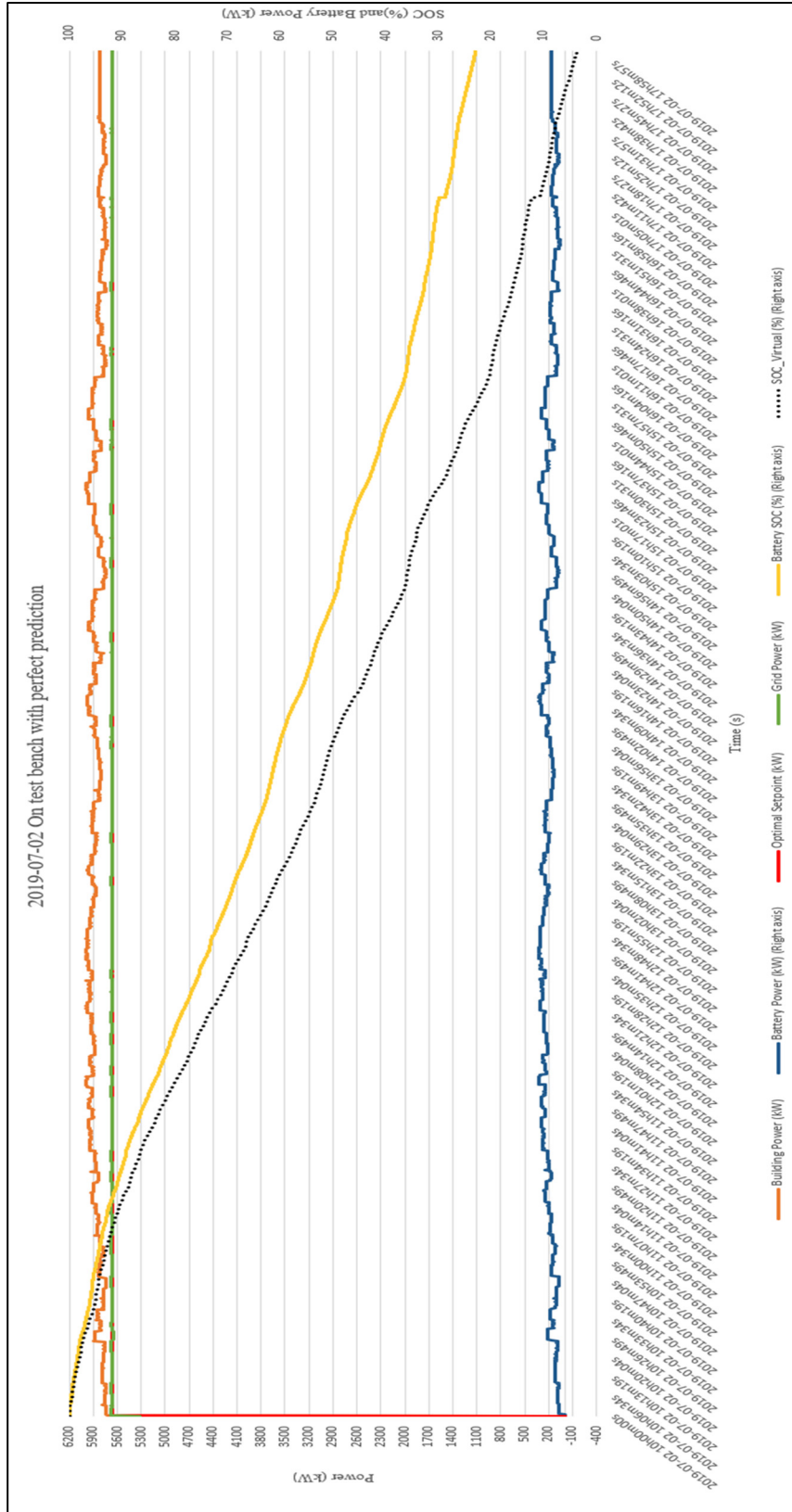


Figure 5.10 2019-07-02 on Test Bench with Perfect Load Prediction

The simulation results of constant setpoint is shown in Figure 5.6, and the test with real equipment is displayed in Figure 5.10. It can be obtained that the charging time period is from 0:00 to 9:30 and the discharge is between 9:30 and 17:30. During the summer, the peak load demand occurs later in the day compared to winter. However, the constant power setpoint method has some issues. When the setpoint is too high, it can cause significant fluctuations in energy storage output, resulting in instability inside the microgrid. When the setpoint is defined too low, it will not achieve the effect of peak load shaving and load valley filling.

Actually, this method has been widely used because of its simplicity and convenience. However, this strategy has relatively high requirements for load prediction accuracy and SOC precision. When the accuracy demand is not met, it becomes difficult to achieve the desired peak load shaving effect.

5.3.2 Past Time Simulation and Test with ANN Prediction Algorithm

The configuration of the simulation is listed below:

- Mode: Past simulation with ANN prediction
- Date: 2019-01-03
- Time slot: 24 hours
- Time ratio: 1.5
- Power ratio: 500
- SOC_min: 20%
- SOC_max: 100%

The results of the simulation are depicted in the Figure 5.10. It is evident from the battery's power curve that the battery was not permitted to charge for the entire day. The ANN algorithm has successfully managed the battery discharge to achieve the objective of peak load shaving in the period of higher power demand, especially from 7:00 to 18:00.

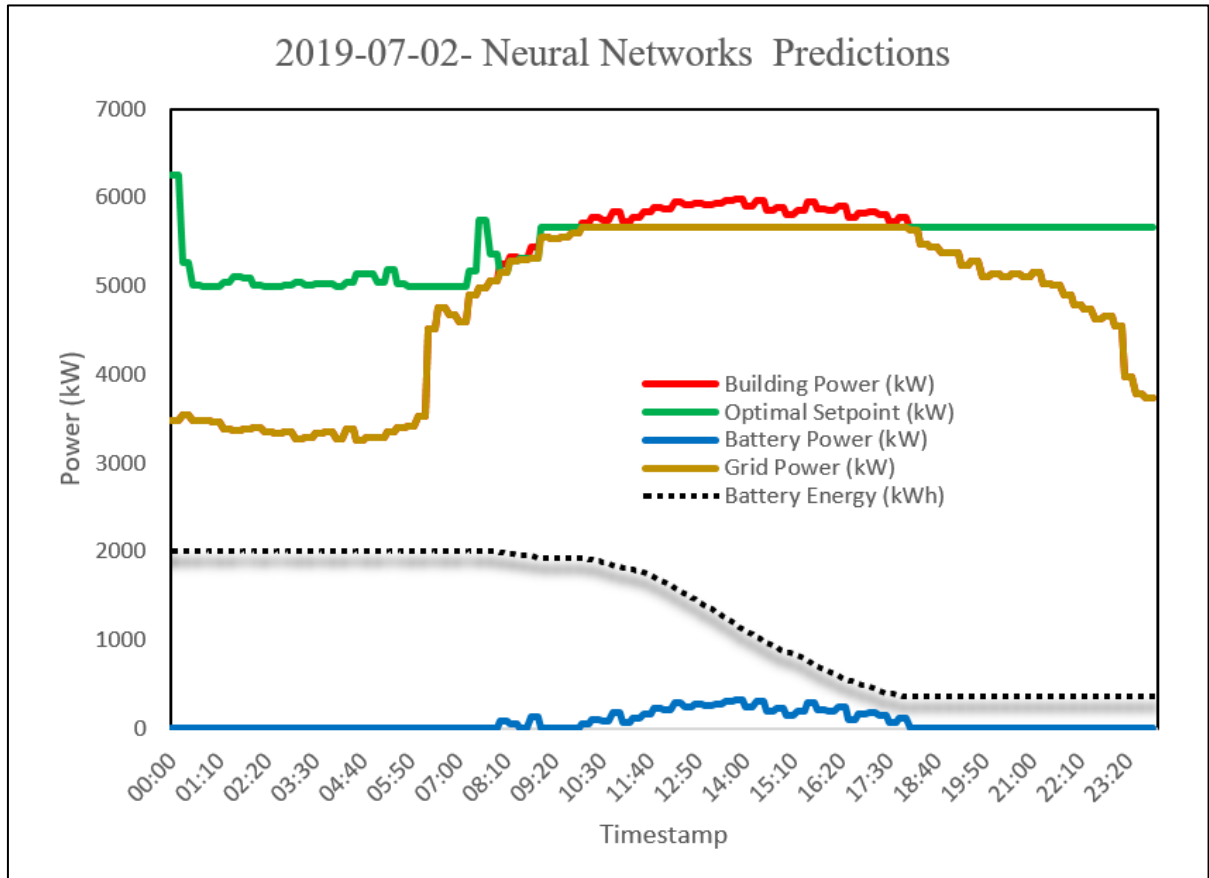


Figure 5.11 2019-07-02 Simulation Power Curve with ANN Load Forecasting

The configuration of the on test bench test is listed below:

- Mode: Past simulation with ANN prediction
- Date: 2019-07-02
- Time slot: 7:00 – 17:45
- Time ratio: 1.5
- Power ratio: 500
- SOC_min: 20%
- SOC_max: 100%

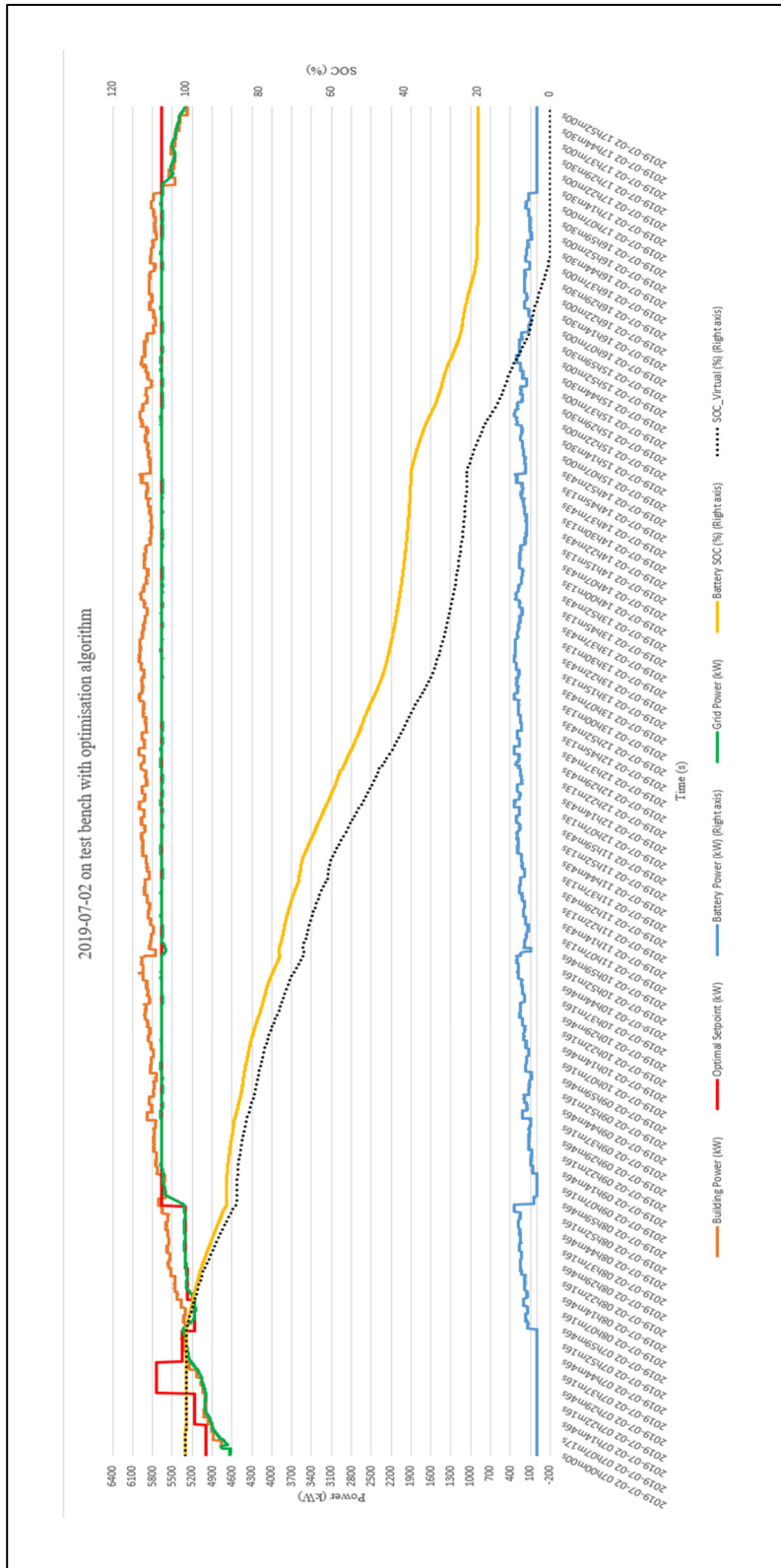


Figure 5.12 2019-07-02 On Test Bench with ANN Load Forecasting

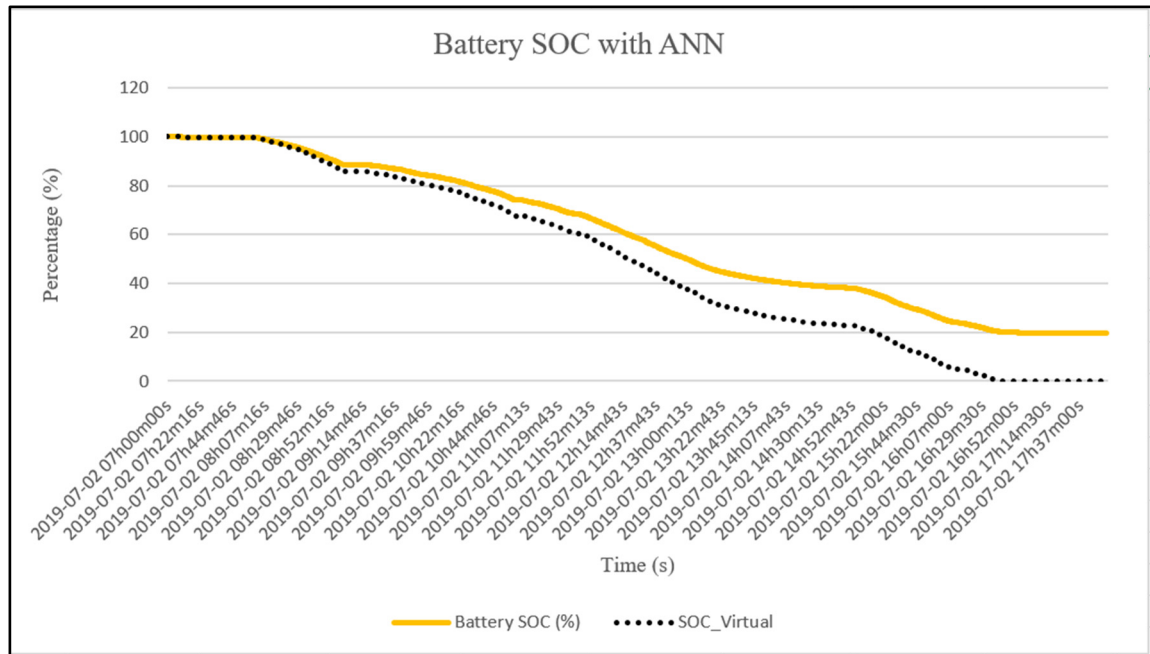


Figure 5.13 Battery SOC with ANN on 2019-07-02

In Figure 5.12, it is shown that the power setpoint is over optimistic, which leads to an abnormal curve between 7:00 and 9:00, for instance, the power setpoint is too high from 7:00 to 7:45, and too low from 8:00 to 9:00, as reflected in the simulation results as well. However, after 9:00 am, the power setpoint returns to reasonable value, and the grid power follows the power setpoint until the end of the test. It is worth mentioning that, unlike the 3rd January test, the battery was discharged steadily until the end of the high load demand, which can be witnessed in the declining slope of the SOC curve in Figure 5.13. This is due to the fact that the optimization algorithm will locate any opportunity to charge the battery during the day if there are no constraints on the charging permissible conditions, and the battery will not drain to the given lower limit. In an ideal scenario, the total authorized discharge of the battery bank is used to minimize excessive power demands on the grid, and the battery bank is charged to full capacity overnight. At this juncture, the algorithm has not attained the anticipated outcome; consequently, further enhancements are required.

5.4 Chapter Summary

This chapter first briefly describes the load forecasting methods and optimization algorithm. Then analyze and compare the simulation results and on test bench test results on selected dates. The experimental results valid the accuracy of the optimization algorithm and contribute to further improvement.

CONCLUSION

With the maturation of distributed energy generation technology, the research significance and practical utility of MG are gaining prominence. As a new type of distribution network, it can achieve more efficiently power consumption peak-shaving and valley-filling, leading to reduce electricity bill. This paper first expounds the research background and significance of microgrids, and then introduced the research status of the microgrid experimental platform both domestically and internationally. By constructing a microgrid central control platform, the exchange and interoperability between various devices in the system was solved, and the microgrid load prediction and power optimization model was validated in combination with actual tests. At the same time the practical problems encountered in monitoring and power management in the operation of the microgrid were remedied, and the stability and economy of microgrid are improved. The main work of this paper is summarized as follows:

- 1) The overall design and operation of the experimental microgrid platform are outlined, as well as the selection of hardware equipment and parameter settings are thoroughly studied.
- 2) Using LabVIEW to build a control module for each device and integrate them into the remote monitoring system for the entire microgrid, where the inverter and power meter communicate using the Modbus TCP protocol. The main body of this system is composed of collecting remote signal collection VI and control and adjustment action VI. On this premise, a user-friendly, straightforward, and easy-to-use human-computer interaction interface is developed.
- 3) Operational evaluation of the test bench is performed, including functional tests of each hardware device and overall performance assessment.
- 4) The viability of the load power optimization strategy and load prediction algorithm is valid through on test bench tests.

RECOMMENDATIONS

The current research work shows that the accuracy of battery SOC has a crucial impact on the entire energy optimization algorithm. Therefore, adding a Conext Battery Monitor (ANNEX X) will greatly reduce the workload of SOC prediction through programming, and also enable to use SOC instead of battery voltage for control mode transitions.

In addition, the next phase of work will focus on two areas: real time tests and adding photovoltaics generation. This test bench has strong extensibility, and various distributed power sources and distributed energy storage system can be introduced to accommodate future research criteria.

APPENDIX I

POWER METER PM5340 DATASHEET

Product data sheet

Specifications



power meter PowerLogic PM5340, ethernet, up to 31st Harmonic, 256KB 2DI/2DO 35 alarms

METSEPM5340

Main

Range	PowerLogic
Product name	PowerLogic PM5000
Device short name	PM5340
Product or component type	Power meter

Complementary

Power quality analysis	up to the 31st harmonic
Device application	Multi-tariff Power monitoring
Type of measurement	Current Voltage Frequency Power factor Energy Active and reactive power
Supply voltage	90...450 V AC 45...65 Hz 100...300 V DC
Network frequency	60 Hz 50 Hz
[In] rated current	5 A 1 A
Type of network	3P 1P + N 3P + N
Maximum power consumption in VA	11.9 VA 415 V
Ride-through time	100 ms 120 V AC typical 400 ms 230 V AC typical 50 ms 125 V DC typical
Display type	Monochrome graphic LCD
Display resolution	128 x 128 pixels
Sampling rate	64 samples/cycle
Measurement current	5...9000 mA
Analogue input type	voltage 10 M(Ohm) current <= 0.3 m(Ohm)
Measurement voltage	35...760 V AC 45...65 Hz between phases 20...400 V AC 45...65 Hz between phase and neutral
Frequency measurement range	45...65 Hz

4-Feb-2023  1

Figure-A I-1 PM5340 Data Sheet Page 1
Taken from (Power Meter Powerlogic PM5340, 2023)

Number of inputs	2 digital
Measurement accuracy	Active energy +/- 0.5 % Reactive energy +/- 2 % Active power +/- 0.5 % Apparent power +/- 0.5 % Frequency +/- 0.05 % Power factor +/- 0.5 Current +/- 0.5 % Voltage +/- 0.5 % Apparent energy +/- 0.5 % Reactive power +/- 2 %
Accuracy class	Class 0.5S active energy IEC 62053-22
Number of outputs	2 relay 2 digital
Information displayed	Tariff 4)
Communication port protocol	Modbus TCP/IP 10/100 Mbit/s 2500 V BACnet IP
Communication port support	ETHERNET
Data recording	Data logs Alarm logs Time stamping Event logs Min/max of instantaneous values Maintenance logs
Memory capacity	256 kB
Connections - terminals	Voltage circuit screw terminal block4 Control circuit screw terminal block2 Current transformer screw terminal block6 Input/output circuit screw terminal block6 Relay output screw terminal block4 Ethernet network RJ45 connector
Mounting mode	Flush-mounted
Mounting support	Framework
Standards	EN 50470-1 IEC 62053-24 IEC 60529 UL 61010-1 IEC 62053-22 EN 50470-3 IEC 61557-12
Product certifications	CE IEC 61010-1 CULus UL 61010-1
Width	3.78 in (96 mm)
Depth	2.83 in (72 mm)
Height	3.78 in (96 mm)
Net weight	15.17 oz (430 g)
Environment	
Electromagnetic compatibility	Limits for harmonic current emissionsclass A IEC 61000-3-2 Electrostatic dischargelevel 4 IEC 61000-4-2 Conducted RF disturbanceslevel 3 IEC 61000-4-6 Magnetic field at power frequencylevel 4 IEC 61000-4-8 Conducted and radiated emissionsclass B EN 55022
IP degree of protection	Display IP51 IEC 60529 Rear IP30 IEC 60529
Relative humidity	5...95 % 122 °F (50 °C) non-condensing
Pollution degree	2
Ambient air temperature for operation	-13...158 °F (-25...70 °C) meter -4...158 °F (-20...70 °C) display -13...-4 °F (-25...-20 °C) with reduced performance) display
Ambient air temperature for storage	-40...185 °F (-40...85 °C)
Operating altitude	<= 3000 m

Figure-A I-2 PM5340 Data Sheet Page 2
Taken from (Power Meter Powerlogic PM5340, 2023)

Packing Units	
Unit Type of Package 1	PCE
Number of Units in Package 1	1
Package 1 Height	4.72 in (12.0 cm)
Package 1 Width	4.88 in (12.4 cm)
Package 1 Length	4.21 in (10.7 cm)
Package 1 Weight	19.40 oz (550.0 g)
Unit Type of Package 2	S03
Number of Units in Package 2	12
Package 2 Height	11.81 in (30.0 cm)
Package 2 Width	11.81 in (30.0 cm)
Package 2 Length	15.75 in (40.0 cm)
Package 2 Weight	15.04 lb(US) (6.82 kg)
Offer Sustainability	
Sustainable offer status	Green Premium product
REACH Regulation	REACH Declaration
EU RoHS Directive	Compliant EU RoHS Declaration
Mercury free	Yes
China RoHS Regulation	China RoHS declaration
RoHS exemption information	Yes
Environmental Disclosure	Product Environmental Profile
Circularity Profile	End of Life Information
WEEE	The product must be disposed on European Union markets following specific waste collection and never end up in rubbish bins
Recommended replacement(s)	

Figure-A I-3 PM5340 Data Sheet Page 3
 Taken from (Power Meter Powerlogic PM5340, 2023)

APPENDIX II

XW PRO 6848 HYBRID INVERTER DATASHEET

Life Is On


XW Pro

6.8/8.5 kW Hybrid Inverter for North America

865-6848-21



Protect your home's power supply when the grid goes out. Save on energy costs with utility time of use and demand charge optimization. The XW Pro solar hybrid inverter is the heart of your home power system, connecting solar and battery storage with the grid for backup power and energy security. It can be used for solar and storage, or backup power systems without solar.

Backup power performance

- Reliable operation of backup power and off-grid loads with a high overload power rating (2x)
- Seamless transition to backup power with an integrated high-speed transfer switch
- Grid and Generator input ports
- Field proven product quality and reliability, building on two decades of experience in solar and storage

Flexible

- 120/240 V output with stacking capability up to 4 units
- Configurable for 120 V output for 3 phase systems
- Connects solar with Conext™ MPPT Charge Controllers or PV inverters for DC-coupled or AC-coupled systems
- Lithium Ion battery integration
- Grid tied and off-grid systems, Rule 21, HECO Rule 14H and PREPA compliant

Easy to install

- Configures quickly using Insight
- AC Out port for backloads
- Full ecosystem and accessories for single unit or scalable systems

Smart energy management

- Optimize energy consumption for time of use rates or demand charges
- Self-consumption of solar energy

Compatible with Insight

- Remote monitoring & control with advanced data security
- Web and mobile app
- Multi-site management for installers



solar.se.com

Figure-A II-1 XW Pro 6848 Data Sheet Page 1

Taken from (XW Pro 120/240V, 2022)

	XW Pro 6848 NA 120/240 V	XW Pro 6848 NA 120 V
Inverter AC Output (Standalone)		
Output power (continuous) at 25°C	6800 W	5760 W
Overload 30 min/60 sec at 25°C	8500 W/12000 W	7200 W/12000 W
Output power (continuous) at 40°C	6000 W	5760 W
Maximum output current 60 seconds (rms)	52 A (240 V)	104 A (120 V)
Output frequency	50/60 Hz	50/60 Hz
Output voltage	Split phase 120/240 V +/- 3%	120 V +/- 3%
Total harmonic distortion at rated power	< 5 %	< 5 %
Idle consumption search mode	< 8 W	< 8 W
Input DC voltage range	40 to 64 V (48 V nominal)	40 to 64 V (48 V nominal)
Maximum input DC current	180 A	180 A
Charger DC Output		
Maximum output charge current	140 A	120 A
Output charge voltage range	40 – 64 V (48 V nominal)	
Charge control	Three stage, two stage, boost, external BMS, custom	
Charge temperature compensation	Battery temperature sensor included	
Power factor corrected charging	0.98	
Compatible battery types	Flooded (default), Gel, AGM, Lithium ion, custom	
AC Input		
AC 1 (grid) input current (selectable limit)	3 – 60 A (60 A default)	3 – 60 A (60 A default)
AC 2 (generator) input current (selectable limit)	3 – 60 A (60 A default)	3 – 60 A (60 A default)
Automatic transfer relay rating/typical transfer time	60 A / 8 ms	60 A / 8 ms
AC input voltage limits (bypass/charge mode)	L-L: 156 - 280 V (240 V nominal)	L-N: 78 - 140 V (120 V nominal)
AC input frequency range (bypass/charge mode)	52 – 68 Hz (allowable)	52 – 68 Hz (allowable)
AC Grid-Tie Output		
Grid sell power	6000 W	5760 W
Grid sell current (selectable limit)	0 to 27 A (240 V)	0 to 48 A (120 V)
Efficiency		
Peak	96.1%	94.8%
CEC weighted efficiency	94.1%	93.6%
General Specifications		
Part number	865-6848-21	
Product/shipping weight	55.2 kg (121.7 lb)/ 76.7 kg (169.0 lb)	
Product dimensions (H x W x D)	58 x 41 x 23 cm (23 x 16 x 9 in)	
Shipping dimensions (H x W x D)	71.1 x 57.2 x 39.4 cm (28.0 x 22.5 x 15.5 in)	
IP degree of protection	NEMA Type 1 Indoor	
Operating air temperature range	-25°C to 70°C (-13°F to 158°F) (power derated above 25°C (77°F))	
Features		
System monitoring and network communications	Available (through Insight)	
Intelligent features	Grid sell, peak load shave, generator support, solar self-supply	
Auxiliary port	0 to 12 V, maximum 250 mA DC output, selectable triggers	
Off-grid AC coupling	Frequency shifting	
Regulatory Approval		
Safety	UL 1741, CSA 107.1	
EMC directive	FCC and Industry Canada Class B	
Interconnect	IEEE 1547, UL 1741-SA, Rule 21, Rule 14H, PREPA, and CSA 107.1	
Compatible Products Part Numbers		
Power Distribution Panels	XW Mini PDP (865-1013-01), XW PDP (865-1015-01)	XW PDP without AC Breakers (865-1014-01), 60 A Three Phase Breaker Kit (865-1315-01)
MPPT Charge Controllers	MPPT 100 600 (865-1034), MPPT 80 600 (865-1032), MPPT 60 150 (865-1030-1)	
Monitoring	InsightHome (865-0330), InsightFacility (865-0335)	
Accessories	Automatic Generator Start (865-1060), Battery Monitor (865-1080-01), Configuration Tool (865-1155-01)	

© 2022 Schneider Electric. All Rights Reserved. All trademarks are owned by Schneider Electric Industries S.A.S. or its affiliated companies. All information is preliminary and will need to be confirmed at the time of order.
DS2020118_XW Pro UL.indd

Life Is On | Schneider Electric

Figure-A II-2 XW Pro 6848 Data Sheet Page 2

Taken from (XW Pro 120/240V, 2022)

APPENDIX III

SIMPLIPHI PHI 3.8 BATTERY DATASHEET

PHI 3.8™ BATTERY



CHEMISTRY	Lithium Ferro Phosphate (LFP) The safest Lithium Ion chemistry available No cobalt or risk of thermal runaway
OCPD	Built-in, accessible 80 Amp DC breaker on/off switch
BMS	Built-in Battery Management System
COMPATIBILITY	Compatible with all industry standard inverters and charge controllers Battery bank-to-inverter output sizing must adhere to a 2:1 ratio: $\text{battery quantity} = \frac{\text{inverter kW}_{AC} \text{ rating} \div \text{inverter efficiency}}{\text{battery MAX Continuous Discharge Rate (kW}_{DC})}$
MAINTENANCE	Maintenance-free No ventilation, cooling or thermal regulation required

PHI 3.8 kWh Module	24V	48V
DC Voltages - Nominal	25.6 VDC	51.2 VDC
Amp-Hours	151 Ah	75 Ah
Rated kWh Capacity	3.8 kWh DC @ 100% DOD 3.04 kWh DC @ 80% DOD	3.8 kWh DC @ 100% DOD 3.04 kWh DC @ 80% DOD
MAX Discharge Rate (10 minutes)	60 Amps DC (1.53 kW DC)	60 Amps DC (3.07 kW DC)
MAX Continuous Discharge Rate	45 Amps DC (1.15 kW DC)	37.5 Amps DC (1.92 kW DC)
MAX Continuous Charge Rate	45 Amps DC (1.15 kW DC)	37.5 Amps DC (1.92 kW DC)
DC Voltage Range ¹	24 VDC to 28 VDC	48 VDC to 56 VDC
Depth of Discharge ¹	up to 100%	
Operating Efficiency	98%	
Charging Temperature ¹	32° to 120° F (0° to 49° C)	
Operating Temperature ¹	-4° to 140° F (-20° to 60° C)	
Storage Temperature	6 months: 14° to 77° F (-10° to 25° C) 3 months: -4° to 113° F (-20° to 45° C)	
Self-Discharge Rate	< 1% per month	
Cycle Life	10,000+ cycles (@ 80% DOD)	
Memory Effect	None	
Warranty	10 Years or 10,000 cycles (@ 80% DOD)	
Weight	78.24 lbs. (35.5 kg)	
Dimensions (W x H x D)	13.5 x 14 x 8 in. (15.5" H w/terminals) / 0.88 ft ³ (34.3 x 35.6 x 20.3 cm / 0.025 m ³)	

1. Max operating ranges. Refer to Installation Manual for recommended conditions.
- All specifications listed are typical/nominal and subject to change without notice.
 - UN 3480, Lithium ion batteries, 9, II
 - UL, CE, UN/DOT and RoHS compliant components - UL Compliant
 - Designed and manufactured in California, USA

CERTIFIED
TO UL 1973



805-640-6700 • techsupport@simpliphipower.com
© SimpliPhi Power, Inc. REV202106281043

Figure-A III-1 PHI 3.8 Battery Page 1
Taken from (PHI 3.8 BATTERY, 2021)

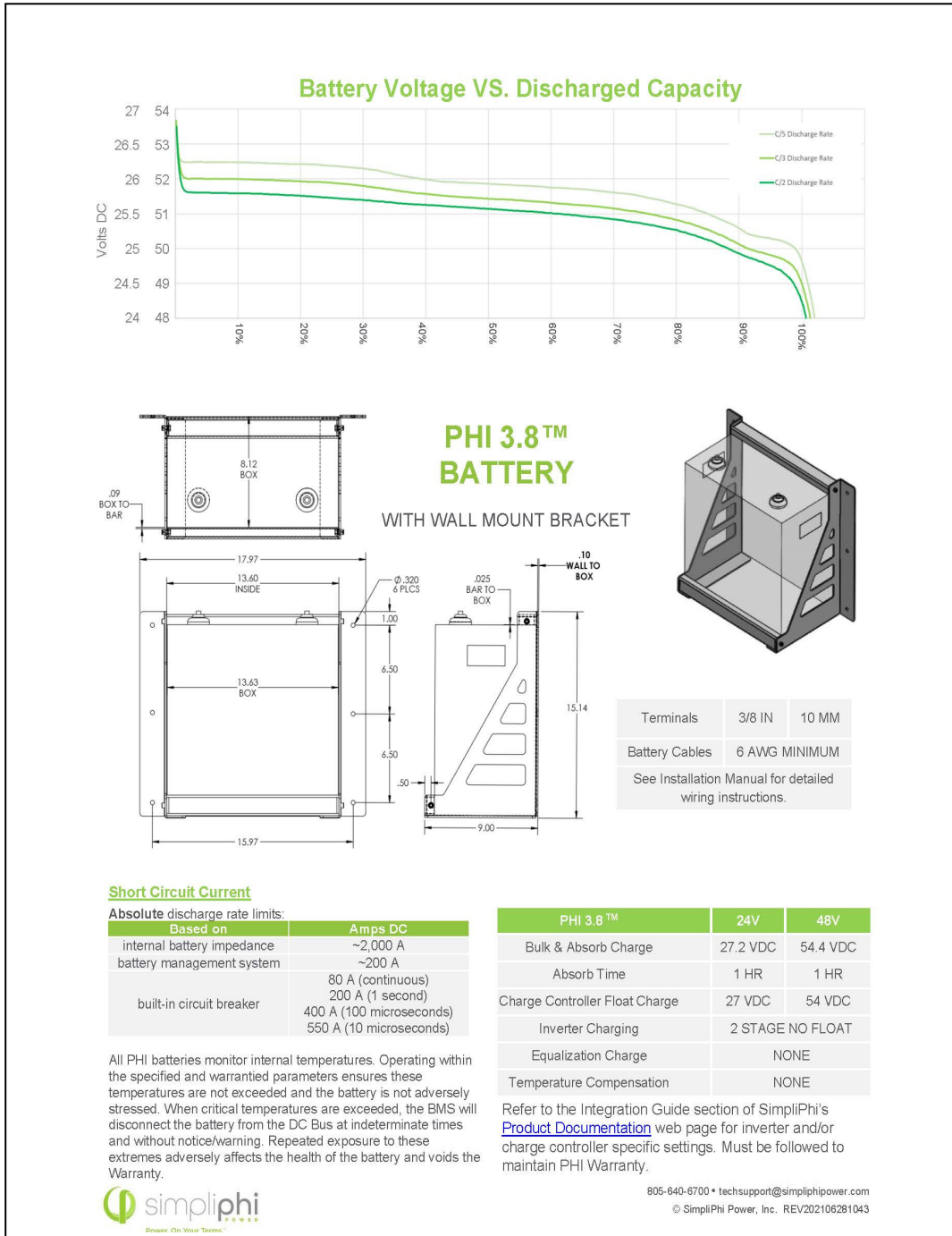


Figure-A III-2 PHI 3.8 Battery Page 2
Taken from (PHI 3.8 BATTERY, 2021)

APPENDIX IV

CONEXT GATEWAY DATASHEET


Life Is On | **Schneider**
Electric

Simplified management of solar and storage systems

Conext™ Gateway

Introducing a powerful new control solution that provides local system configuration and management as well as live system monitoring for the residential and commercial range of solar and storage products





Solution at a glance

The new Conext™ Gateway provides local system configuration and management as well as live system monitoring for the residential and commercial range of solar products.

To accelerate the installation and system setup process, the Conext™ Gateway offers wireless connectivity along with more intuitive configuration and system management tools. To give users better insights into your solar system performance, the Conext™ Gateway's graphing and reporting interfaces are completely updated.

The Conext™ Gateway together with Conext™ Insight 2 will bring system monitoring and remote management to the cloud.

The Conext™ Gateway is compatible with the new Conext™ XW Pro and the rest of the residential and commercial range of solar and storage products.

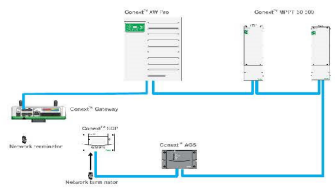


Figure-A IV-1 Conext Gateway Page 1

Taken from (Conext Gateway, 2020)

Conext™ Gateway | 2

Conext™ Gateway

Advanced diagnostics for solar and battery systems

Higher return on investment

- Monitor solar system performance in real time on your local network
- Monitor your system from anywhere using Conext™ Insight 2
- Measure and compare energy performance over varying time frames

Flexible

- Multiple visualizations for trend analysis as well as custom data logging for diagnostics
- Built-in wireless access point (WAP) connectivity for easy configuration (wirelessly connect a laptop to your Gateway)
- Built-in wireless station mode for connection to a local area network
- Dual Xanbus channels to support larger networks of devices
- Modbus support for string inverters and third-party Modbus devices*
- Canbus for compatible storage systems (e.g., Li-Ion batteries)*

Easy to service

- View or download an events log for faster troubleshooting
- Upgrade Conext™ Gateway and other Conext™ devices firmware through Gateway's web application
- Remotely manage system settings and firmware updates from Conext™ Insight 2*

Easy to install

- Configure devices remotely on the web
- Surface or DIN-Rail mounting options
- Multiple power supply options; AC adapter or Xanbus

* This feature is in development as of November 21, 2019. Please contact your local sales representative for more information on features under development.

Applications

- 
Rooftop for feed-in-tariff / net metering
- 
Rooftop for self-consumption with storage
- 
PV-Diesel hybridization
- 
Storage / backup power
- 
Commercial off-grid
- 
Microgrids
- 
Telecom towers
- 
Residential grid-tie solar with battery backup
- 
Residential self-consumption with storage
- 
Residential off-grid
- 
Residential backup power

solar.schneider-electric.com



Figure-A IV-2 Conext Gateway Page 2
Taken from (Conext Gateway , 2020)

Conext™ Gateway | 3

Technical Specifications

Conext™ Gateway

Device short name	Conext™ Gateway
Electrical Specifications	
Power consumption	2 W average / 10 W peak
AC/DC adapter (supplied)	Input: 100-240V AC, 50-60Hz, 0.6A, Output: 12V DC, 1.5A, 5.5mm outer, 2.1mm center-positive jack
Xanbus	When connected to Conext XW Pro / SW or MPPT 80 600 providing network power
24V on 26-pin connector	24V DC, 1A max input only through pins 1 and 2 Accepts 16 - 24 AWG pin wire size
Physical Specifications	
Part number	865-0329
Weight (device only)	340 g / 0.75 lb
Dimensions (device only) (W × H × D)	134 × 137.4 × 48.5 mm / 5.3 × 5.4 × 1.9 inches
Shipping package dimensions	153 × 158 × 138 mm / 6.2 × 6.2 × 7.4 inches
Shipping package weight	2 kg / 4.5 lb
Housing / Mounting system	ABS Plastic / 35-mm DIN rail clip
IP rating / Mounting Location	IP 20, NEMA 1, Indoor only
Status Display	7 x LEDs
Temperature	Operating: -4 to 122 °F / -20 to 50 °C Storage: -40 to 185 °F / -40 to 85 °C
Humidity	Operating: < 95%, non-condensing Storage: <95%
Features	
Programmable dry contact relay	Screw 3-terminal, 16-24 AWG, NC-Com-NO, Form: Class 2, 24 V DC, 4 A max SELV input only
Graphical user interface	Internet Browser
Remote firmware upgrades	Yes (Conext Gateway and connected Xanbus devices)
Custom Data logger	Yes
Max. number of Xanbus devices	Up to 20 (depending on the device type)
Micro-SD card (supplied)	Read-only
Regulatory	
EMC immunity	EN61000-6-1
EMC emissions	EN61000-6-3, FCC Part 15 Class B, Ind. Canada ICES-003 Class B
Substances / environmental	RoHS
Compatible products part numbers	
Conext XW Pro UL (120/240 V)	865-6343-21
Conext XW+ IEC (230 V)	XW+ 8543 E: 865-8543-61
Conext XW+ UL (120/240 V)	XW+ 6343 NA: 865-6343-01
Conext SW IEC (230 V)	SW 4024: 865-4024-55 / SW 4048: 865-4048-55
Conext SW UL (120/240 V)	SW 4024: 865-4024-21 / SW 4048: 865-4048-21
Conext CL-60 E	PVSCL60E
Conext CL36 IEC	PVSCL36E
Conext MPPT 80 600	865-1032
Conext MPPT 60 150	865-1030-01
Conext System Control Panel	865-1050-01
Conext Automatic Generator Start	865-1060-01
Conext Battery Monitor	865-1080-01

Specifications are subject to change without notice.



For indoor use only

© 2020 Schneider Electric. All Rights Reserved. All trademarks are owned by Schneider Electric Industries SAS or its affiliated companies. All information is preliminary and will need to be confirmed at the time of order. DS20200117_Conext Gateway.indd



Figure-A IV-3 Conext Gateway Page 3
Taken from (Conext Gateway , 2020)

APPENDIX V

LABVIEW INVERTER READ AND WRITE PROGRAM

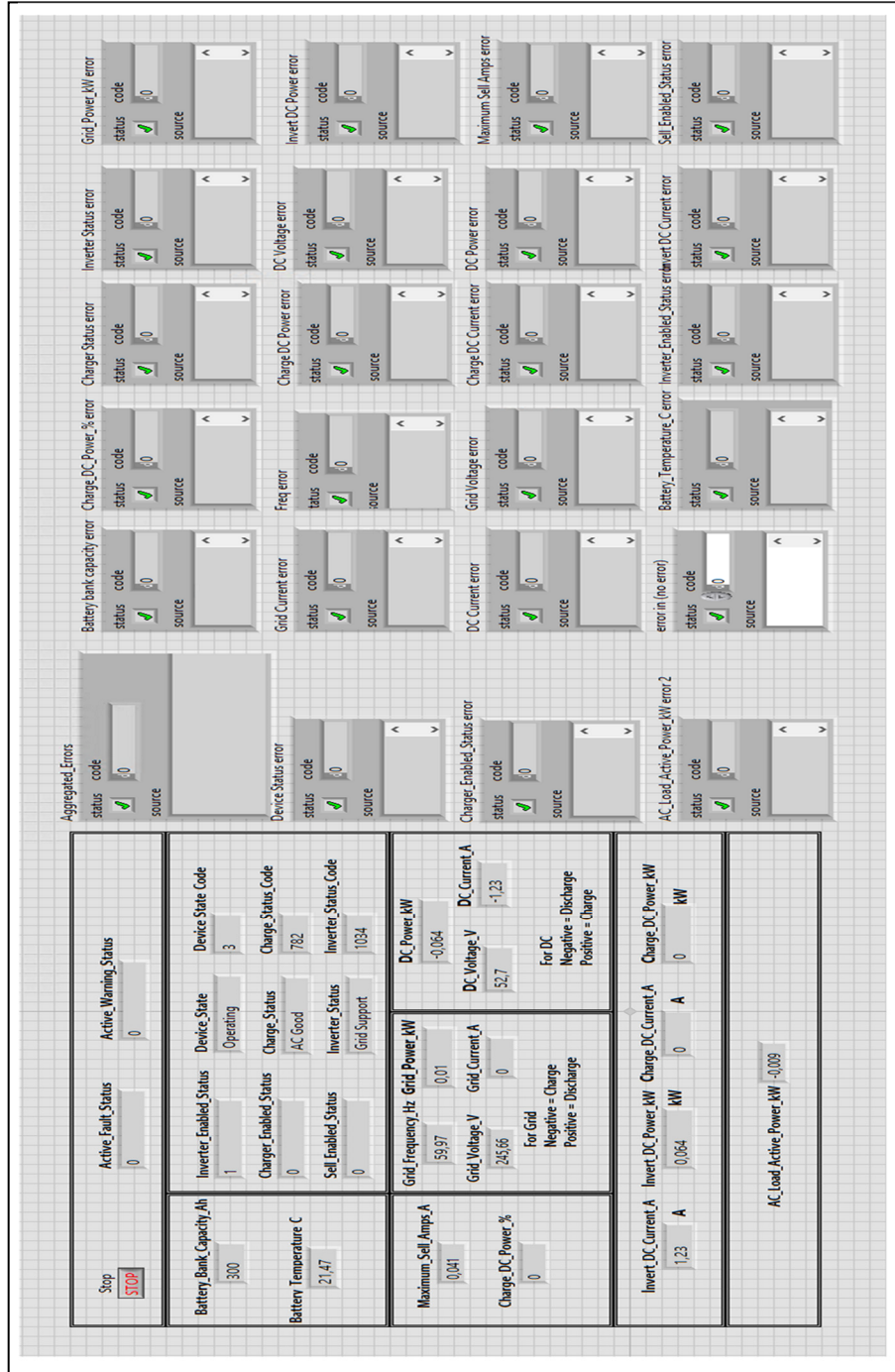


Figure-A V-1 XW Pro Read Front Panel

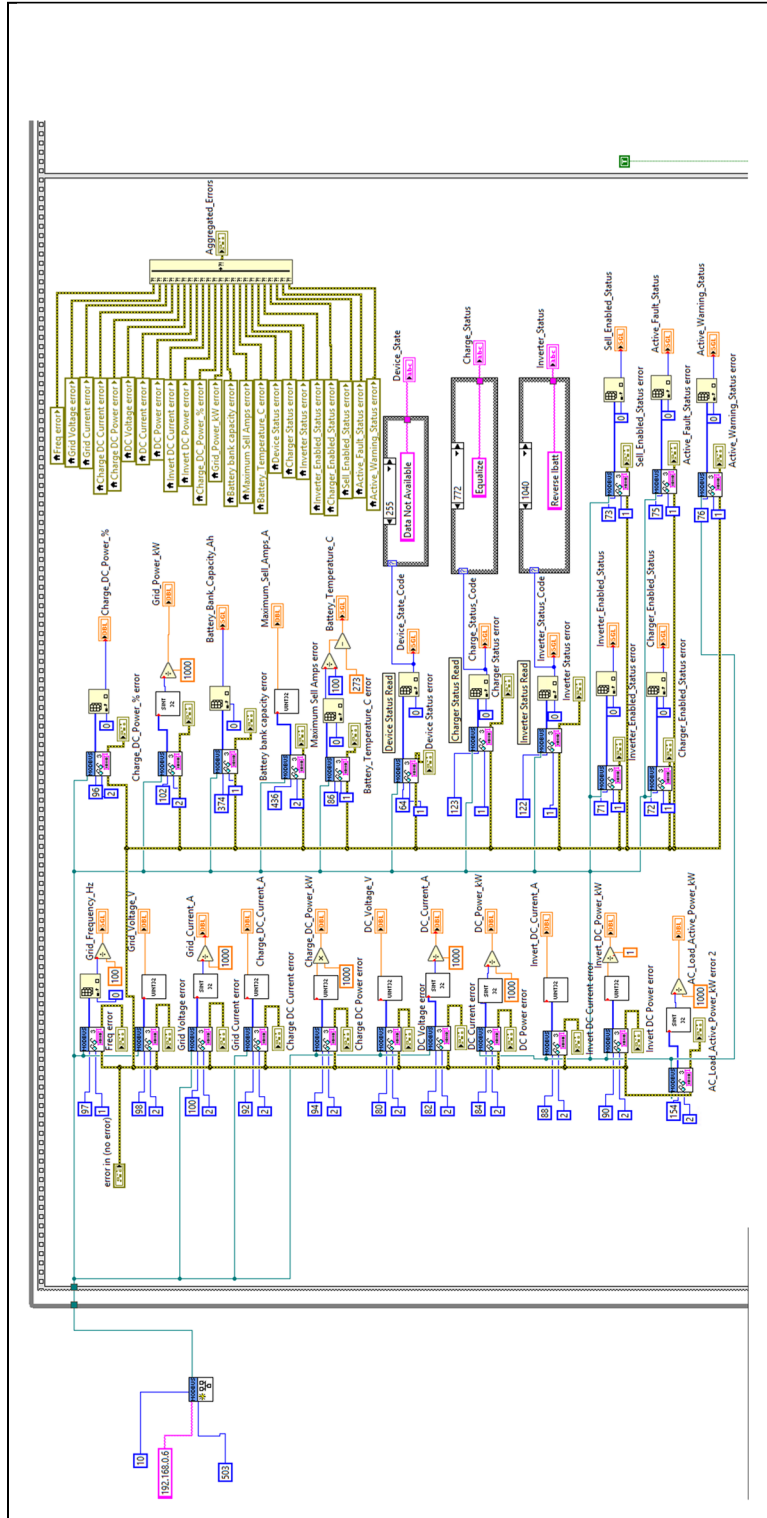


Figure-A V-2 XW Pro Read VI Block Diagram

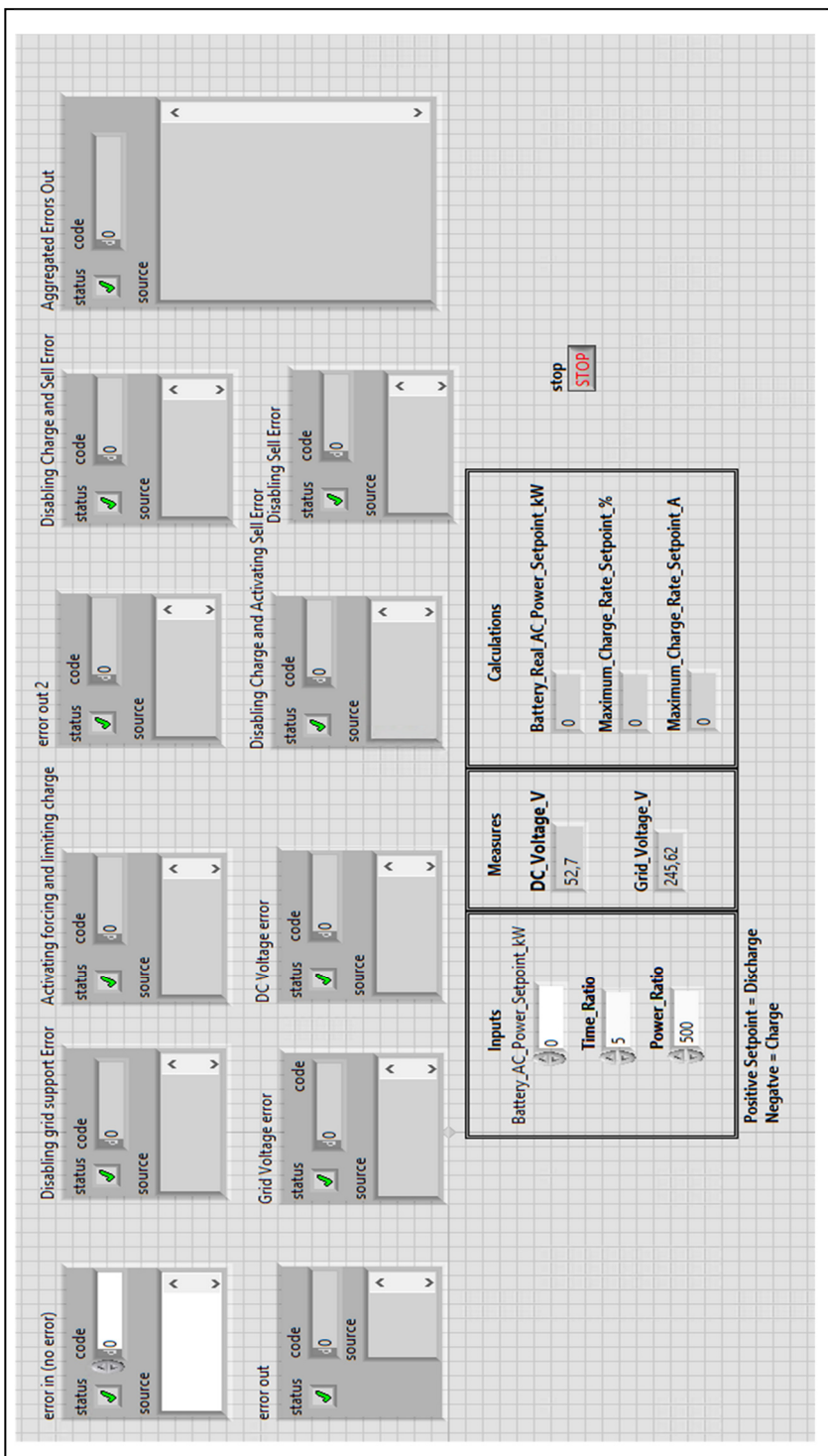


Figure-A V-3 XW Pro Write VI Front Panel

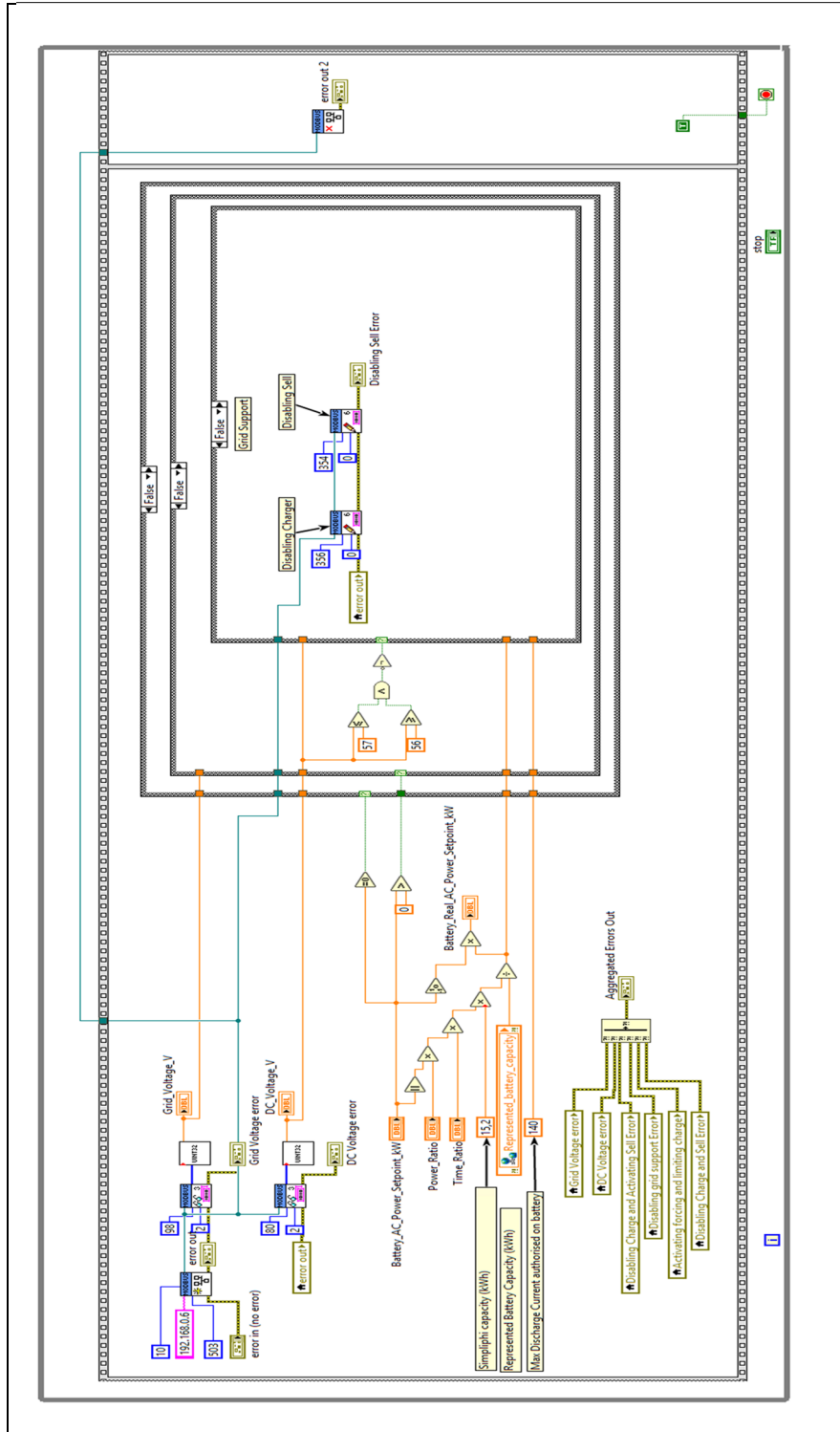


Figure-A V-4 XW Pro Write VI Block Diagram

APPENDIX VI

LABVIEW INVERTER INITIALIZATION PROGRAM

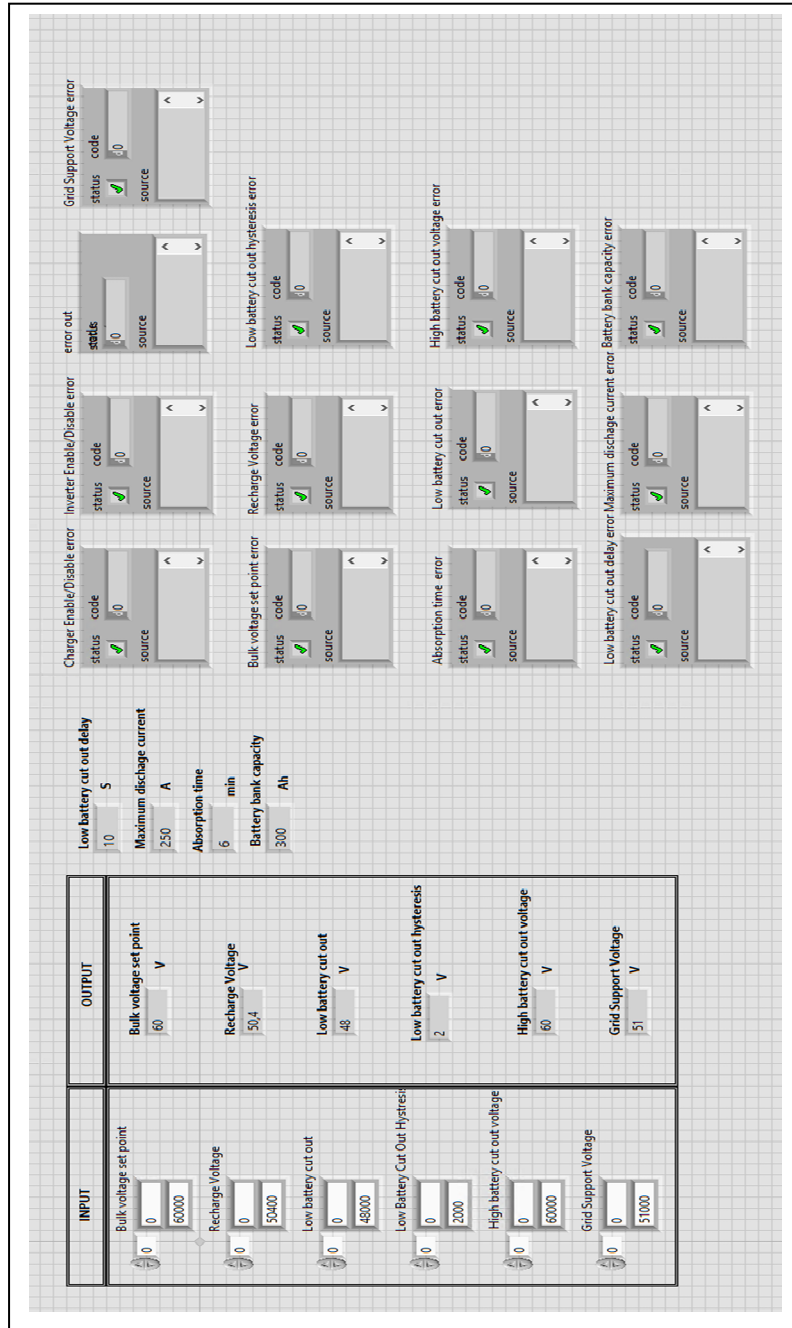


Figure-A VI-1 XW Pro Initialization VI Front Panel

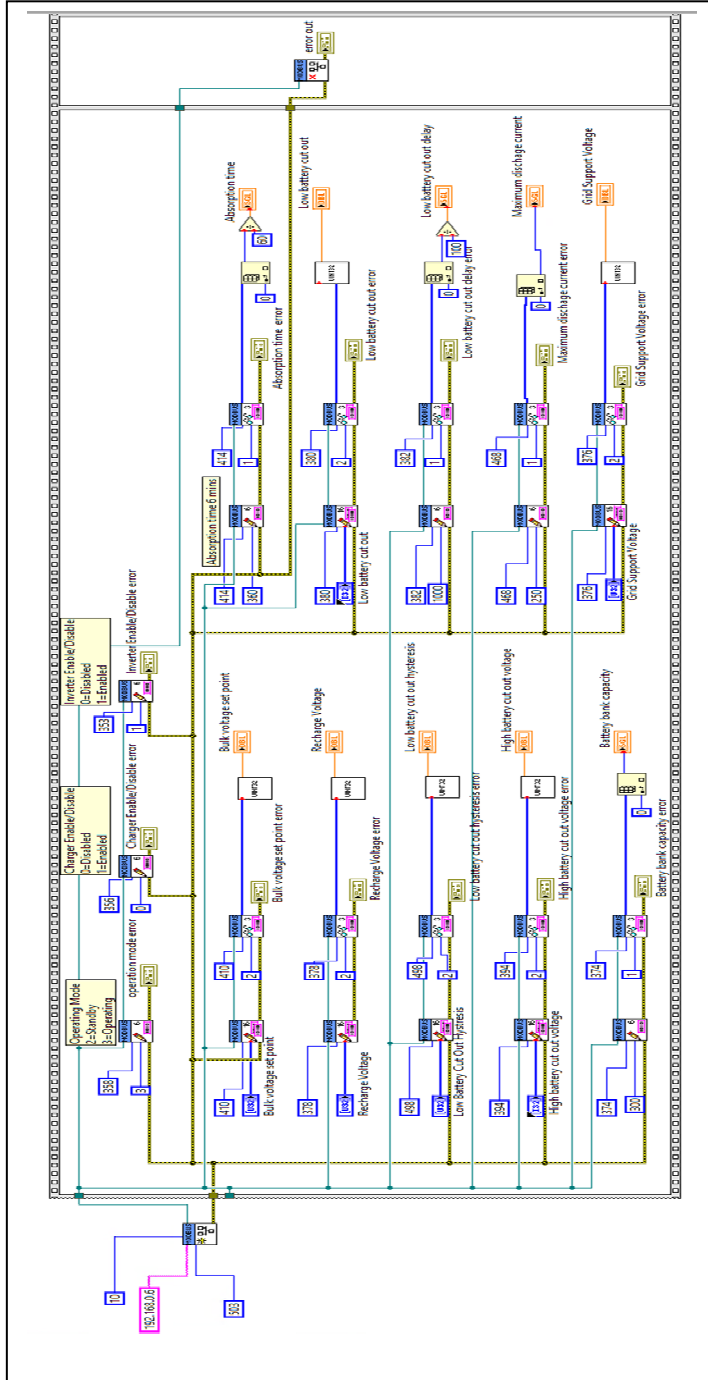


Figure-A VI-2 XW Pro Initialization VI Block Diagram

APPENDIX VII

LABVIEW CHROMA LOAD PROGRAM

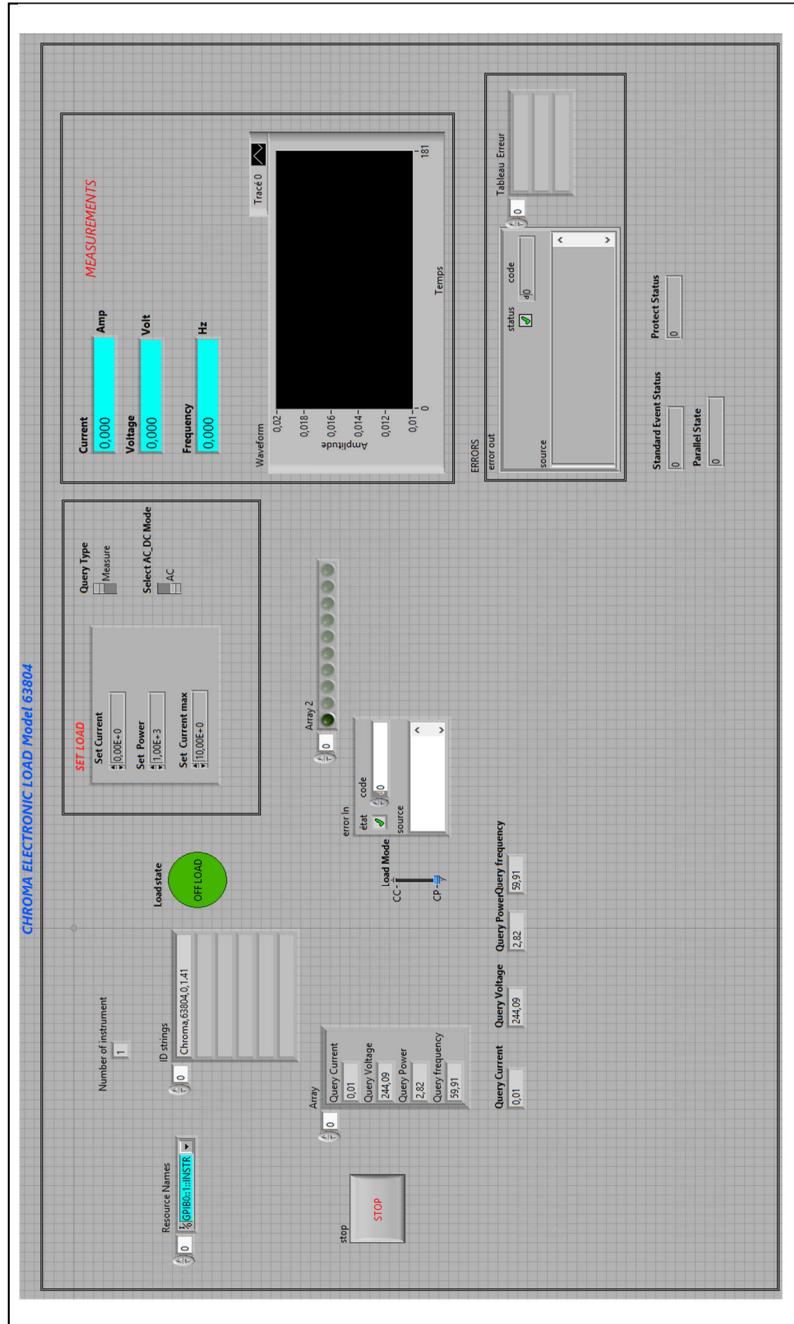


Figure-A VII-1 Chroma Load VI Front Panel

APPENDIX VIII

LABVIEW POWER METER PROGRAM

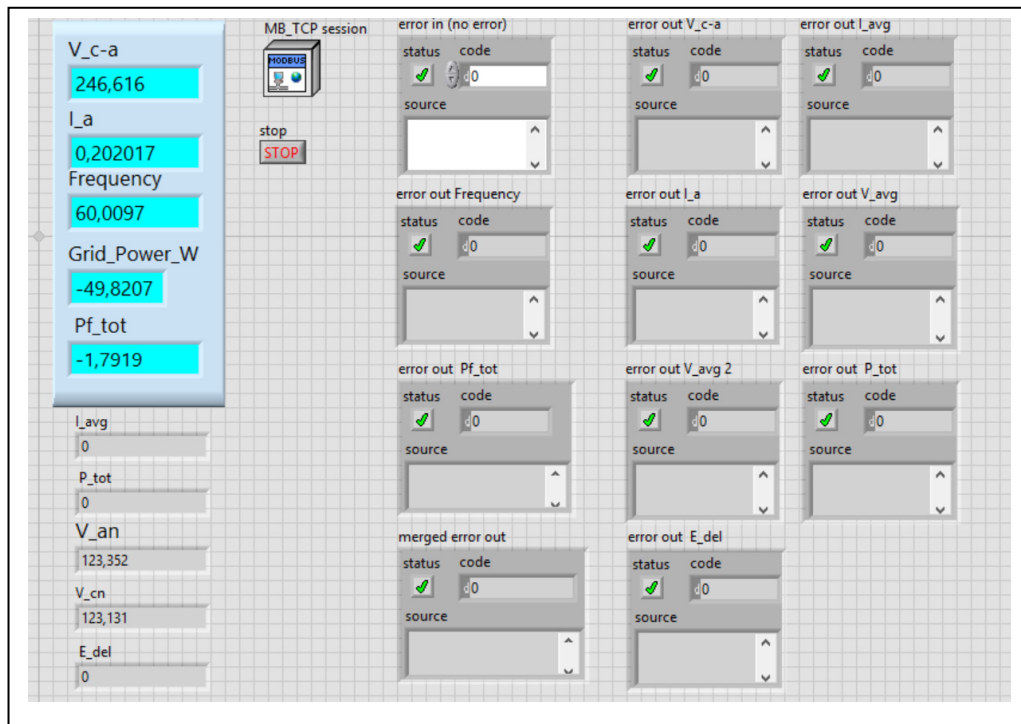


Figure-A-VIII-1 PM5340 VI Front Panel

APPENDIX IX

XW PRO INVERTER READ PROGRAM INTEGRATION

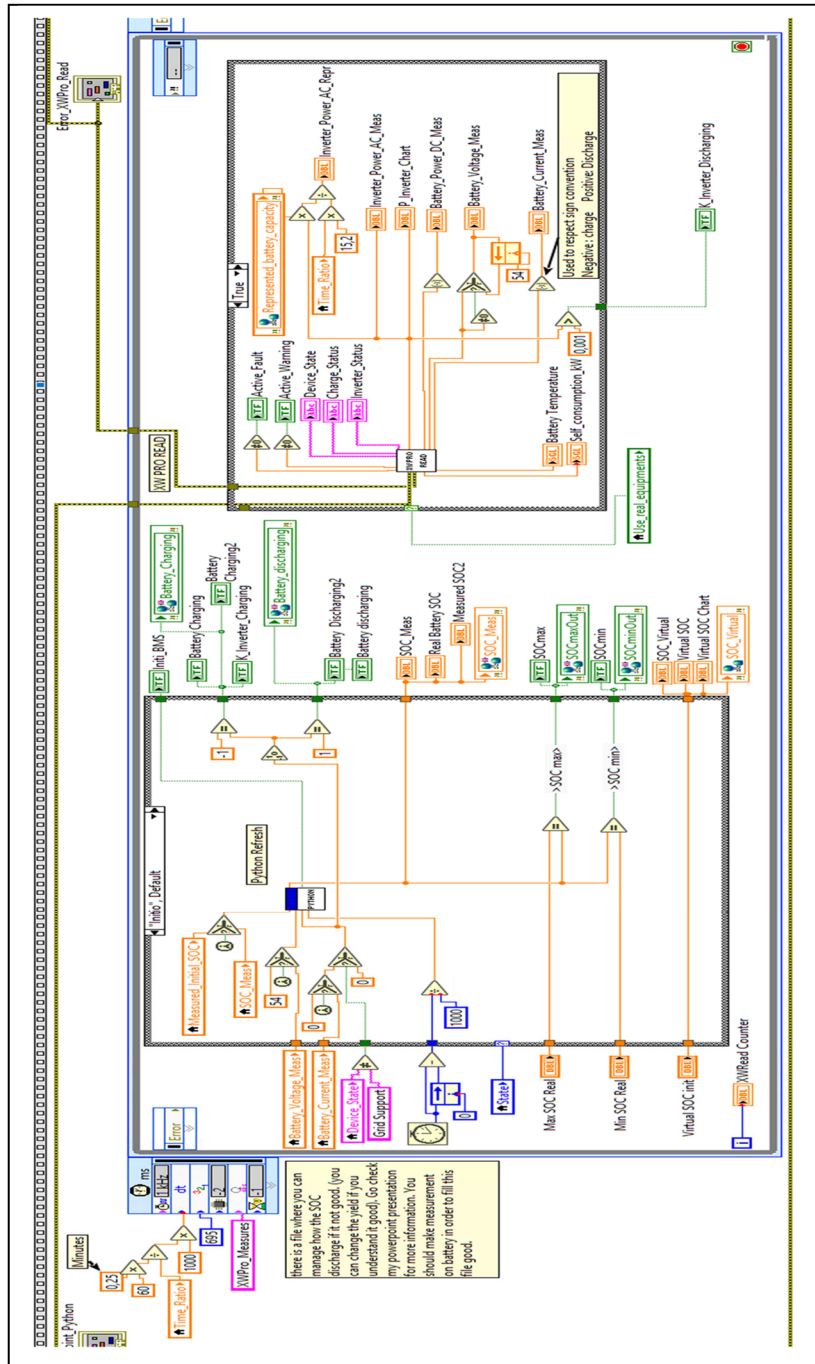


Figure-A IX-1 Inverter Read Program Integration

APPENDIX X

CONEXT BATTERY MONITOR DATASHEET

Life Is On | **Schneider**
Electric

Conext Battery Monitor

Battery bank monitoring with
battery string health detection.



Product at a glance

Conext™ Battery Monitor indicates hours of battery-based runtime and determines battery bank state of charge. It shares key battery bank parameters with Conext™ Pro and XW+ Inverter/chargers improving overall system performance of 24 V and 48 V battery banks. Detecting battery string imbalance is determined using innovative mid-point sensing technology providing time to address the issue before performance is significantly impacted.

Conext™ Battery Monitor features built-in data logging and a local display to selectively show the voltage, current, consumed amp-hours, remaining capacity, and remaining hours. The same information and battery bank data is reported by Conext™ Gateway and distributed to other Conext devices such as XW Pro or XW+ Inverter chargers, MPPT Solar Charge Controllers, Automatic Generator Start module, and System Control Panel via Xanbus™ network connectivity, enhancing performance of the overall system.

Industrial and telecom customers can integrate Conext™ Battery Monitor with energy management systems over Modbus RS485.

Why choose Conext Battery Monitor?

Higher return on investment

- Get the most out of battery-based Conext inverter/charger systems
- Clearly understand hours of available battery-based autonomy
- Detect imbalance between battery strings before it becomes an issue

Designed for reliability

- Extensive quality and reliability testing
- Highly Accelerated Life Testing (HALT)

Flexible

- Stand-alone application or integration with Conext™ XW Pro or XW+ inverter charger systems
- Enables state of charge triggers for AGS module control of diesel generators
- Enables balancing of multi-battery bank systems for large clustered Conext.XW+ inverter/charger systems

Easy to service

- Remotely monitor, troubleshoot, or upgrade firmware with Conext Gateway
- Built-in data logger

Easy to install

- Wall-mount, DIN-rail mount, panel mount
- RJ45 connections for Xanbus network and battery signals
- Configure with front-panel buttons, Conext™ Gateway, or RS485 Modbus

Product applications



Backup power



Residential grid-tie solar with backup power



Off-grid solar



Community electrification




Self-consumption

Figure-A X-5.1 Conext Battery Monitor Datasheet Page 1

Taken from (Conext Battery Monitor, 2020)

Conext Battery Monitor		solarschneider-electric.com 2
Device short name	Conext™ Battery Monitor	
Electrical specifications		
Supply voltage	18 – 66 Vdc	
Supply current (backlight off, logging-disabled)	80 mA @ VIN=48 Vdc, 150 mA @ VIN=24 Vdc	
Input voltage range	0 – 70 Vdc	
Input current range	-9999 – +9999 A	
Battery capacity range	20 – 10,000 Ah	
Operating temperature range	-20 – +50 °C	
Displayed increments		
Voltage	0 – 70 V (0.01 V)	
Current	0 – 200 A/200 – 9999 A (0.1 A/1 A)	
Amp-hours	0 – 200 Ah/200 – 99990 Ah (0.1 Ah/1 Ah)	
State of charge	0 – 100% (0.1%)	
Time remaining	0 – 24 hrs/24 – 240 hrs (1 min/1 hr)	
Temperature	-20 to +50 °C (0.1 °C)	
Accuracy		
Voltage measurement	+/- 0.3%	
Current measurement	+/- 0.4%	
Features		
Network	Protocol: Xanbus/Connectors: RJ45	
USB 2.0	Protocol: MSD (data extraction) Connector: USB mini-B	
Modbus	Isolated RS-485, 2-wire serial	
Data logging	10 data points every 10 mins for 10 years	
Display	Backlight LCD	
Front-panel interface	3 menu buttons, 1 power button	
Battery string imbalance detection	Two point sensing	
Temperature sensor (included)	762 cm	
Warranty	Please refer to our website, SESolar.com for the latest version of the warranty statement.	
General specifications		
Product dimensions (H x W x D)	8.5 x 8.5 x 9.0 cm (3.3 x 3.3 x 3.5 in)	
Product/shipping weight	0.2 kg (0.4 lb)/1.95 kg (4.3 lb)	
Mounting options	Panel-mount, wall-mount, DIN rail: 35 mm	
IP rating/location	IP 20, NEMA 1, indoor only	
Storage temperature range	-30 – +70 °C	
Part number	865-1080-01	
Battery interface kit with shunt (included)		
Connection to battery	300 cm cable with ring terminals	
Connection to battery monitor	500 cm CAT5 cable RJ45	
Shunt	500 A/50 mw	
Regulatory approvals		
Markings	CE, RCM, UL, CSA	
Safety	IEC/EN62109-1, UL1741, CSA 107.1	
EMC	Directive 2004/108/EC, IEC/EN61000-6-3, IEC/EN61000-6-1, FCC Part 15 Class B, Industry Canada ICES-003 Class B	
Compatible products part numbers		
Conext XW Pro (120/240 V)	XW Pro 6848 NA: 865-6848-21	
Conext XW+ (230 V)	XW 8548 E: 865-8548-61	
Conext XW+ (120/240 V)	XW 8848 NA: 865-8848-01	
Conext SW (230 V)	SW 4024: 865-4024-55 / SW 4048: 865-4048-55	
Conext SW (120 V)	SW 4024: 865-4024-21 / SW 4048: 865-4048-21	
Conext MPPT 80 600	865-1032	
Conext MPPT 60 150	865-1030-1	
Conext Gateway	865-0329	
Conext System Control Panel	865-1050	
Conext Automatic Generator Start	865-1060	
Conext Configuration Tool	865-1155-01	

Schneider Electric
Head Office
35 rue Joseph Monier
92500 Rueil-Malmaison, France
Tel: +33 (0)1 41 29 70 00
solar.schneider-electric.com



Specifications are subject to change without notice.
© 2020 Schneider Electric. All Rights Reserved. Schneider Electric | Life Is On is a trademark and the property of Schneider Electric SE, its subsidiaries, and affiliated companies. DS20200117 - Conext Battery Monitor

Figure-A X-5.2 Conext Battery Monitor Datasheet Page 2

Taken from (Conext Battery Monitor, 2020)

LIST OF BIBLIOGRAPHICAL REFERENCES

- 2021 Texas power crisis. (2021). Retrieved from Wikipedia: https://en.wikipedia.org/wiki/2021_Texas_power_crisis#cite_note-winterize2-9
- A. A. Jabbar, A. Y. (2019). Development of Hybrid AC/DC Laboratory-scale Smart Microgrid Testbed with Control & Monitoring System Implementation in LabVIEW. *2019 IEEE PES GTD Grand International Conference and Exposition Asia (GTD Asia)*, (pp. 889-894). Bangkok, Thailand. doi:10.1109/GTDAAsia.2019.8715942
- A. N. Akpolat, Y. Y. (2021, April 13). Design Implementation and Operation of an Education Laboratory-Scale Microgrid. *IEEE Access*, 9, 57949-57966. doi:10.1109/ACCESS.2021.3072899
- Application Development with Modbus*. (2022, February 11). Retrieved from National Instrument: <https://www.ni.com/en-ca/innovations/white-papers/14/application-development-with-modbus.html>
- Beckers, R. (2022, September 9). *How to Find Happiness With LiFePO4 (Lithium-Ion) Batteries*. Retrieved from Solacity Inc.: <https://www.solacity.com/how-to-keep-lifepo4-lithium-ion-batteries-happy/#:~:text=Discharging%20an%20LFP%20Battery&text=Most%20of%20the%20time%20during,99%25%20to%2030%25%20SOC.>
- Conext Battery Monitor*. (2020). Retrieved from Schneider Electric Solar: <https://solar.se.com/us/wp-content/uploads/sites/7/2021/10/Conext-Battery-Monitor-Datasheet.pdf>
- Conext Gateway*. (2020). Retrieved from Schneider Electric Solar: <https://solar.se.com/us/wp-content/uploads/sites/7/2021/11/DS20200117-Conext-Gateway.pdf>

- D. K. Nichols, J. S. (2006). Validation of the CERTS microgrid concept the CEC/CERTS microgrid testbed. *2006 IEEE Power Engineering Society General Meeting*, (p. 3). Montreal. doi:10.1109/PES.2006.1709248
- David R Baker, S. S. (2021, October 5). *Global energy crisis is the first of many in the clean-power era*. Retrieved from BNN Bloomberg: <https://www.bnnbloomberg.ca/global-energy-crisis-is-the-first-of-many-in-the-clean-power-era-1.1661753>
- E. Nasr-Azadani, P. S. (2020, March 04). The Canadian Renewable Energy Laboratory: A testbed for microgrids. *IEEE Electrification Magazine*, 8(1), 49-60. doi:10.1109/MELE.2019.2962889
- Espina, E. B.-M.-G. (2020). Experimental Hybrid AC/DC-Microgrid Prototype for Laboratory Research. *2020 22nd European Conference on Power Electronics and Applications (EPE'20 ECCE Europe)*, (pp. 1-9). Lyon, France. doi:10.23919/EPE20ECCEurope43536.2020.9215751
- Geli, Y. (2021). *Optimisation et mise en place sur un simulateur d'une commande d'écrêtage de puissance d'un bâtiment universitaire utilisant les prédictions d'un réseau de neurones*. Montreal.
- IEA. (2021, July). *Electricity Market Report*. Retrieved from IEA: <https://www.iea.org/reports/electricity-market-report-july-2021>
- M. H. Saeed, W. F. (2021). A Review on Microgrids' Challenges & Perspectives. *IEEE Access*, 9, 166502-166517. doi:10.1109/ACCESS.2021.3135083
- Mary, N. (2016). *Étude technico-économique de l'installation d'un système de production solaire photovoltaïque accompagné de batteries ayant pour objectif de réaliser de*

l'écèlement de puissance au sein du campus de l'école de technologie supérieure.
Montreal.

Mary, N. (2022). Neural Network based Predictive Algorithm for Peak Shaving Application using Behind the Meter Battery Energy Storage System.

PHI 3.8 BATTERY. (2021, June 28). Récupéré sur SIMPLIPHI POWER:
<https://simpliphipower.com/wp-content/uploads/documentation/phi-3-8/simpliphi-power-phi-3-8-kwh-60-amp-specification-sheet.pdf>

Power Meter Powerlogic PM5340. (2023, Februray 03). Récupéré sur Schneider Electric/ Life is on: <https://www.se.com/ca/en/product/METSEPM5340/power-meter-powerlogic-pm5340-ethernet-up-to-31st-harmonic-256kb-2di-2do-35-alarms/>

Schneider Electric, i. (2020, June 4). Conext Gateway Modbus Interface Specification (503) Conext XW Inverter/Chargers. (990-6268B, Éd.) Retrieved from <http://solar.schneider-electric.com>

SimpliPhi Power, I. (2021, June 28). *impliphi-power-phi-3-8-kwh-60-amp-specification-sheet.*

Singh, J. S. (2021, July 21). Recent control techniques and management of AC microgrids: A critical review on issues, strategies, and future trends. *International Transactions on Electrical Energy Systems*, 31(11), 13035. doi:doi.org/10.1002/2050-7038.13035

T. Gühna, D. S. (2021). Hardware and Software Concept for Distributed Grid-Forming Inverters in Microgrids. *2021 23rd European Conference on Power Electronics and Applications*, (pp. P.1-P.10). Ghent, Belgium.

T. Mindra, G. F. (2022). Combined peak shaving/time shifting strategy for microgrid controlled renewable energy efficiency optimization. *2022 21st International*

Symposium INFOTEH-JAHORINA (INFOTEH), (pp. 1-6). East Sarajevo.
doi:10.1109/INFOTEH53737.2022.9751266

V. Y. Kondaiah, B. S. (2022, July). A review on short-term load forecasting models for micro-grid application. *The Journal of Engineering*(7), 665-689. doi: 10.1049/tje2.12151

Xianyong Feng, A. S. (2017, July 30). Comparison of Hierarchical Control and Distributed Control for Microgrid. *Electric Power Components and Systems*, 45(10), 1043-1056.
doi:10.1080/15325008.2017.1318982

XW Pro 120/240V. (2022). Retrieved from Schneider Electric Solar:
<https://solar.se.com/us/wp-content/uploads/sites/7/2021/10/XW-Pro-UL-Datasheet.pdf>

Zakaria, R. (2022, January 10). *Are we entering an age of increasing power supply disruptions?* Retrieved from IHS Markit: <https://ihsmarkit.com/research-analysis/are-we-entering-an-age-of-increasing-power-supply-disruptions.html>